Coordination Chemistry Reviews 553 (2026) 217509

Contents lists available at ScienceDirect

Coordination Chemistry Reviews

journal homepage: www.elsevier.com/locate/ccr

Review

The dynamic adaptability of mixed-ligand zinc MOFs: from fundaments to applications☆

Andrea Daolio [a,1], Dario Giovanardi [a,1], Paolo Pio Mazzeo [a,b], Paolo Pelagatti [a,c], Alessia Bacchi [a,b,d,*]

[a] Dipartimento Di Scienze Chimiche, Della Vita e Della Sostenibilità Ambientale, Università degli Studi di Parma, Viale Delle Scienze, 17A, 43124 Parma, Italy.
[b] Biopharmanet-TEC, University of Parma, Parco Area Delle Scienze 27/A, Parma 43124, Italy.
[c] Centro Interuniversitario di Reattività Chimica e Catalisi (CIRCC), Via Celso Ulpiani 27, 70126 Bari, Italy.
[d] CSGI: Center for Colloid and Surface Science, Via Della Lastruccia 3, 50019 Sesto Fiorentino, Italy.

ARTICLE INFO

Keywords:
Chemical bonds
Noncovalent interactions
Synthesis
Catalysis
Design of materials

ABSTRACT

Metal-Organic Frameworks (MOFs) are functional materials composed of metal nodes linked by organic ligands, often displaying empty pores or channels. Their dynamic structural rearrangement upon guest sorption and desolvation makes them uniquely adaptable and suitable for a wide range of applications. In particular, mixed-ligand Zinc MOFs represent an attractive subset of those materials for their extensive flexibility in coordination and topology. In this review we first discuss the coordination geometries, resulting topologies, and possible structural and dynamic rearrangement modes of different Zn mixed-ligand MOFs families. Like modular tools, the knowledge of these classes and modes make possible the *a priori* design of tailored materials displaying specific properties. The review follows with a selected list of applications in which the dynamic interplay between framework dynamics and guest molecules properties play an important role. These includes the separation of chemical mixtures of industrial relevance, the controlled release of active pharmaceutical ingredients (APIs) and capture and sensing of hazardous chemicals. We demonstrate the feasibility of this approach by focusing on the PUM (Parma University Materials) family of MOFs, that were specifically engineered to find applications in the controlled release of APIs and smart packaging. These materials are able to trap a wide range of APIs, often more than one at a time, adapting their framework geometry to better allocate guest with different shape and functionalities.

1. Introduction

1.1. MOFs as dynamic functional materials

In the realm of functional materials, coordination polymers (CPs) occupy a prominent role. [1–4] They are defined as coordination compounds with repeating coordination entities extending in 1, 2, or 3 dimensions [5], or as polymers whose repeating unit is a coordination complex. [6] These repeating units extend in one, two, or three dimensions, forming various architectures, including chains [7], layers [1], or more complex frameworks. [6,8] In the early years of the twenty-first century, the metal-imposed geometrically ordered ligands arrangement combined with the structural rigidity of linear or *quasi*-linear organic linkers, was strategically harnessed by researchers such as Yaghi, Kitagawa, and collaborators to engineer materials exhibiting porous crystalline architectures. [9–13] These frameworks initially contained solvent molecules in otherwise empty pores and channels, most notably *N*,*N*′-dimethylformamide (DMF), which now can frequently be substituted by less toxic alternatives. [14–16] Kitagawa and coworkers proposed an efficient way to classify porous coordination polymers based on the stability of their frame upon guest removal: first generation materials shows loss of crystallinity and morphology after

☆ This article is part of a Special issue entitled: 'Chemical Bonds' published in Coordination Chemistry Reviews, dedicated to Professor Resnati, celebrating a career in chemical bonds on the occasion of his 70th birthday.

* Corresponding author at: Dipartimento Di Scienze Chimiche, Della Vita e Della Sostenibilità Ambientale, Università Degli Studi di Parma, Viale Delle Scienze, 17A, 43124 Parma, Italy.
E-mail address: alessia.bacchi@unipr.it (A. Bacchi).

[1] These authors contributed equally to this paper.

https://doi.org/10.1016/j.ccr.2025.217509
Received 28 October 2025; Received in revised form 2 December 2025; Accepted 18 December 2025
Available online 5 January 2026
0010-8545/© 2025 The Authors. Published by Elsevier B.V. This is an open access article under the CC BY license (http://creativecommons.org/licenses/by/4.0/).

removal of the guests; second generation materials retain their topology and dimensionality after guest removal, being featured by rigid frameworks; finally, third generation materials undergo a significant reduction of the pore dimensions upon extrusion of the guest, but the initial architecture can be rebuilt after exposure of the material to the same guest. [17,18] Upon solvent removal, in fact, many of these materials retained their crystalline structure while preserving porosity, although substantial structural rearrangements often occurred during desolvation (Fig.1.). [19–23] Unlike traditional porous materials such as zeolites, [24,25] the ability of these frameworks to undergo dynamic structural transformations upon solvent loss was recognized as a functional asset rather than a drawback. [26,27] Through the incorporation of more flexible structural motifs, early innovators in the development of Metal-Organic Frameworks (MOFs in the following) successfully synthesized responsive crystalline materials capable of tailoring their architecture to specific applications, including gas sorption and chemical sensing. [28–31] Nowadays, *a priori* design of materials based on sound coordination chemistry principles proves invaluable in the formulation of a huge number of systems with predictable and tailored properties, making the study of MOFs one of the most active, flourishing and promising fields of modern chemistry, as demonstrated by the 2025 Chemistry Nobel Prize awarded to Susumu Kitagawa, Richard Robson and Omar Yaghi. [32–36] Two main factors are exploited in the formulation of these cutting-edge materials. The first is the coordination geometry of the metal nodes, often arranged in mono- or poly-nuclear assemblies known as Secondary Building Units (SBUs). A specific geometry can hence be imparted by a combination of synthetic conditions, oxidation state of the metal and nature of the bridging ligands, providing foreseeable topology and connectivity. [37–40] The second lies in the nature of the ligand which, either rigid or flexible, linear or bent, and possessing various functional groups in nature and number, can be chosen to impart specific properties to the resulting material. [41–46]

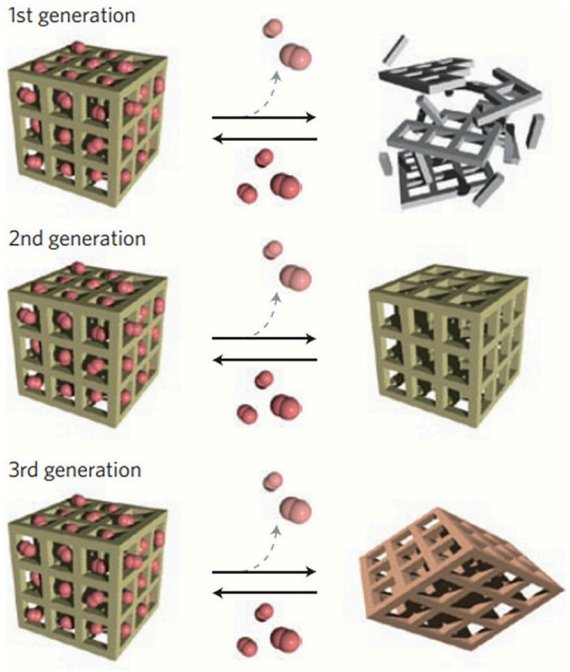


Fig. 1. Graphical representation of MOF generations as a consequence of guest removal. In first generation materials the framework collapses upon guest removal. In second generation materials, thanks to the rigid and stable frame, the architecture of the frame is maintained. Lastly, in third generation materials, the framework is maintained but it adapts to the absence of guests. Reproduced with permission from [23].

1.2. Isoreticularity, interpenetration and polycatenation

In the analysis of porous CPs, the possibility of engineering "empty" pore space is as important as it is the engineering of the chemical structure itself. The first paramount achievement of Yaghi et Al. on this account is the introduction of the isoreticularity concept, dictating that the dimensions of the pores are strictly commanded by the length of the organic ligand. Using similar, yet elongated, ligands brought to the obtainment of a series of isoreticular MOFs, defined as IR-MOFs, whose dimension of grids were directly dependent on the length of the dicarboxylate linkers used in the syntheses. This phenomenon was termed "isoreticular expansion" (Fig. 2., a). [47] It follows that, alongside the increase of the dimensionalities of the grids, the void space must increase accordingly, and indeed important progresses have been made on that account. [48] However, with the expansion of the empty space within a single grid, one of the most recurrent phenomena in MOFs is the occurrence of entanglement. [49] This characteristic, related to the need of the framework to satisfy energetic conditions establishing favorable interframe interactions, [50] leads to intertwining of independent frames in order to maximize the contact and limit the extension of voids in the crystal structure. [51] Depending on the geometrical requirements of the inorganic and organic constituents, entangled frameworks can be classified into two main categories: interpenetrated and polycatenated. The most recurrent MOF interpenetration deals with the entanglement of identical frames, each having the same dimensionality of the whole framework, like in the case of 3D + 3D ➔ 3D expansions(Fig.2, b). [52–54] Less common are the examples dealing

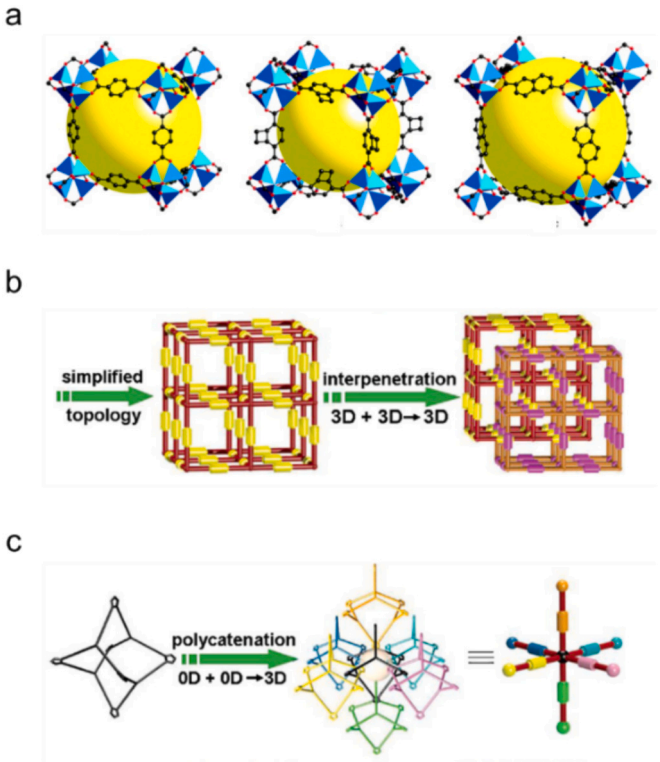


Fig. 2. a) three MOFs exemplifying the concept of isoreticularity. Three ligands with different lengths give rise to topologically similar structures, differing from the dimension of the empty space inside of the channels (graphically represented by yellow spheres). Reproduced with permission from [47]. b) Schematic illustration of the concept of interpenetration, two pcu nets interpenetrating each other in a 3D + 3D ➔ 3D fashion. c) Schematic illustration of the concept of polycatenation, different cages polycatenating each other giving rise to a framework in a 0D + 0D ➔ 3D fashion. b and c reproduced with permission from [52]. (For interpretation of the references to colour in this figure legend, the reader is referred to the web version of this article.)

with 2D + 3D➔3D expansions. [55] The magnitude of interpenetration depends strongly on the length of the organic ligands and on their steric hindrance, with the implementation of ligands possessing bulky substituent favoring the obtainment of lower degrees of interpenetration. [52] Literature presents several examples, from non-interpenetrated framework to degree of interpenetration greater than 10-fold, [56] and up to 54-fold interpenetrated structures. [57] The degree of interpenetration affects the physical properties of the materials, as the pore dimension is typically reduced compared to the one of the non-interpenetrated framework, generating more rigid structures. At the same time the stabilization induced by the interactions between neighboring nets might allow for some degrees of flexibility that would result in disruption of the isolated single framework. [58,59] The formation of an interpenetrated framework may lead to formation of pores narrower than expected, improving the overall selectivity shown toward guest molecules. [60–63] Interpenetration can be either thermodynamically favored (due to van der Waals interactions between nets) or kinetically controlled (depending on crystal growth rate). [64] Several synthetic strategies have been developed to control interpenetration, including the use of templating agents, [65,66] specific solvents, [67,68] temperature control or dilution, [69] incorporation of sterically bulk ligands [70] or post synthetic modifications. [71]

The second typical entanglement displayed by MOFs is polycatenation. Here, the dimensionality of the single frame is lower compared to the dimensionality of the whole framework. For instance, either 1D or 2D frames intertwined to obtain a 3D framework. Examples of polycatenated frameworks derived from 1D + 1D ➔ 2D, [72] 1D + 1D➔3D, [73,74] 1D + 2D➔3D, [75] 2D + 2D ➔ 3D [76,77] are reported. Structurally, polycatenation can occur in several geometries such as parallel, [78] inclined, [79] or interwoven [80] orientations. The reasons behind these lowering of dimensionality are often linked to a sudden stop in the growth of the framework, favored by coordinating monotopic molecules blocking the elongation over one or more directions of the frame or by the ligand-induced deformation of the framework. [81] Notable examples are found in catenated chains, where supramolecular cages or interlocked polyhedra form mechanically bonded assemblies (Fig.2, c). [82]

1.3. *Mixed-ligand MOFs and flexibility*

The possibility of constructing mixed-ligand crystalline architecture proved to be an additional step toward the functionalization and complexity of MOFs. These materials derived by the combination of multiple ligands with different functionalities, also known as heteroleptic MOFs, represent a less explored subclass compared to homoleptic MOFs, which instead are built from a single ligand type. By employing linkers with different functionalities, it is possible to impart the resulting material with a plethora of features often inaccessible through the inclusion of a single organic functional group. [83–86] Additionally, this approach opens to the possibility of building a variety of specific architectures available only when more than a single functional ligand is employed. [87,88] Such materials often display characteristic dynamic modes that are the main subject of this work. [89–91] In fact, mixed-ligand MOFs are often flexible because the combination of different organic linkers introduces structural variability and dynamic coordination environments. One of the main reasons for this behavior is the different length of the two (or more) ligands, which create a non-isotropic environment promoting the bending or twisting of the ligands themselves. [92,93] The possibility of building MOFs with ligand that bind to the metal nodes in different fashion allows a *piori* design of flexibility in a material. The presence of more labile or “soft” coordinative bonds around a metal allows for a finite number of chemical flexible modes. The prototypical example, and a major focal point of this review, is the difference between a “hard” anchoring point of a carboxylate linker and the “soft” coordination impaired by pyridinic linkers. [94] Said ligands can also be designed with inherently flexible moieties on one of the ligands, allowing certain degrees of flexibility while preventing others, hence keeping intact the overall crystallinity of the sample upon movement of the framework. [95–97] Lastly, it must be noted that designing materials with different “dangling” functional groups on the ligand allows the material to respond anisotropically to the presence of guest molecules, prompting specific flexibility modes while keeping intact the rest of the structure. [98,99]

The synthesis of heteroleptic MOFs represent a significant advancement in the rational design of porous materials, allowing for precise tuning of pore geometry, chemical functionality, and dynamic behavior. Achieving such controlled heterogeneity requires a deep understanding of both thermodynamic and kinetic factors, as well as careful manipulation of coordination chemistry to direct the self-assembly process toward the desired mixed-linker structure. One of the primary strategies relies on thermodynamic control, where the relative binding affinities of different linkers toward the metal nodes dictate their preferential incorporation into the framework. Linkers with stronger coordinating groups tend to occupy the most favorable coordination sites, while weaker linkers are incorporated in less constrained positions. By exploiting these differential affinities, researchers can bias the assembly process to generate predictable heteroleptic architectures. Combining, for example, metal atoms in their +2 oxidation state with carboxylate ligands may bring to the formation of two-dimensional layers with open metal sites orthogonal to the plane, in which the coordinative environment of the metal can be filled by neutral linkers. [100] Complementary to thermodynamic strategies is the use of kinetic control, which focuses on the reaction rate and nucleation processes. Fast reactions may trap metastable phases or favor certain linkers at specific nodes due to temporal accessibility, allowing for selective incorporation of multiple linkers that would not coexist under equilibrium conditions. Adjusting solvent composition, temperature, concentration, and the use of modulators can modulate the kinetic landscape, enabling selective crystallization of mixed-linker frameworks. [101,102]

A crucial aspect of heteroleptic MOF design is the management of competing linker coordination. In a multi-linker system, the linkers may differ in length, rigidity, functional groups, or steric demand, and these differences influence which nodes they can access and how they orient within the lattice. Rational design often employs a complementary geometry approach, pairing linkers whose lengths and angles are compatible with the target topology to minimize strain and maximize framework stability. In addition, steric hindrance and functional group positioning can be leveraged to prevent homoleptic domains, encouraging an ordered distribution of the distinct linkers. [103,104] The use of modulators, such as monocarboxylic acids or small chelating molecules, further aids in controlling nucleation and growth, as they can transiently block metal coordination sites and slow down linker incorporation, enhancing the probability of forming the desired heteroleptic configuration. [105]

Another common strategy involves stepwise or sequential linker incorporation, where a primary framework is first assembled using a dominant linker, followed by post-synthetic incorporation of a secondary linker through solvent-assisted linker exchange or post-synthetic modification. This approach allows greater control over the distribution and ratio of the linkers within the structure and can facilitate the incorporation of functional or responsive moieties that may not survive direct solvothermal synthesis. [106,107]

Once the materials have been synthetized, investigating MOF flexibility requires a combination of experimental and computational techniques capable of probing structural changes, local dynamics, and mechanical responses at multiple length and time scales.

Diffraction techniques remain foundational for characterizing framework flexibility. Single-crystal X-ray diffraction provides high-resolution information on unit cell parameters, bond lengths, angles, and local distortions, enabling the visualization of subtle structural transformations during guest adsorption or external stimuli. Powder X-ray diffraction, particularly *in situ* or variable-temperature/pressure

modes, allows monitoring of phase transitions, breathing behavior, and gate-opening phenomena in bulk samples. Complementarily, neutron diffraction is highly valuable for locating light atoms, such as hydrogen, within pores and for tracking guest molecules that may induce framework transformations, offering insights often inaccessible *via* X-ray techniques. [108]

Spectroscopic methods offer complementary local information. Raman and infrared (IR) spectroscopy detect variations in bond vibrations, ligand conformations, and coordination environments associated with framework deformation. Solid-state nuclear magnetic resonance (NMR) spectroscopy probes the local dynamics of ligands, metal nodes, and guest molecules, revealing dynamic processes on molecular timescales. UV–Vis absorption and fluorescence spectroscopy can further monitor guest-induced conformational changes, particularly in optically active or luminescent MOFs. [109–111]

Gas adsorption and sorption studies are instrumental in revealing framework flexibility, particularly guest-responsive phenomena. Stepwise or hysteretic adsorption isotherms provide indirect evidence for breathing, gate-opening, or other structural transitions. High-pressure adsorption experiments allow examination of framework response under extreme conditions, providing insight into mechanical robustness and reversible structural changes. [22,112]

Microscopy techniques offer spatially resolved information on framework deformation. Transmission electron microscopy (TEM) and scanning electron microscopy (SEM) allow visualization of morphological changes, crystal swelling, or pore collapse at high resolution. Atomic force microscopy (AFM) can quantify nanoscale mechanical properties and detect subtle deformations, offering insight into local flexibility and elasticity. [113]

Computational approaches provide atomistic and molecular-level understanding of dynamic behavior. Molecular dynamics (MD) simulations predict breathing modes, guest-induced transformations, and energy barriers associated with structural transitions, enabling visualization of flexibility over time. Density functional theory (DFT) calculations complement experimental observations by evaluating the energetics of different conformational states, stability of flexible frameworks, and potential response pathways to external stimuli. [108]

Thermal and mechanical analyses further contribute to understanding MOF flexibility. Differential scanning calorimetry (DSC) and, to a lesser extent, thermogravimetric analysis (TGA) detect phase transitions, decomposition events, and thermally induced structural rearrangements. [114,115]

Collectively, these experimental and computational techniques provide a comprehensive, multi-scale perspective on MOF flexibility. By integrating structural, spectroscopic, mechanical, and theoretical insights, researchers can elucidate the mechanisms governing dynamic behavior, optimize framework design, and predict performance under realistic operating conditions. This holistic understanding is critical for the rational development of flexible MOFs for advanced technological applications, enabling exploitation of their unique adaptive properties while ensuring stability, reproducibility, and functionality in practical environments.

1.4. Zinc coordination geometries and relative families of functional materials

Given the vast number of possible metals and ligands exploited to build MOFs that exceed the scope of this review, here we focus on a specific group of mixed-ligand MOFs that contain pyridinic and carboxylic acid linkers bound to Zn(II) metal atoms. Zinc-based coordination polymers are among the most studied materials for many kinds of applications. [116–118] This is due to the many key benefits Zn possesses over other transition metal elements. Among them, we cite:

- Biocompatibility: Zn is a biologically essential element, naturally present in the human body. [119,120] This makes zinc-based MOFs more biocompatible compared to other metals, which may be toxic or environmentally harmful. Its non-toxic nature allows the resulting MOFs to be used in biomedical applications, such as drug delivery systems. [121] Additionally, their compatibility with biological systems reduces the likelihood of adverse reactions, paving the way for their use in imaging and sensing [122] or even tissue engineering. [123]

- Cost-Effectiveness: zinc is an abundant and relatively inexpensive metal, making it a cost-efficient choice for synthesizing MOFs. [124] The affordability of Zn-based MOFs makes them attractive for industrial use, particularly in areas like carbon capture, where scalability and economic viability are critical. [125,126]

- Structural versatility: The chemistry of Zn allows for the formation of a wide array of SBUs, giving rise to diverse architectures. Zinc readily coordinates with various organic ligands, such as carboxylates and imidazolates, enabling the creation of frameworks with tailored properties. In its common +2 oxidation state, Zn is a d^{10} metal that does not usually tend to oxidize or reduce in the relatively mild conditions in which MOFs are constructed. Therefore, orbital directing interactions are weak to absent, and the metal can adopt several different coordination modes. Tetrahedral and octahedral coordination complexes are known, common and stable. [124] In addition, square pyramidal complexes in the form of so-called "paddlewheels" are a common occurrence due to coordination of the metal to the carboxylic acid moiety, capped by nitrogen-containing pillaring ligands (Fig.3). [127–129] Synthetic conditions such as the use of a specific solvent or the stoichiometric ratios of linkers can impart a geometry on the metal node. In combination with the geometry of the organic ligands employed, this often translates to materials with predictable topology and functionality. [32] In the following, we will explore the different coordinative environments of this metal with a strong focus on the structure of the resulting materials.

1.4.1. Tetrahedral Mixed-Ligand Zn MOFs

When Zn(II) combines with carboxylic acids (or carboxylates) and pyridine-containing ligands in a 1:2:2 ratio, it can form tetrahedral molecular complexes. [130,131] When multitopic ligands are employed, those complexes may arrange in one of two main possible framework topologies, diamondoid (**dia**) and square planar (**sql**). The synthesis of the tetrahedral connectivity is generally aided using water as a solvent in hydrothermal reactions. [53,132] Additionally, when asymmetric ligands bearing both pyridinic and carboxylic acid functionalities are employed, the material often displays this coordination. [133–135] The nature and geometry of the ligands seem to play a major role in the formation of **dia** or **sql** topologies. Following the tetrahedral geometry of the metal node, the use of linear and generally rigid linkers usually promotes the formation of MOFs with **dia** topology. In these structures, carboxylate groups bridge zinc atoms in a bis(monodentate) binding mode, forming undulating chain submotifs. Bis-pyridinic likers forms similar undulating chains running perpendicular to the former. An additional ancillary interaction between the carboxylate oxygen and the ortho-hydrogens of the pyridinic ligands is often present, likely contributing to the stabilization of the framework. These structures exhibit adamantanoid cages, which are fundamental units of the diamondoid net, and display six-membered windows. Interpenetration is a highly common and defining feature of **dia** Zn-MOFs, as the large void spaces in single diamondoid nets often lead to multiple networks interweaving to stabilize the structure and minimize large empty volumes. The degree of interpenetration varies widely, with instances of 2-fold [133], 3-fold [136], 4-fold [137], 5-fold [138], 6-fold [139], 7-fold [140], 8-fold [141], and even 10-fold [142] interpenetration reported. Many of these materials are non-porous, with interpenetrated nets filling all available space. They typically demonstrate good thermal and chemical stability, especially to water, which can be enhanced by factors like hydrophobic groups. [141].

If more flexible or bent ligands are employed, the tetrahedral coordinative environment of Zn(II) can produce MOFs with **sql** topology, in which the distortion on at least one of the ligands produces corrugated

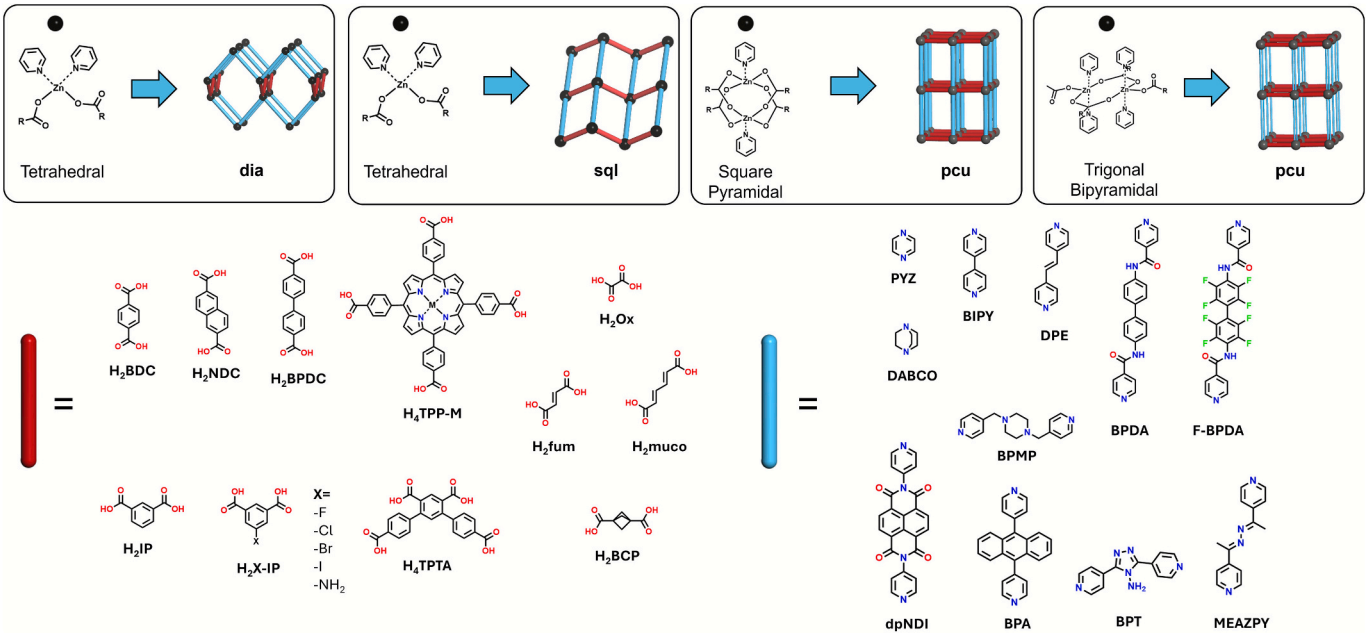


Fig. 3. *Above, inlets* schematical representation of the geometry of the metallic node and its extension to one of the material classes discussed in this work. The topology of the framework is indicated near it, black spheres represent the SBU, red bars the carboxylate linkers and light blue bars the bis-pyridinic linkers. *Below*, a collection of carboxylate and bis-pyridinic linkers discussed in this work. The abbreviation used in the text is reported at the bottom of the 2D representation. (For interpretation of the references to colour in this figure legend, the reader is referred to the web version of this article.)

2D sheets that forms layers by virtue of additional noncovalent interactions such as π-π stacking. [143] Given the different resulting topology, high degrees of interpenetration are uncommon, but not absent from literature. In this case, the layer described is often referred to as an interdigitated bilayer. [144] The resulting pore shape is generally squared, as consistent with the **sql** lattice. Most of the features highlighted for tetrahedral Zn-MOFs with **dia** topology are also held for this class of materials, especially water and thermal stability [88,139].

1.4.2. Square pyramidal mixed-ligand Zn MOFs

When reacted with carboxylic acids and pyridine-containing ligands in a 2:1:1 ratio, Zn(II) can usually form dimeric complexes often referred to as "paddlewheels" in which the coordination of two Zn metals is forced into a square pyramidal geometry by the coordination of four carboxylates. The formation of square pyramidal Zn(II) complexes is known in literature [145] and zinc "pillared" MOFs (PL-MOFs) are a prominent class of materials characterized by this distinctive dinuclear paddlewheel SBU based on $[Zn_2(COO)_4]$ units. [4,87,146] The $[Zn_2(COO)_4]$ paddlewheel SBUs are connected by dicarboxylate linkers to form two-dimensional square-grid layers. The pillaring and the formation of the 3D architecture is then achieved when the two-dimensional layers are connected by additional N-topic organic linkers, known as "pillars," to form a three-dimensional structure, in which each Zn(II) center adopts a distorted square pyramidal geometry. These pillars bridge the layers, enhancing the stability of the framework and creating additional porosity. [147] The design allows for great control over the pore size, shape, and functionality of the MOFs, making them highly versatile. [148–150] The resulting materials display a primitive cubic (**pcu**) topology with approximately rectangular windows and mono-, bi- or tri-directional channels running through the material. [62,151] It is brilliantly shown by Schmid [152] that pillaring in Zn(II)-MOFs is the source of the inherent softness and flexibility of this coordination networks, owing to the arrangement being an energetic saddle point rather than the ground state of the system. [153] These diverse structural characteristics enable a wide range of applications for paddlewheel Zn MOFs. [154–157] Many are employed in gas storage and separation, including H_2, N_2, CO_2, and hydrocarbons. [146,158,159] The ability of these MOFs to undergo structural transformations in response to external stimuli, like guest molecules or pressure, is a crucial feature that enhances their performance in these applications, allowing for tailored properties and highly selective interactions. [160,161]

1.4.3. Trigonal bipyramidal mixed-ligand Zn MOFs

Zn(II) complexes can also show trigonal bipyramidal coordination and mixed-ligand MOFs containing pentacoordinated Zn atoms in dinuclear SBUs are known. While the stoichiometry is the same as in tetrahedral MOFs, a choice of a solvent different from water (*i.e.* a solvothermal reaction, most notably DMF) usually promotes the formation of octahedral coordination. [139,162] In this coordinative environment, all the metal atoms have a $[ZnN_2O_3]$ distorted trigonal bipyramidal coordination geometry, which is formed by thee O atoms from three different dicarboxylate ligands and two N atoms from two different bis-pyridinic ligands. [163] In a single SBU, four different carboxylates bind two Zn(II) metals over a plane. However, differently from paddlewheel SBUs, the two carboxylate groups of a dianionic ligand display different coordination modes: two carboxylate groups from two ligands bridge two Zn(II) centers to form a $[Zn_2(COO)_2]$ unit, while other two bind each a Zn atom through one of their oxygens, hence composing the trigonal bipyramid, $[Zn_2(\mu\text{-}COO)_2(COO)_2]$. In some cases, a k^2-chelating behavior of the non-bridging carboxylates is also found, giving rise to highly distorted octahedrons. The other dicarboxylate groups on the ligands bridge together the SBUs forming distinctive distorted square layers topologically similar to the paddlewheel ones. [164–167] It should be noted that employing bent dicarboxylic acids as reagents produces a similar coordinative environment for the metal but with different connectivity between the SBUs, which can vary widely across multiple MOFs architectures. [132,135] The apical positions of the octahedral coordination are then filled by two pyridinic linkers for each Zn(II) atom, forming a double pillaring unit extending over the third direction of the coordination and forming the crystalline lattice. The resulting materials, much like the pillared MOFs described above, display a primitive cubic (**pcu**) topology with rectangular windows and directional channels. [168] For structural reasons to be detailed in the

following, the resulting materials are usually more rigid and resistant than paddlewheel pillared MOFs, although some degree of mobility can be imparted mostly thanks to flexible ligands. Materials with this topology are less present in literature in respect to the other classes described in this work. As a result, a specific name for this class is not so widely recognized. For the sake of clarity, we will refer to them as "double-pillared" MOFs throughout the discussion, which is a term employed by some authors. [169–171]

2. Main dynamic modes of mixed-ligand Zn MOFs

In addition to their rich coordinative and topological ranges, MOFs are often capable of undergoing structural changes in response to external stimuli maintaining their overall framework integrity. [23,172] These transformations are often referred to framework dynamics or flexibility. [173] Unlike traditional rigid porous materials, flexible MOFs can adapt their internal geometry such as distances between nodes, angles between linkers and relative position of different interpenetrated nets. This dynamic nature allows the framework to respond to its environment, optimizing pore volume and interactions between the nets and guest molecules. [174] This tunability allows to design MOFs that are not only porous but also capable of adjusting their internal architecture to optimize performance under specific conditions, producing responsive materials and allowing for applications that require adaptability, such as sensing, separation, and storage. [175]

The most common external stimuli that can induce flexibility in MOFs include changes in temperature, [176] pressure, [177] and most notably the presence or removal of guest molecules such as gases or solvents. [178] Mechanical stresses, such as compression or shear, [179] can also prompt deformations or phase transitions. Additionally, light or electric fields may influence certain photo- or electro-responsive MOFs. [180]

Often, even extreme degrees of structural adaptabilities do not compromise the crystallinity of the materials. [181] Instead, flexibility introduces a level of structural responsiveness that can be finely tuned through the choice of metal nodes, organic linkers, and overall topology. [182,183] This feature allows to study the framework dynamics with crystallographic and magnetic resonance techniques. As a result, a parallel can often be drawn between the structural changes in a material and their behavior in a variety of applications, the most sensible of this is undoubtedly their isothermal gas loading, in which events such as "gate opening" can be directly linked to framework dynamics. [184–187]

Usually, the coordination geometry dictated by the SBU allows for a finite number of structural deformations so that it is possible to group these modes on the basis of the MOF classes described above. [172,188] It is hence convenient, in the following, to list the main flexibility modes that mixed-ligand Zn-MOFs can undergo classifying them first by their class and then dividing the modes by how the framework respond to external stimuli (Table 1).

2.1. Tetrahedral mixed-ligand Zn MOFs

This class of MOFs is widely recognized for its pronounced rigidity, [87,88,189] primarily attributable to the robust tetrahedral coordination between Zn(II) metal centers and organic linkers, [130,190] as well as the propensity to form networks featuring a high degree of interpenetration that limits pore volume and, hence, structural flexibility. [137,141] As a consequence, literature often reports the absence of structural modifications upon guests inclusion or gases sorption. [190,191] Nonetheless, certain dynamic behaviors can still be identified, and some studies conducted on this class provide insights into the responsive mechanisms of these MOFs under external stimuli, often focusing on guest molecule adsorption and desorption. [192,193] These examples highlight that while framework dynamics is a mechanism of adaptability common in many MOFs classes, their occurrence in tetrahedral Zn(II) MOFs depends on the specific cases defined by ligand combinations and resulting network characteristics, leading to either dynamic flexibility or notable rigidity. [137]

2.1.1. Ligand distortion

Ligand mobility, characterized by conformational changes and distortion in the organic linkers, is the fundamental property that dictates the dynamic behavior of tetrahedral Zn-MOFs. This inherent flexibility allows these materials to respond to external stimuli, directly impacting their structural parameters and functional performance. [144] Two papers by Lee at *Al.* highlight the possibility of building tetrahedral, diamondoid networks including flexible, photoactivatable moieties as part of the pyridinic linker. Employing 1,4-bis(4-pyridyl) piperazine as a linker, the group was able to photochemically switch the linker from a chair to twist-boat conformation. A similar transformation was also reported by exchanging the guest solvent from DMA (N,N-dimthylacetamide) to benzene. Critically, the materials produced in this way displayed marked differences in their photoluminescence spectra. This behavior was investigated both employing 4,4′-oxybis (benzoic acid) and benzene-1,3-dicarboxylic acid as carboxylate linkers. [194,195] While it is not always possible to gain detailed information about the ligand rearrangement during guest uptake or release, it is interesting to notice that the type and inherent flexibility of the bridging ligands critically influence the overall framework dynamic behavior. For example, the choice between 1,2-bis(4-pyridyl)ethane (BPA) and 1,2-bis (4-pyridyl)ethylene (BPE) as pillars in Zn-1,4-naphthalenedicarboxylate (1,4-NDC) systems influences the structural versatility and ultimately, the properties of the MOF. [88] The two MOFs bear an almost identical structure, differing just for the nature of the bis-pyridinic linker and the number of interpenetrated nets (three for BPA and four for BPE). When guest DMF is removed from their channels they both undergo significant changes in their PXRD patterns consistent with extensive structural transformations, but only $[Zn(BPE)(1,4\text{-}NDC)]_n$ is capable of returning to its original structure after being exposed to DMF vapors for 2 days. When the 1,4-NDC moieties are substituted for more flexible dicarboxylic acids such as fumarate and muconate, [141,190] the resulting compounds show interesting and complex sorption behavior of different gases, again suggesting that the specific interactions between the framework, guest molecules and the ligands play a pivotal role in the sorption processes, often displaying unexpected gate-opening events associated with dramatic changes in the material architecture.

2.1.2. Framework breathing in dia networks

Characterized by the reversible expansion and contraction of the MOF's framework, "breathing" represents a dynamic response to changes in the chemical environment, often triggered by guest exchange or desolvation (Fig.4, a). While it is not always possible to detail this behavior in single crystals, stepped sorption isotherms are a strong diagnostic sign of a "gate-opening", where pores reversibly expand and contract. One notable example is $[Zn_2(4\text{-pyridilbenzene-1,3-dicarbohydrazide})_2(4,4'\text{- oxybis(benzenedicarboxylate)}_2]_n$ (**JUK-8**), an eightfold interpenetrated **dia** MOF, which.

demonstrates distinct switchability triggered by guest molecules like water and CO_2, or by changes in temperature (Fig.4, b). [196] Its unique "breathing" mechanism involves collective motions of all eight interpenetrated diamondoid subnetworks with only minor relative displacements, changing the entire volume of the cell from 3831 $Å^3$ to 4063 $Å^3$. This synchronized motion is primarily stabilized by strong hydrogen bonds between carboxylate oxygen and N—H groups of the 4-pyridilbenzene-1,3-dicarbohydrazide linker, and π-π stacking interactions between aromatic rings of adjacent interpenetrating networks. **JUK-8** shifts between a closed-pore phase, an intermediate-pore phase, and an open-pore phase. CO_2 sorption at 195 K exhibits a two-step adsorption isotherm, where the material first fills the intermediate pore phase, then undergoes an abrupt expansion to the open-pore phase. This process is fully reversible, with very narrow hysteresis. Similarly, water vapor adsorption at 298 K also shows a two-step uptake,

Table 1
shorthand name (when available), structural formula, type of flexibility encountered and potential application of the MOFs listed in the review.

Shorthand Name	Chemical Formula	Type of Flexibility	Application	Citation
ADES-1	$[Zn_2(5NO_2\text{-IP})_2((E)\text{-N}'\text{-(pyridin-3-ylmethylene)nicotinohydrazide})_2](H2O)]_n$	Framework Breathing	Dye Adsorption	[229]
CID series	[Zn(R-IP)(BIPY)]	Pillar Tilting and Rotational dynamics	Molecular Switches, Guest Adsorption	[230]
CID-23	$[Zn(isophthalate)(1,4\text{-bis}(4\text{-pyridyl})acetylene)]_n$	Breathing Behavior and Plane Sliding	Molecular Switches, Guest Adsorption	[232]
f-MOF-1	[Zn(1,4-naphthalenedicarboxylate)(1,2-bis-(4-pyridyl)ethane)]	Framework Breathing	Gas adsorption - Structural Studies	[223]
f-MOF-1a	(desolvated phase of f-MOF-1)	Framework Breathing	Gas adsorption - Structural Studies	[223]
f-MOF-1b	(desolvated phase of f-MOF-1)	Framework Breathing	Gas adsorption - Structural Studies	[223]
FTR-P1	$[Zn(bicyclo[1.1.1]pentane\ dicarboxylic)_2(bipyridine)]$	Ligand Rotation and Torsion	Molecular Switches	[211]
FTR-P2	$[Zn(bicyclo[1.1.1]pentane\ dicarboxylic)_2(4,4'\text{-azobipyridine})]$	Network Displacement	Molecular Switches	[210]
IITKGP-24	$[Zn_2(1,2\text{-Di}(4\text{-pyridyl})ethylene)(1,2,4,5\text{-tetrakis}[(4\text{-carboxy})phenoxymethyl]benzene)]_n$	Rigid	Acetylene/CO_2 Separation	[252]
IRMOF-1	$Zn_4O(1,4\text{-benzenedicarboxylate})_3$	Rigid	Structural Studies, API Targeted Release	[332]
IRMOF-3	$Zn_4O(2\text{-amino-}1,4\text{-benzenedicarboxylate})_3$	Rigid	Structural Studies, API Targeted Release	[332]
IRMOF-8	$Zn_4O(2,6\text{-naphthalenedicarboxylate})_3$	Rigid	Structural Studies, API Targeted Release	[332]
IRMOF-10	$Zn_4O(4,4'\text{-biphenyldicarboxylate})_3$	Rigid	Structural Studies, API Targeted Release	[332]
IRMOF-16	$Zn_4O(p\text{-terphenyldicarboxylate})_3$	Rigid	Structural Studies, API Targeted Release	[332]
JUK-8	$[Zn_2(4\text{-pyridilbenzene-}1,3\text{-dicarbohydrazide})_2(4,4'\text{-oxybis}(benzenedicarboxylate)_2]_n$	Framework Breathing in dia Network	Gas Adsorption	[196]
JUK-8F	$[Zn_2(4\text{-pyridilbenzene-}1,3\text{-dicarbo-}5\text{-fluorohydrazide})_2(4,4'\text{-oxybis}(benzenedicarboxylate)_2]_n$	Framework Breathing in dia Network	Structural Studies - Gas Adsorption	[197]
JUK-8Cl	$[Zn_2(4\text{-pyridilbenzene-}1,3\text{-dicarbo-}5\text{-chlorohydrazide})_2(4,4'\text{-oxybis}(benzenedicarboxylate)_2]_n$	Framework Breathing in dia Network	Structural Studies - Gas Adsorption	[197]
JUK-8Br	$[Zn_2(4\text{-pyridilbenzene-}1,3\text{-dicarbo-}5\text{-bromohydrazide})_2(4,4'\text{-oxybis}(benzenedicarboxylate)_2]_n$	Framework Breathing in dia Network	Structural Studies - Gas Adsorption	[197]
JUK-8I	$[Zn_2(4\text{-pyridilbenzene-}1,3\text{-dicarbo-}5\text{-iodohydrazide})_2(4,4'\text{-oxybis}(benzenedicarboxylate)_2]_n$	Framework Breathing in dia Network	Structural Studies- Gas adsorption	[197]
MOF-1	$[Zn_2(DPT)_2(BIPY)]_n$	Framework Breathing	Gas adsorption - Structural Studies	[220]
MOF-2-Zn	$[[Zn_2(BPT)(2,5\text{-thiophenedicarboxylate})_2]\cdot 2(DMF)]_n$	Pillar Tilting	CO_2 Adsorption Studies, Solvent Exchange Flexibility	[87]
MOF-508	$[Zn_2(1,4\text{-benzenedicarboxylate})_2(4,4'\text{-BIPY})]_n$	Pillar Tilting	Gas-Chromatographic Separation of Alkanes	[218]
MRT-3	$\{[Zn(BPDC)(4\text{-BPMHZ})]\cdot(MeOH)\cdot 0.5(H2O)\}_n$	Breathing Behavior and Plane Sliding	Structural Studies	[192]
SNU-9	$[Zn_2(BPnDC)_2(BIPY)]$	Framework Breathing	Structural Studies - Gas adsorption	[224]
PCP-NH2-bdc	$[Zn_2(NH_2\text{-BDC})_2(BIPY)]_n$	Pillar Tilting	Gas adsorption	[217]
PTA-DMF	$[Zn_2(PdTCPP)(Bpa)]\cdot DMF$	Guest Mediated Flexibility	Adsorption of n-hexane	[258]
PUM168	$[Zn_3(N,N'\text{-}(1,1'\text{-biphenyl})\text{-}4,4'\text{-diylbis-}4\text{-pyridinecarboxamide})_{1.5}(4,4'\text{-biphenyldicarboxylate})_3(DMF)]_n$	Pillar tilting	API Encapsulation and Controlled Release, Structure Determination of Small Molecules	[308][309][310] [311] [312,313]
PUM210	$[Zn_4(N,N'\text{-}(1,1'\text{-biphenyl})\text{-}4,4'\text{-diylbis-}4\text{-pyridinecarboxamide})_{1.5}(2,6\text{-naphthalenedicarboxylate})_4\cdot(H_2O)]_n$	Framework rigidity	Solid-phase microextraction of aromatics	[254,255,311,313]
PUM210F	$[Zn_3(N,N'\text{-(perfluoro-}1,1'\text{-biphenyl-}4,4'\text{-diyl)diisonicotinamide})(2,6\text{-naphthalenedicarboxylate})_3(DMF)]_n$	Breathing Behavior and Plane Sliding	Gas Adsorption	[255]
UCLA-Ph	$[Zn_2(triptycene\text{-}9,10\text{-dicarboxylate})_2(1,4\text{-bis}(4\text{-pyridylethynyl})benzene)]_2(DMF)_5$	Ligand Rotation and Torsion	Molecular Switches	[213]
UCLA-R1	$[Zn_2(1,4\text{-benzenedicarboxylate})_2(9,10\text{-bis}(4\text{-pyridylethynyl})triptycene)]_2(DMF)_5$	Ligand Rotation and Torsion	Molecular Switches	[212]
UCLA-R2	$[Zn_2(4,4'\text{-biphenyldicarboxylate})_2(9,10\text{-bis}(4\text{-pyridylethynyl})triptycene)]_2(DMF)_5$	Ligand Rotation and Torsion	Molecular Switches	[212]
UCLA-R3	$[Zn_2(triptycene\text{-}9,10\text{-dicarboxylate})_2(9,10\text{-bis}(4\text{-pyridylethynyl})triptycene)]_2(DMF)_5$	Ligand Rotation and Torsion	Molecular Switches	[212]

(*continued on next page*)

Table 1 (*continued*)

Shorthand Name	Chemical Formula	Type of Flexibility	Application	Citation
UCLA-Tp	$[Zn_2$(triptycene-9,10-dicarboxylate)$_2$(9,10-bis(4-pyridylethynyl) triptycene)$]_2(DMF)_5$	Ligand Rotation and Torsion	Molecular switches	[213]
UTSA-300-Zn	$[Zn(4,4'$-dipyridylsulfide$)_2(SiF_6)]_n$	Rigid	Acetylene/Ethylene Separation	[250]
YO-MOF	$[Zn_2(4,4',4'',4'''$-benzene-1,2,4,5-tetrayltetrabenzoic acid$)(N,N'$-di-(4-pyridyl)-1,4,5,8-naphthalenetetracarboxydiimide$)]_n$	Network Displacement	Structural Studies - Gas Adsorption	[226]
X-pcu-3-Zn	$[Zn_2(4,4'$-biphenyldicarboxylate$)_2$(1,4-bis(4-pyridyl)benzene$)]_n$	Framework Breathing	Gas Adsorption	[221] [222]
X-pcu-5-Zn	$[Zn_2(4,4'$-biphenyldicarboxylate$)_2$(DPE$)]_n$	Framework Breathing	Gas Adsorption	[221] [222]
X-pcu-6-Zn	$[Zn_2(4,4'$-biphenyldicarboxylate$)_2$(1,2-bis(4-pyridyl)ethane$)]_n$	Framework Breathing	Gas Adsorption	[221] [222]
X-pcu-7-Zn	$[Zn_2(4,4'$-biphenyldicarboxylate$)_2$(1,2-bis(4-pyridyl)acetylene$)]_n$	Framework Breathing	Gas Adsorption	[221] [222]
X-pcu-8-Zn	$[Zn_2(4,4'$-biphenyldicarboxylate$)_2(4,4'$-azopyridine$)]_n$	Framework Breathing	Gas Adsorption	[221] [222]
ZIF-8	Zeolitic Imidazolate Framework-8	Rigid	Membrane Preparation	[247]
Zn-BDC	$[Zn(BDC)(H2O)\cdot DMF]_n$	Plane Sliding	Separation of C6 Hydrocarbons	[257]
Zn-BDC-NH2	$[Zn(BDC\text{-}NH_2)(H_2O)\cdot DMF]n$	Plane Sliding	Activity against *E. coli* in Combination with Thymol	[305]
ZJNU-406	$\{[Zn_2(TPTA)]\cdot 2DMA\}$	Rigid	Separation of Acetylene from CO_2 and Methane	[251]
ZJNU-407	$[Zn_4(TPTA)(BDC\text{-}F)(OH)_2]\cdot 0.5DMF\cdot H_2O$	Rigid	Separation of Acetylene from CO_2 and Methane	[251]
ZJNU-408	$[Zn_4(TPTA)_2(BDC\text{-}F)(CH_3NH_3)_2]\cdot 5NMF\cdot 3EtOH$	rigid	Separation of Acetylene from CO_2 and Methane	[251]
N/A	$[Zn$(1,4-benzenedicarboxylate)(1,4-di(1H-imidazol-4-yl)benzene$)]_n$ series	Framework Breathing in dia Network	Structural Studies	[198]
N/A	[Zn(1,2-bis(4-pyridyl)ethene)(BDC)]·DMF	[2 + 2] Cyclization Reactions	Structural Studies - Intraframe reactions	[233]
N/A	[Zn-(1,2-bis(4-pyridyl)ethene)(fum)]·H_2O	[2 + 2] Cyclization Reactions	Structural Studies - Intraframe reactions	[233]
N/A	[Zn(1,2-bis(4-pyridyl)ethene)(muco)]·DMF·H_2O	[2 + 2] Cyclization Reactions	Structural Studies - Intraframe reactions	[233]
N/A	$[Zn$(2,5-bromo-1,4-benzenedicarboxylate$)_2$(DABCO$)]_n$	Guest Mediated flexibility	C1-C3 Alkane Mixture Separation	[253]
N/A	[Zn(4,4'-(4,4,5,5,6,6-hexafluoro-9a,9b-dimethyl-5,6,9a,9b-tetrahydro-4H-indeno[5,4-b:6,7-b']dithiophene-2,8-diyl)dipyridine)(BPDC)·solvents]	Photo-Induced Isomerization	CO_2 Adsorption Mediated by Photoswitching	[259]
N/A	$[Zn(\mu_2$-isophthalate$)(\mu_2$–1,2-bis(4-pyridyl)ethane$)]_n$·nDMF	Interbilayer Separation in sql Network	Structural Studies	[144]
N/A	$[Zn(\mu_2$–5-methoxyisophthalate$)(\mu_2$–1,2-bis(4-pyridyl)ethane$)]_n$	Interbilayer Separation in sql Network	Structural Studies	[144]
N/A	[Zn((E)-5-(phenyldiazenyl)isophthalate)(1,2-bis(pyridin-4-yl) hydrazine)]$_n$	Interbilayer Separation in sql Network	Gas Adsorption - Structural Studies	[202]
N/A	[Zn((E)-5-((2,4-dimethylphenyl)diazenyl)isophthalate)(1,2-bis(pyridin-4-yl)hydrazine)]$_n$	Interbilayer Separation in sql Network	Gas Adsorption - Structural Studies	[202]
N/A	[Zn(5-(tert-butyl)isophthalate)(1,2-bis(pyridin-4-yl)hydrazine)]$_n$	Interbilayer Separation in sql Network	Gas Adsorption - Structural Studies	[202]
N/A	$[Zn_2$(1,4-benzenedicarboxylate$)_2$(1,2-bipyridylethene$)]_n$	Guest Mediated Flexibility	Detection of Nitro-Containing Compounds	[264]
N/A	$[Zn_2$(1,4-benzenedicarboxylate$)_2$(dipyridyl naphthalenediimide$)]_n$	Guest Mediated Flexibility	Detection of Small Aromatic Compounds	[265]
N/A	$[Zn_2$(1,4-benzenedicarboxylate$)_2$(triethylenediamine$)]_n$	Breathing Behavior and Plane Sliding	Gas Detection - CO_2 Adsorption	[266]
N/A	$[Zn_2(4,4'$-oxybis(benzoate$))_2(4,4'$-bipyridine$)]_n$	Guest Mediated Flexibility	Removal of Nitro-Containing Compounds	[263]
N/A	$[Zn_2$(aminotriazole$)_2$oxalate$]_n$	Guest Mediated Flexibility	Separation of Ethylene/Acetylene Mixture	[256]
N/A	$\{[Zn(AZPY)_{0.5}(GLUT)(H_2O)]\cdot(AZPY)_{0.5}\}_n$	Rigid	Water Stability – H_2 Adsorption	[228]
N/A	$\{[Zn(MEAZPY)_{0.5}(GLUT)(H_2O)]\cdot(H_2O)_2\}_n$	Rigid	Water Stability – H_2 Adsorption	[228]
N/A	$\{[Zn_2(bpp)_2(bdc)_2]\cdot 4DMF\cdot 4H_2O\}_n$	Ligand Distortion	Photoluminescence Properties	[194]
N/A	{[Zn2(bpp)2(bdc)2]·4DMA·6H2O}n	Ligand Distortion	Photoluminescence Properties	[194]
N/A	$\{[Zn(bpp)(obc)]\cdot 3H_2O\}_n$	Ligand Distortion	Structural Studies - Solvent Exchange	[195]
N/A	$\{[Zn_3(bpp)_3(obc)_3]\cdot 2DMF\cdot 4H_2O\}_n$	Ligand Distortion	Structural Studies - Solvent Exchange	[195]
N/A	$\{[Zn(bipy)(1,4\text{-}ndc)(H_2O)_2]\cdot 2H_2O\}$	Ligand Distortion	Gas Adsorption	[88]
N/A	$\{[Zn(bpe)(1,4\text{-}ndc)]_2\cdot 2DMF\}$	Ligand Distortion	Gas Adsorption	[88]
N/A	$\{[Zn(bpee)(1,4\text{-}ndc)]_2\cdot 2DMF\}$	Ligand Distortion	Gas Adsorption	[88]
2-bpe	$[Zn_2(\mu_4$-succinate$)(\mu_3$-succinate$)(\mu_2$-bpe$)]\cdot(H_2O)_{4.5}$	Ligand Distortion	Gas Adsorption	[190]

(*continued on next page*)

Table 1 (*continued*)

Shorthand Name	Chemical Formula	Type of Flexibility	Application	Citation
3-bpe	[Zn(μ_2-fumarate)(μ_2-bpe)]·(H_2O)$_{0.5}$(DMF)	Ligand Distortion	Gas Adsorption - Iodine Adsorption	[190]
5-bpe	[Zn(μ_4-adipate)$_{0.5}$(μ_2-adipate)$_{0.5}$(μ_2-bpe)]·(H_2O)	Ligand Distortion	Gas Adsorption	[190]
6-bpe	[Zn(μ_2-muconate)(μ_2-bpe)]·(H_2O)$_2$(DEF)	Ligand Distortion Framework	Gas Adsorption - Iodine Adsorption	[190]
1	([Zn(4-(3,5-dimethyl-1H-pyrazol-4-yl) benzoate)$_2$]$_n$	Breathing in dia Network Framework	Structural Studies - Gas Adsorption	[199]
2	([Zn(4-(3,5-dimethyl-1H-pyrazol-4-yl) benzoate)$_2$]$_n$	Breathing in dia Network	Structural Studies - Gas Adsorptiom	[199]
3	([Zn(4-(3,5-dimethyl-1H-pyrazol-4-yl) benzoate)$_2$]$_n$	Non-flexible and Non-porous Framework	Structural Studies - Gas adsorption	[199]
N/A	Zn(trans-2-(4-pyridyl)-4-vinylbenzoate)$_2$]$_n$·DMF	Breathing in dia Network	Second Harmonic Generation for NLO Devices - Structural Studies	[200]

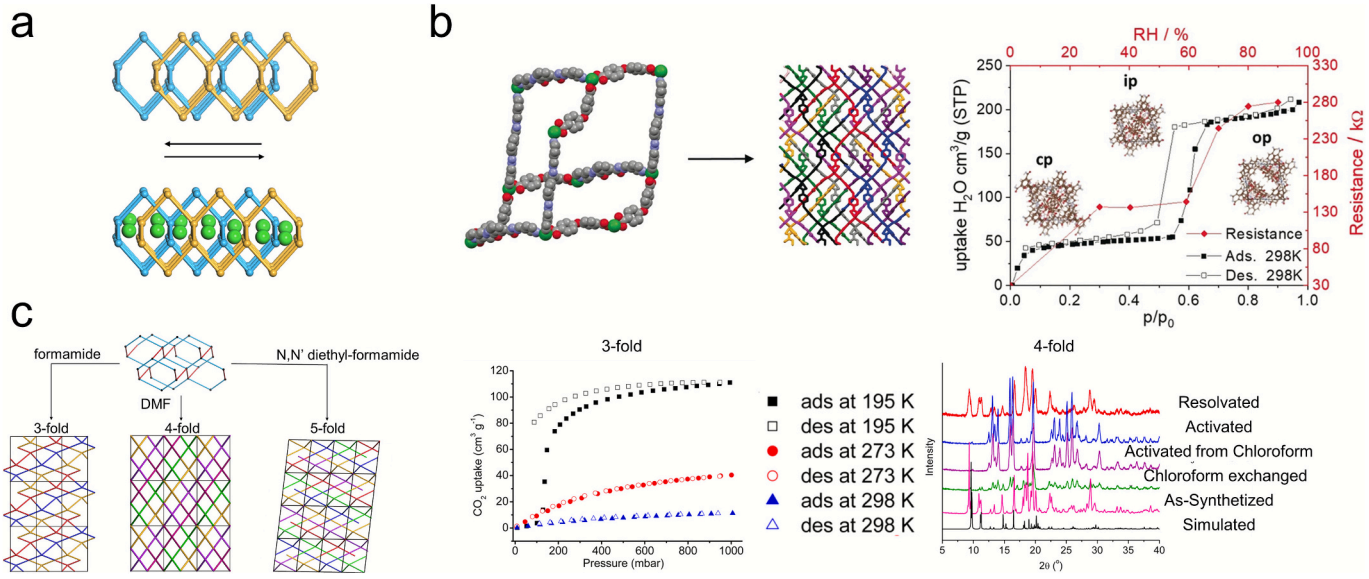


Fig. 4. a) Schematic representation of framework breathing in **dia** frameworks. Guest molecules are schematized as green spheres. b) *left*, **JUK-8** framework representation. One net on the left and cell content on the right. *Right*, H_2O isotherm of the framework, highlighting the closed-pore phase and its transitions to the intermediate-pore and open-pore phases. Reprinted with permission from [197]. c) representation of the behavior of the series of [Zn(terephthalate)(1,4-Di(1H-imidazol-4-yl)benzene)]$_n$ frameworks. *Left*, schematic representation of how a different solvent induces a different degree of interpenetration in the structure. *Middle*, CO_2 adsorption isotherms of the 3-fold interpenetrated network displaying gate-opening events. *Right*, adaptive behavior of the 4-fold interpenetrated network upon the adsorption of different solvents. Reproduced with permission from [198]. (For interpretation of the references to colour in this figure legend, the reader is referred to the web version of this article.)

first forming the intermediate-pore phase followed by expansion to the open-pore phase. The material also exhibits remarkable stability and reversibility upon repeated adsorption and desorption cycles.

The flexibility of **JUK-8** has been further explored and modulated in the **JUK-8**× series, where halogen substituents (F, Cl, Br, I) were introduced to the dicarboxylate linker. [197] Interestingly, while fluorine or chlorine functionalization did not significantly alter the maximum molar CO_2 uptake compared to **JUK-8**, larger bromine or iodine atoms counter-intuitively increased this uptake by 59 % and 48 % respectively. This enhanced uptake is attributed to the formation of an "extended pore" phase for **JUK-8Br**, characterized by a 38.1 % unit cell volume expansion. The adsorption mechanism also varied: while **JUK-8** and most **JUK-8**× (X = Cl, Br, I) derivatives followed a closed-pore → intermediate-pore → open-pore pathway, **JUK-8F** exhibited a direct closed-pore → open-pore transformation, bypassing the intermediate phase due to enhanced halogen-oxygen and carbon-fluorine interactions within its closed-pore structure, which "freeze" framework deformations at low pressures.

While in specific cases interpenetration permits dynamic behaviors by opposing the collapse of the framework, intuitively framework breathing should be hindered by the degree of interpenetration, the neighboring networks contrasting the expansion of any single one. This is remarkably illustrated by a series of [Zn(1,4-benzenedicarboxylate)(1,4-di(1H-imidazol-4-yl)benzene)]$_n$ frameworks, in which the degree of interpenetration was controlled through accurate choice of the solvent during synthesis and was found to influence framework flexibility (Fig.4, c). [198] The 3-fold interpenetrated **dia** network, displayed a CO_2 gate-opening pressure at 0.13 bar, indicating flexibility. The 4-fold interpenetrated network exhibited reversible structural transformations during activation and resolvation cycles. In contrast, the 5-fold interpenetrated network proved robust with no significant structural flexibility upon solvent exchange. Further insights into the subtle nature of flexibility in **dia** MOFs come from studies on interpenetration-direction isomerism. Three isomeric Zn(II) **dia** frameworks, **1**, **2**, and **3** ([Zn(4-(3,5-dimethyl-1H-pyrazol-4-yl).

benzoate)$_2$]$_n$), despite sharing the same 4-fold interpenetrated entanglement, exhibited drastically different pore features, framework flexibilities, and sorption behaviors due to their distinct polarity

arrangements and the shape-asymmetry of the ligand. [199] For instance, compound **1**, with parallel interpenetration, had isolated pores and, after desolvation, showed significant shrinkage and became highly selective for CO_2 over N_2. Its CO_2 adsorption was a two-step process, with structural expansion occurring at higher pressures. Compound **2**, with an orthogonal arrangement, possessed a continuous 3D channel system and exhibited a three-step adsorption for both N_2 and CO_2, indicating a more accessible pore network. Notably, the desolvated phase of compound **2** showed an initial shrinkage upon CO_2 adsorption at low loadings, before subsequent expansion. Compound **3**, with an anti-parallel arrangement, was nonporous.

Lastly, a remarkable example of transformation in **dia** MOFs is the single-crystal-to-single-crystal transformation of [Zn(trans-2-(4-.

pyridyl)-4-vinylbenzoate)$_2$]$_n$·DMF, a 7-fold interpenetrated MOF, to an 8-fold interpenetrated one, upon the loss of DMF. [200] This transformation involves alternating diamondoid fragments from adjacent structures moving toward each other to fill voids, which necessitates the breaking and reforming of Zn(II)-ligand bonds. This process resulted in a significant decrease in cell volume. In contrast, a similar Cu(II) analogue did not undergo such a structural change, emphasizing that not all isostructural **dia** MOFs display similar flexibility.

2.1.3. *Interbilayer separation in sql networks*

Inter-network displacement is a rarely described phenomenon in which **sql**-interwoven structures can subtly shift relative to each other, altering the accessible pore space in a manner similar to clay intercalation of guests (Fig. 5, a). [201] A compelling illustration of this phenomenon is observed in the pair of isoreticular, 2-periodic Zn(II)-based

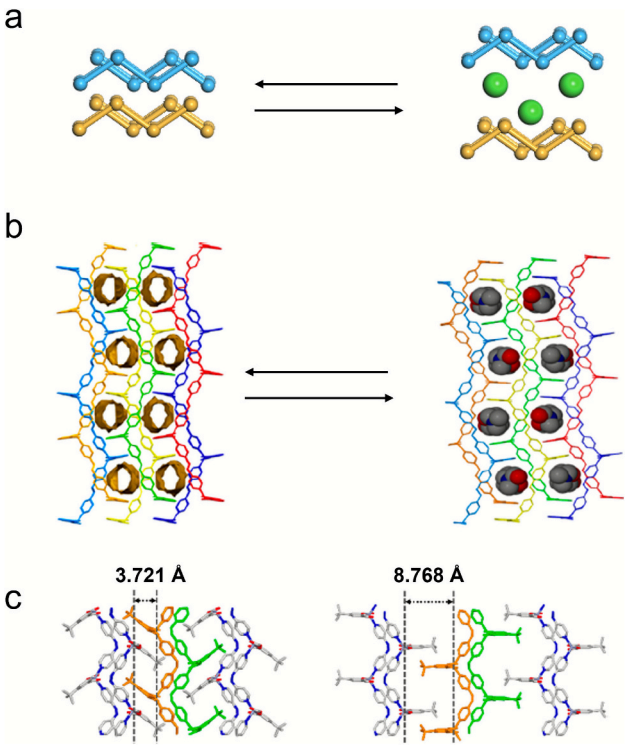


Fig. 5. a) Schematic representation of interbilayer separation in **sql** frameworks. Guest molecules are schematized as green spheres. b) Crystal structure of the guest-free 2-periodic MOF described by Oliver et Al. and its as-synthetized, DMF-solvated phase. Channels in the structures are exemplified by solid yellow contours. Reprinted with permission from [144]. c) Similarly, narrow-pore phase and open phase of compound **4** as reported by Zaworotko et Al. Interbilayer separation in Ångstrom is reported near the structure and exemplified by dotted linea. Reproduced with permission from [202]. (For interpretation of the references to colour in this figure legend, the reader is referred to the web version of this article.)

mixed-ligand MOFs, [Zn(μ^2- isophthalate)(μ^2–1,2-bis(4-pyridyl)ethane)]$_n$·nDMF and [Zn(μ^2–5-methoxyisophthalate)(μ^2–1,2-bis(4-pyridyl)ethane)]$_n$ (Fig. 5, b). [144] These structures exhibit entanglement through the interpenetration of neighboring frameworks, forming a two-dimensional interdigitated bilayer. Activated samples of these MOFs, once desolvated, demonstrate distinct changes in their pore volumes and unit cell axes when subjected to hydration, especially in the axis parallel to bilayer stacking. The observed differences in pore volumes and unit cell axes during solvent exchange and desolvation are not merely localized breathing but involve a change in the overall arrangement of these bilayers. This separation effectively represents a concerted shift and sliding of the interpenetrating networks relative to each other, optimizing the void space for guest accommodation. The authors suggest that the differing degrees of this displacement between [Zn(μ^2- isophthalate)(μ^2–1,2-bis(4-pyridyl)ethane)]$_n$·nDMF and [Zn(μ^2–5-methoxyisophthalate)(μ^2–1,2-bis(4-pyridyl)ethane)]$_n$, is influenced by the methoxy group in the latter that retards the separation of bilayers, further underscoring the complexity of this dynamic mode. Zaworotko et Al. [202] introduced three novel MOFs capable of undergoing such transformation in which the effect of the substituents on the carboxylate also influence the dynamic transformation (Fig. 5, c). The study examined a family of [Zn(5-R-isophthalate)(1,2-bis(pyridin-4-yl)hydrazine)]$_n$, where the nature of the pendent R group profoundly impacted their structural and gas sorption properties. [Zn(5-(*tert*-butyl)isophthalate)(1,2-bis(pyridin-4-yl)hydrazine)]$_n$, [Zn((*E*)-5-(phenyldiazenyl)isophthalate)(1,2-bis(pyridin-4-yl)hydrazine)]$_n$ and [Zn((*E*)-5-((2,4-dimethylphenyl)diazenyl)isophthalate)(1,2-bis(pyridin-4-yl)hydrazine)]$_n$ were identified as flexible networks, consistently demonstrating reversible transformations from small to large pore phases upon desolvation and subsequent gas sorption, a behavior not observed in the other compounds analyzed in the study. [Zn(5-(*tert*-butyl)isophthalate)(1,2-bis(pyridin-4-yl)hydrazine)]$_n$, featuring a short but bulky *tert*-butyl pendent group, exhibited flexibility primarily driven by interbilayer separation. Upon activation and guest inclusion, it demonstrated dramatic solvent-triggered phase changes, transitioning through three distinct phases: a low-porosity phase, an intermediate-porosity one, and a high-porosity phase. The interlayer distance significantly changed across these phases from 3.7 Å, expanding to 7.3 Å in, and even reaching 8.8 Å (Fig. 5, c). Structural analysis suggested that weaker noncovalent interactions ($\pi - \pi$, C-H···π, and C-H···O) between adjacent **sql** layers in the narrow-pore phase, characterized by longer average distances compared to rigid analogues, contributed to its guest-triggered interlayer motion. For [Zn((*E*)-5-((2,4-dimethylphenyl)diazenyl)isophthalate)(1,2-bis(pyridin-4-yl)hydrazine)]$_n$, structural changes involved a decrease in the perpendicular distance between **sql** planes upon activation, specifically from 8.7 Å in the open phase to 6.3 Å in the narrow-pore phase. This transformation was facilitated by the hinge-like motion of the pendent isophthalate moieties and an additional twisting of the isophthalate ligand around the azo bond, which introduced another source of flexibility. CO_2 sorption displayed "closed-to-open" switching isotherm. CO_2 sorption isotherm of [Zn((*E*)-5-(phenyldiazenyl)isophthalate)(1,2-bis(pyridin-4-yl)hydrazine)]$_n$ showed an "open-to-more open" step, suggesting that, differently from the other two MOFs, some porosity was maintained in its narrow-pore phase even after activation. In essence, the study demonstrates that the systematic modification of pendent groups can be used to harness flexibility in **sql** MOFs.

2.2. *Pillared mixed-ligand Zn MOFs*

Among the material classes highlighted in this review, pillared Zn(II) MOFs are by far the most studied in terms of frameworks dynamics and adaptability. [203–206] This is undoubtedly due to the vast number of possible dynamic modes that the framework can undergo without compromising the overall material's crystallinity. [207,208] The orthogonality of the two ligand functionalities, in tandem with the

known methods to control interpenetration, often provide MOFs with available free space around the ligands that can prompt rotational and motional freedom. [90] The resulting materials might then possess freely rotating ligands to be used as molecular rotors to be applied in sensing. [209] At the same time, the overall framework is able to respond to guest uptake and removal thanks to two main dynamic modes. The first one involves the pillaring ligand that can bend around their coordination axis producing "closed" and "open" materials able to efficiently trap guests. [88] The second, in case of interpenetrated structures and particularly prominent in two-fold interpenetrated ones, involves the relative slippage of the two nets along the pillaring direction, opening or closing additional channels and providing new gate opening events associated with the entire framework readjustment. [8] The presence or co-presence of these modes depends massively on the functional groups attached to the ligands and the strength of their interactions with the second net, as well as the specific interaction held between the framework and their guests.

2.2.1. *Ligand rotation and torsion*

Zn pillared-MOFs are known to allow for ligand rotations and torsions, the magnitude of those can be usually triggered and controlled by external stimuli such as temperature or guest sorption. This behavior is particularly noticeable for the pillaring ligands decorating the directional channels of this MOF class, in which the Zn metal atoms act as stators (Fig. 6, a). [209] Depending on the nature of the pillaring ligand, its rotational and torsional energetic barriers and their steric hindrance and chemical functionalities, the motion of the rotor can be free, in that differing pillaring ligands cannot interact with one another. [210] On the contrary, especially if the carboxylic acid employed to construct the layers is short enough to allow for some interaction between neighboring pillars, their motion can be concerted, with the extreme cases of cascade dynamics in which the rotation of a single rotor triggers the rotation of all following ones. [8] We note here that, despite the length of the carboxylic acid, concerted motion can also be present when interpenetration prompts the vicinity of pillaring ligands owning to different nets. [211]

A prototypical example of this behavior is given by Garcia-Garibay and co-workers. [212] Their tryptycene-based 9,10-bis-(pyridylethynyl)-triptycene pillar linker can be employed to build a variety of isoreticular pillared MOFs employing different carboxylic acid linkers, including terephthalate (**UCLA-R1**), biphenyl-4,4′-dicarboxylate (**UCLA-R2**), and triptycene-9,10-dicarboxylate (**UCLA-R3**)(Fig. 6, b). In theory, all three nets may possess the necessary chemical requirements to rotate around the Zn—Zn coordination axis. However, thanks to the two-fold and four-fold polycatenation of **UCLA-R1** and **UCLA-R2**, respectively, the rotor does not display any significant motion. In contrast, the noncatenated **UCLA-R3** displays low rotational barriers of about 13.5 kcal/mol. It follows that limiting the space for rotor motion is a prime strategy to control the dynamic behavior of these compounds. In a subsequent paper, Garcia-Garibay and co-workers also demonstrated that rotor dynamic can be modulated by other factors such as guest inclusion. [213] In this work, two different rotors were considered: a triptycene-based one and a phenylene-based one. Changing guest molecules inside the channels by means of solvent exchange had dramatically different effects on the two rotors. The triptycene rotor (in **UCLA-Tp**) displayed solvent-independent rotational symmetry but with activation parameters that varied significantly from solvent to solvent. Instead, the more compact phenylene rotator (in **UCLA-Ph**) exhibited rotational trajectories and dynamic modes that varied by solvent but showed relatively low and constant apparent activation energies. This suggests "slip" behavior, where the phenylene rotator can undergo relatively independent rotation and slip past neighboring solvent molecules.

A second known case is the motorized-MOFs by Feringa et Al., in which the overcrowded alkene-based dipyridyl pillar employed retains its unhindered 360° motion thanks to the free space available in the

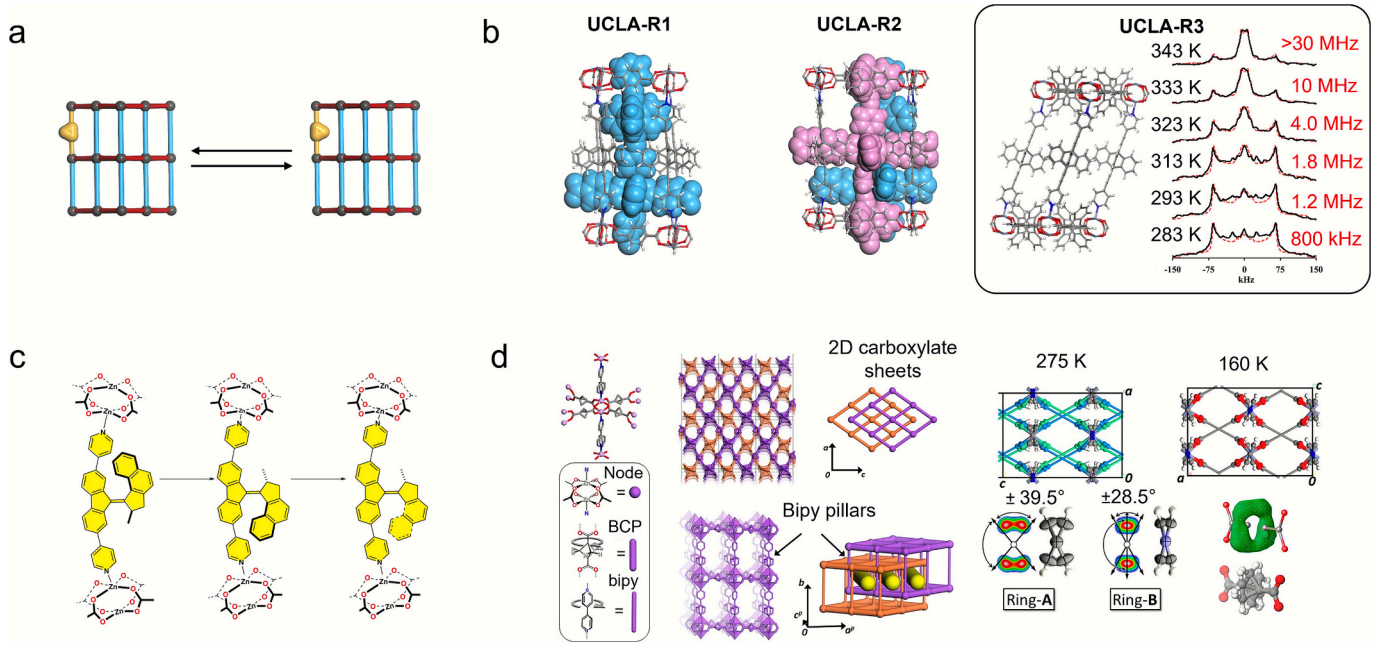


Fig. 6. a) Schematic representation of a pillar ligand tilting in response to a generic stimulus in pillared frameworks. b) Representation of the interpenetration of UCLA series and the relative mobility of the triptycene-based pillared frameworks. **UCLA-R1** and **UCLA-R2** are static as interpenetrated nets (in light blue and pink) hamper their movement, **UCLA-R3**, non-interpenetrated, presents free motion of the ligand as revealed from NMR analysis displayed in the inlet. Reproduced with permission from [212]. c) Graphical representation of an overcrowded alkene-based dipyridyl pillar highlighting the free space induced by the pillared framework structure and its subsequent unidirectional unhinged motion. Reprinted with permission from [214]. d) Representation of the structure of **FTR-P1** (left) and of the crystallographic information retrievable from the structure about the formation of the pillaring ligand (disorder at higher temperatures) and the dicarboxylic one (smeared electron density in the direction of rotation). Reproduced with permission from [211]. (For interpretation of the references to colour in this figure legend, the reader is referred to the web version of this article.)

structure (Fig. 6, c). [214] In a subsequent work, authors were also able to trigger the rotor dynamic by employing a photosensitizer as the porphyrin-containing tetracarboxylic acid constructing the layers, achieving rotary speeds of these rotors similar to those observed in solution. [215]

Comotti et Al. provides compelling examples on how temperature and gas sorption can trigger or hinder the dynamical response of molecular rotors embedded in MOFs. For example, in [Zn(bicyclo[1.1.1]pentane dicarboxylic)$_2$(bipyridine)], **FTR—P1**, the bipyridyl pillaring ligand spins over its axis only with temperatures above 200 K. Below these temperature, PXRD, SC-XRD, SS-NMR and computational analysis reveal a less disordered phase in which the pillaring ligand is static (Fig. 6, d). [211]

In the same work, dicarboxylate acids-based molecular rotors are also studied extensively. In Comotti's work, the dynamics of BCP (bicyclo[1.1.1]pentane-dicarboxylate) molecules within Zn-based MOFs center around their role as ultra-fast rotors. In this material, BCP rotors spin at frequencies up to 10^7 Hz even at cryogenic temperatures, thanks to their extremely low activation energy. [211]

The dynamics are not just fast, they're also complex and temperature dependent. Comotti's studies show a cascade of motions unfolding at different thermal thresholds, with individual rotors activating sequentially in conrotary and disrotary patterns. Variable-temperature solid-state NMR and X-ray diffraction studies reveal how these motions evolve and interact. Intriguingly, external stimuli such as CO_2 gas can influence the system. When CO_2 diffuses into the porous framework, it affects rotor dynamics by modifying the ordering and energy barriers within the structure. Additionally, in similar frameworks constituted by the same BCP dicarboxylate acid and 4,4′-1,2-diazenediylbispyridine as a pillaring ligand, the insertion of iodine into the channels provided an increased mobility of the rotors. The shifting of the interpenetrated frameworks pushed closer different BCP units, then destabilized by the rotation of its neighbors. For 4,4′-1,2-diazenediylbispyridine, the same network shift provided more available free space for the pyridyl rings to be able to rotate thanks to flipping (rotation of the ring around its axis) and crank-like (swinging of the azo- group) motion. [210]

Besides BCP, a number of dicarboxylate linkers have been studied as potential rotors. Among them, we cite terephtalic acid and its fluorinated or methylated substituents, and 1,4-naphthalenedicarboxylic acid. An interesting example of such analysis is given by Garcia-Garibay, proving that 2,3-difluorophenylene dicarboxylic acid ligand presents a lower rotation barrier compared to its non-fluorinated counterpart. This is achieved by virtue of the steric and electrostatic interactions between the aryl substituents and the carboxylate oxygens. [216]

2.2.2. *Pillar tilting*

Beyond simple rotation, paddlewheel MOFs are known to undergo "breathing" or gate-opening transitions, especially when the framework integrates flexible linkers such as bipyridyl-based systems. These transitions involve collective movements of the framework units. While these effects are usually referred to as "breathing effects", they encompass a few different dynamic modes that can occur individually or in tandem, depending on the relative flexibility of different parts of the structure. Hence, we considered to discuss them separately.

Framework tilting, as a broader outcome of these internal distortions, involves the macroscopic rearrangement, shifting, or relative movement of MOF layers or interpenetrated networks (Fig. 7, a). In some MOFs, 2D layers can shift reciprocally along a crystallographic direction, driving the tilting of pillar ligands and reducing interlayer distances in a single net. While an idealized, schematic representation of a paddlewheel MOF has its pillaring ligands orthogonal to the carboxylate layers, noncovalent interaction between interpenetrated frameworks and between the framework and solvated guest molecules create a "push-and-pull" dynamic effect in which the pillaring ligand can experience dramatic restructuring. In the most clear cases of pillar tilting, the system may switch between two different "closed" and "open" states, as in **PCP-NH2-bdc** (NH2-BDC = 2-amino-1,4-benzenedicarboxylate), an interpenetrated framework $[Zn_2(NH_2\text{-}BDC)_2(BIPY)]_n$. [217] **PCP-NH2-bdc** exists in two primary structural phases: an open-phase and a dense-phase (Fig. 7, b). The as-synthesized material is characterized by its open-phase structure, which consists of a twofold interpenetrated framework. In this arrangement, zinc paddlewheel nodes are bridged by **NH2-BDC** ligands in the equatorial plane and pillared by BIPY ligands in the apical positions, collectively forming accessible one-dimensional channels. When this material is activated by heating at 150 °C under vacuum to remove guest molecules, it transforms into a guest-free dense-phase. The transition from the open-phase to the dense-phase involves significant subnetwork distortion and displacement within the MOF. This structural rearrangement leads to a substantial decrease in the void volume, a 71 % reduction from 21.2 % in the open-phase to 6.1 % in the dense-phase. In an early work from Yaghi et Al., [218] the $[Zn_2(COO)_4]$

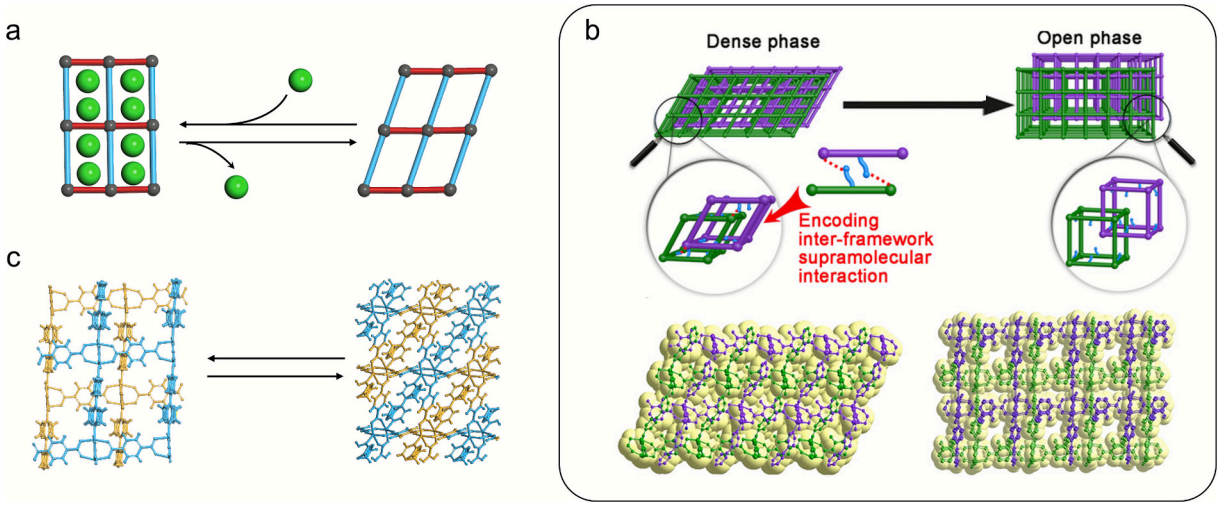


Fig. 7. a) Schematic representation of pillar tilting in pillared frameworks. Guest molecules are schematized as green spheres. b) *Above*, schematic representation of **PCP-NH2-bdc** in its dense and open phase triggered by guest uptake. The figure highlights the role of pending NH_2 groups in switching of the two structures. *Below*, crystal structures of the two phases. Reproduced with permission from [217]. c) Open-pore and closed-pore phases of **MOF-508**, highlighting how the tilting of the pillaring ligand induces the switch from a porous to nonporous phase, the tilting cascading a series of other structural shifts including orientation of the SBUs and angles between carboxylate ligands. (For interpretation of the references to colour in this figure legend, the reader is referred to the web version of this article.)

paddlewheel clusters of **MOF-508** [Zn_2(1,4-benzenedicarboxylate)$_2$(4,4'-BIPY)]$_n$ undergo significant distortion upon solvent removal, and the 4,4'-BIPY linkers become bent (Fig. 7, c). These internal structural changes lead to a considerable compression of the framework, resulting in a 16.7 % reduction in the volume per formula unit (from 410.7 Å^3 to 342.3 Å^3). The desolvated phase then presents as a dense framework with discrete 66 Å^3 voids and no permanent channels connecting them, effectively rendering it non-porous in this state. The process is fully reversible: **MOF-508** can be converted back to its open phase by soaking it in a DMF/ethanol solution. This demonstrates the dynamic behavior of the MOF in response to guest removal and re-inclusion. A milder example of the same phenomenon is given by Lahtinen et Al. [87] When the as-synthesized **MOF-2-Zn**, [[Zn_2(BPT)(2,5-thiophenedicarboxylate)$_2$]·2(dmf)]$_n$ (BPT = 4-amino-3,5-bis(4-pyridyl)-1,2,4-triazole) initially containing DMF, is exposed to different guest solvents like chloroform, its framework undergoes pronounced structural changes. Specifically, the BPT (4-amino-3,5-bis(4-pyridyl)-1,2,4-triazole) ligands, which act as pillars, adopt slightly different molecular conformations. This involves adjustments in the orientation of the NH_2-triazole core unit and tilting of the pyridyl groups. Quantitatively, the N – Zn···Zn – N torsion angles subtly deviate from linearity, and the Zn···Zn angles across the BPT direction show clear changes. While the pyridyl rings in the pristine **MOF-2-Zn** are almost perfectly aligned, in the chloroform-exchanged structure, they become strongly tilted in opposite directions. These pillar conformational changes, accompanied by subtle alterations in the metal-carboxylate bonding scheme, provoke a transformation in the shape of the channels, leading to the emergence of distinct rectangular-shaped channels.

2.2.3. *Framework breathing*

Another distinctive dynamic mode pillared MOFs can undertake when subject to external stimuli is the expansion or contraption of the square grid that composes the dicarboxylate layers. Especially visible in non-interpenetrated frameworks, the approximately square dicarboxylate grid might contract over one direction and extend in the other after the removal of solvent guest to increase the noncovalent interactions between dicarboxylate linkers (Fig. 8, a). Usually this process is reversible: when re-exposed to guest molecules, the now rhombus-shaped grid can return to its original square-like conformation. [219] This transformation can involve various mechanisms, including a direct phase change from a closed to an open structure, or a modification of the pore shape. For instance, from square to rhombic. The driving force for this effect can be the activation conditions, as seen in **MOF-1**, [Zn_2(DPT)$_2$(BIPY)]$_n$ (DPT = 2,5-diphenylbenzene-1,4-dicarboxylic acid) synthesized by Barbour et Al. [220]. This non-interpenetrated **MOF** also undergoes a phase transformation between 25 and 30 bar of CO_2 pressure, partially transforming from phase 1B (closed-pore) to 1C (as-synthesized-like) when activated by guest exchange or supercritical CO_2 drying, respectively. The MOF-1B also shows a distinct pressure-induced phase transitions during CO_2 sorption to MOF—1C, with gate-opening pressures influenced by temperature and exhibiting hysteresis upon desorption.

Some other examples include **X-pcu-3-Zn** ([Zn_2(4,4′-biphenyldicarboxylate)$_2$(1,4-bis(4-pyridyl)benzene)]$_n$), which exhibit reversible switching between closed (nonporous 'b' forms) and open (porous 'a' forms) phases. This leads to significant unit-cell-volume shrinkages when the material transforms from the open 'a' phase to the closed 'b' phase: approximately 33.6 % for **X-pcu-5-Zn** ([Zn_2(4,4′-biphenyldicarboxylate)$_2$(DPE)]$_n$), 31.9 % for **X-pcu-6-Zn** ([Zn_2(4,4′-biphenyldicarboxylate)$_2$(1,2-bis(4-pyridyl)ethane)]$_n$), 36.9 % for **X-pcu-7-Zn** ([Zn_2(4,4′-biphenyldicarboxylate)$_2$(1,2-bis(4-pyridyl)acetylene)]$_n$), and 38.2 % for **X-pcu-8-Zn** ([Zn_2(4,4′-biphenyldicarboxylate)$_2$(4,4′-azopyridine)]$_n$), all relative to their corresponding 'a' forms. The 'b' forms are nonporous. This structural change involves the bending of metal-

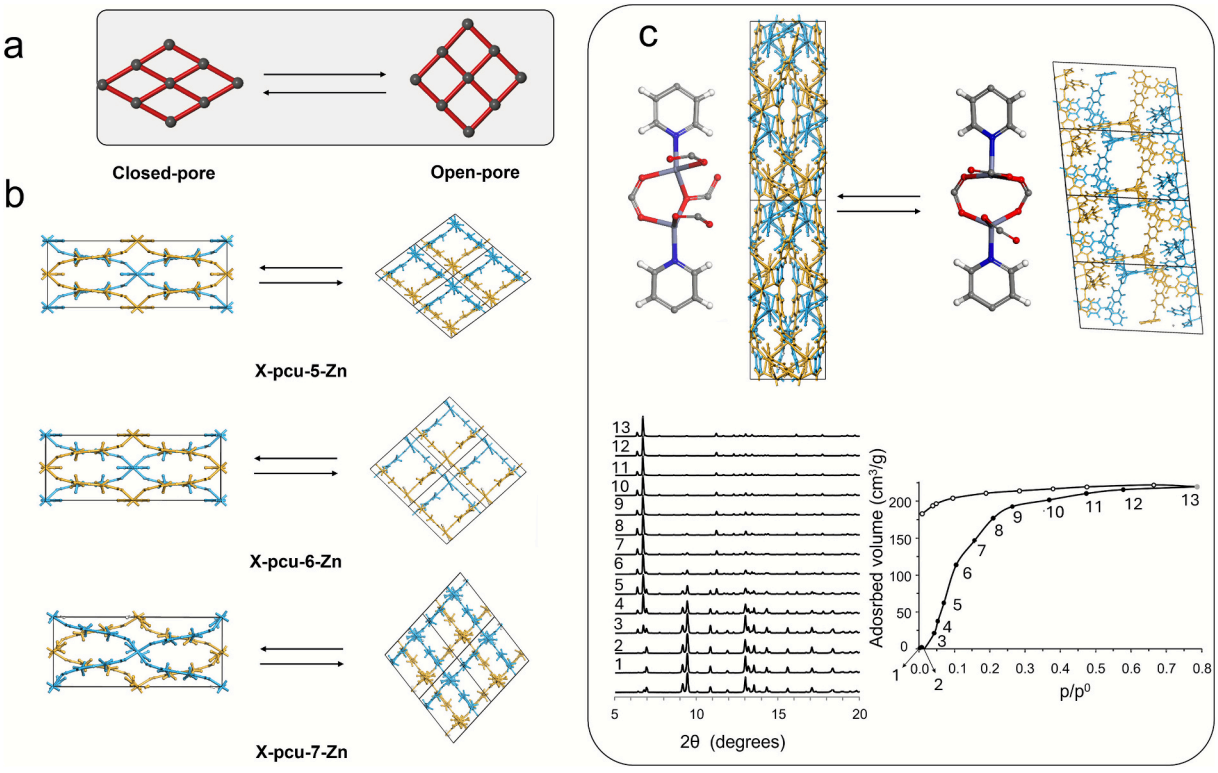


Fig. 8. a) Schematic representation of gate opening in pillared frameworks. b) closed- and open- frameworks of a family of two-fold interpenetrated structures of the series **X-pcu-N-Zn** upon gas sorption. c) closed- and open-pore frameworks of **SNU-9**, highlighting the rearrangement of the Zn—O bonds upon guest insertion. *Below,* variable pressure PXRDS and sorption isotherm of **SNU-9**, displaying a marked gate-opening event between p/p^0 0.43 and 0.53. Reproduced with permission from [224].

carboxylate junctions and rotation of organic linkers. The process of transforming between the open and closed forms is reversible. [221,222] In an important work by Kitagawa et Al. the structural dynamics of **f-MOF-1**, a twofold entangled MOF, in response to external stimuli like temperature, pressure, and guest molecules was investigated. [223] **f-MOF-1** is constructed using 1,4-naphthalenedicarboxylic acid (1,4-NDCH_2) and 1,2-bis-(4-pyridyl)ethane (BPE). The framework consists of [$Zn_2(COO)_4$] paddlewheel SBUs connected by 1,4-NDC to form a 2D grid, which are then pillared by BPE to create a 3D network. When **f-MOF-1** is air-dried, it transforms into a desolvated phase, **f-MOF-1a**. In this transformation, the square-shaped 2D net of [Zn_2(1,4-NDC)$_2$] in **f-MOF-1** is shifted into a rhombic 2D net in **f-MOF-1a**. This deformation of the 3D framework leads to a relative movement of the 3D interpenetrated nets with respect to each other, drastically reducing the void space to 2.4 %. Another desolvated phase, **f-MOF-1b**, is obtained by heating **f-MOF-1** under vacuum. Importantly, **f-MOF-1b** can transform into a structure very similar to the as-synthesized **f-MOF-1** upon CO_2 diffusion, signaling the reopening of the closed structure to an open one. The flexibility observed involves both local changes, such as the rotation of naphthalene and pyridyl rings, and global changes, including the distortion of the 3D nets. **SNU-9** ([Zn_2(BPnDC)$_2$(BIPY)]) features asymmetric paddlewheel SBUs where Zn atoms are coordinated by four carboxylic groups from benzophenone 4,4′-dicarboxylic acid (BPnDC) linkers. [224] The material contains two interpenetrated frameworks with **pcu** topology. Upon activation, the MOF undergoes a structural transformation involving rearrangement of Zn—O bonds (Fig. 8, c), which leads to a contraction of the unit cell along the b-axis and a decrease in unit cell volume of nearly 28 % compared to the as-made structure (from 10,182 Å^3 to 7334 Å^3). The solvent-accessible volume consequently shrinks from 40.8 % to 12.8 %. During CO_2 adsorption, the material transitions to the **CO_2@SNU-9** structure, which is similar to, but not identical with, the as-made phase. This involves an increase in channel size along the direction from 10.7 Å (evacuated phase) to 17.2 Å. For N_2 adsorption, the transformation from the narrow pore form to the open structure occurs quasi-in-one-step, and the resulting **N_2@SNU-9** structure is identical to that of the as-synthesized phase.

2.2.4. Network displacement

Subnetwork displacement is characteristic for 3D interpenetrated structures, which contain chemically non-interconnected frameworks interacting rather through weak forces. [225] The subnets can drift, relocate or shift in regards to each other upon external stimuli action (Fig. 9, a). Early findings of this phenomenon [226] in Zn-MOFs include **YO-MOF**, of formula [Zn_2(4,4′,4″,4‴-benzene-1,2,4,5-tetrayl-tetrabenzoic acid)(*N,N*′-di-(4-pyridyl)-1,4,5,8-naphthalenetetracarboxydiimide)], a twofold interpenetrated with pillared paddlewheel framework. The material displays hysteretic CO_2 uptake, suggesting dynamic structural behavior. While framework collapse is ruled out due to the tight interpenetration, and pillar rotation as a primary mechanism is unlikely, the interpenetrated frameworks are shown to move with respect to each other. Pair distribution function (PDF) analysis reveals that upon solvent removal, the frameworks undergo a torsional motion of a benzene ring of the bis pyridinic ligand. More significantly, simulations indicate that the observed changes in atomic-pair correlations at longer ranges are consistent with a conversion encompassing relative slippage of the two independent frameworks. This suggests that upon complete guest solvent removal, the frameworks shift toward each other to maximize van der Waals interactions. This inter-conversion dominates its dynamic behavior, with displacements occurring at the supramolecular and network level, leading to sizable changes in guest-accessible surface area. Similarly in Hupp [227] the enhanced hydrogen uptake by these materials is explained by a molecular-adsorbate-driven displacement of interwoven frameworks, leading to additional accessible surface area. The overall mechanism for enhanced uptake is identified as the favorable displacement of interwoven frameworks, rather than the creation of new adsorption sites. Moreover,

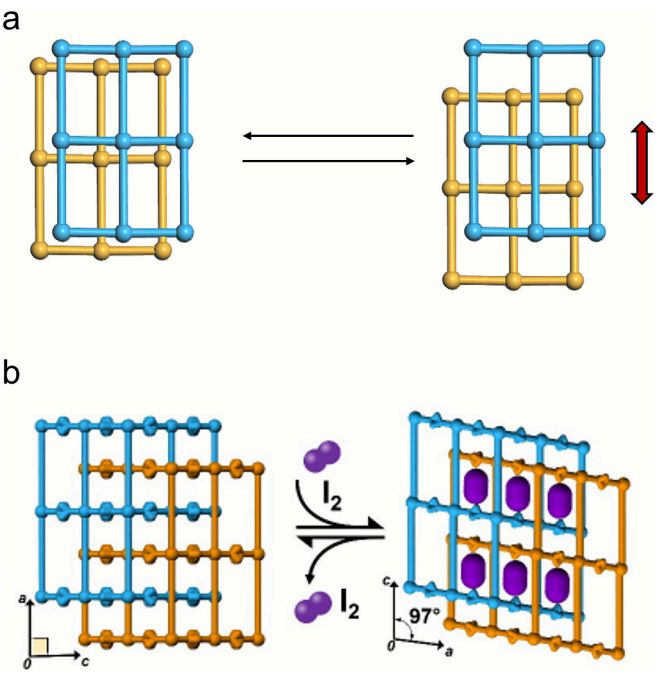


Fig. 9. a) Schematic representation of framework sliding in paddlewheel frameworks. b) Schematic representation of framework sliding in **FTR-P2** by the insertion and removal of I_2. The scheme also reports the change in the unit cell β angle derived from the concomitant pillar tilting in the framework, highlighting how flexibility modes appear *in tandem*, especially in this material class. Reproduced with permission from [210].

the abovementioned **f-MOF-1** [223] and **FTR-P2** [210], ([Zn(bicyclo [1.1.1]pentane dicarboxylic)$_2$(4,4′-azobipyridine)], the deformation of the 3D framework described directly leads to a relative movement of the 3D interpenetrated nets with respect to each other, significantly reducing the void space.

2.3. Doubly pillared mixed-ligand Zn MOFs

Double-pillared MOFs tend to be fairly rigid and display strong structural integrity. For instance, the MOFs described by Dey and colleagues, {[Zn(AZPY)$_{0.5}$(GLUT)(H$_2$O)]·(AZPY)$_{0.5}$}$_n$, {[Zn(MEAZPY)$_{0.5}$(GLUT)(H$_2$O)]·(H$_2$O)$_2$}$_n$, (where AZPY = *N,N*′-bis-pyridin-4-ylmethylene-hydrazine, MEAZPY = *N,N*′-bis-(1-pyridin-4-yl-ethylidene)-hydrazine, GLUT = disodium glutarate) are explicitly noted for their water stability, maintaining the same crystal structure after being activated, and possess good thermal stability up to 250 °C. [228] Similarly, ADES-1 and related compounds [Zn_2(5NO$_2$-IP)$_2$((*E*)-*N*′-(pyridin-3-ylmethylene)nicotinohydrazide))$_2$](H$_2$O)] $_n$ (5OH-IP = 5-nitro isophthalic acid), exhibit "good stability and reusability" in applications like dye adsorption, with framework structures preserving integrity post-adsorption and thermal stability up to around 330 °C. [229] This robustness stems from the intrinsic nature of the bridging ligands and the strong connectivity they establish between individual layers or chains within the framework. Mainly, the octahedral coordination environment of the metal imposes a more rigid arrangement of the pillars and carboxylate ligands, which are then energetically more confined to this position. However scarce, some works highlighting flexible modes of these Zn-MOFs can be found, mimicking the flexibility modes of Cd- or Co-MOFs. [162]

2.3.1. Pillar tilting and rotational dynamics

In double pillared MOFs, the SBU is inherently less flexible than paddlewheel owing to the pillar arrangement. Namely, the two neighboring pillars usually interact with each other due to noncovalent

interactions that limit the flexibility of the ligand over at least one of the two directions orthogonal to the pillaring direction (Fig. 10, a). As an example, the parent compound of the abovementioned **MOF-2-ZN** in Lahtinen et Al. does not display any significant change differently from the paddlewheel analogous. [87] Some authors have achieved some structural modifications in MOFs upon guest capture or removal. Kitagawa et Al. describe an unprecedented behavior in which BIPY ligands of the **CID** ("coordination polymers with an interdigitated structure", with general formula of [Zn(R-IP)(BIPY)], R-IP: differently substituted isophthalic acid) series are able to rotate and act like molecular rotors, allowing, in a "turnstile-fashion", guest molecules to be adsorbed. [230] Once CO_2 is adsorbed in the cavities at room temperature (when the rotors are actively rotating), the system can be subsequently cooled to lower temperatures between 195 K and 233 K, under vacuum. At these lower temperatures, the molecular rotors switch from their rotation to a static mode, effectively reducing the channel windows. This transition to immobility generates steric hindrance that effectively traps the CO_2 molecules within the cavities, preventing their desorption and diffusion even under vacuum or very low pressure (Fig. 10, c). This highlights a strategy where the dynamics of the rotors control the diffusion of CO_2 in the pores. Although not strictly a Zn-MOF, Chen et Al. were recently able to achieve a so-called "pendulum effect" by selective guest uptake in a double-pillared MOF Co(EDBA)(BIPY)]·DMF·H_2O (EDBA = 4,4′-(ethyne-1,2-diyl)dibenzoic acid (Fig. 10, b). This "pendulum effect" of the pillars is selectively induced by larger guest molecules like DMF (or DMA), through a steric hindrance effect. When loaded with DMF, the pillar inclined angle shifts from 67.0° (guest-free) to 100.4° (DMF-loaded), passing over the vertical angle of 90°. This allows the framework to accommodate larger guests by increasing pore height. These dynamic inversions, akin to pendulum behaviors, surmount high-energy intermediate states, leading to observable macroscopic crystal shape changes. The mechanism is supported by single-crystal X-ray diffraction, sorption measurements, and molecular simulations. [231]

2.3.2. *Breathing behavior and plane sliding*

Many of the observed MOFs are doubly interpenetrated, so the plane sliding effect should be prompted by gas adsorption. In practice, however, many of those materials do not display any plane sliding as a result of guest sorption/desorption. This is imputable to the peculiar framework channels generated by interpenetration. As specifically visible in, say, Fonari at Al. [163], the interpenetration of the frameworks generate two distinct channels in reported {[Zn(BPDC)(4-BPMHZ)]·(MeOH)·0.5(H_2O)}$_n$, or **MRT-3** (BPDC = biphenyl 4,4′-dicarboxylate, 4-BPMHZ = 1,2-bis(1-(pyridin-4-yl)ethylidene)hydrazine). A bigger one decorated by the pillaring ligand, akin to the abovementioned paddlewheel frameworks, and a smaller one formed by the two adjacent carboxylate layers. Guest molecules often occupy the latter establishing extremely strong interactions with both the frameworks, providing strong anchoring point for the two planes and not allowing the two to shift relative to each other. However, experimental results suggest that some gate-opening and breathing effect derived from plane-sliding may occur in specific situations, for example in [Zn(isophthalate)(1,4-bis(4-pyridyl)acetylene)]$_n$ (**CID-23**) [232], reported by Kitagawa et Al. This compound exhibits moderate flexibility and undergoes a "large difference between its desolvated and as-synthesized phases". Its benzene adsorption isotherm shows a gate-opening event derived from a structural transformation. While the authors were incapable of obtaining a single crystal structure of the benzene-loaded phase, they argue that the encountered flexibility must depend on the packing system of the 2D sheets, aligning well with the breathing behavior and plane sliding of the interdigitated networks.

2.3.3. *[2 + 2] cyclization reactions*

The uncommon vicinity of the bis-pyridinic ligands in this MOF class allows for post-synthetic structural modification forcing the two neighboring pillars to react (Fig. 11, a). This feature, while not exclusive to double-pillared MOFs, is a defining characteristic of this class. One prominent category of addition reactions discussed involves photochemical [2 + 2] cycloaddition reactions where olefinic bonds within the MOF ligands react to form cyclobutane rings. For example, Mir and colleagues demonstrated this in three-dimensional zinc coordination polymers, specifically [Zn(1,2-bis(4-pyridyl)ethene)-(muco)]·DMF·H_2O, [Zn(1,2-bis(4-pyridyl)ethene)(BDC)]·DMF, and [Zn-(1,2-bis(4-pyridyl)ethene)(fum)]·H_2O. These MOFs incorporate the ditopic ligand trans-1,2-bis(4-pyridyl)ethene (BPE) as a pillar, and upon UV irradiation (wavelength 280–350 nm) at 223 K, the olefinic C═C bonds

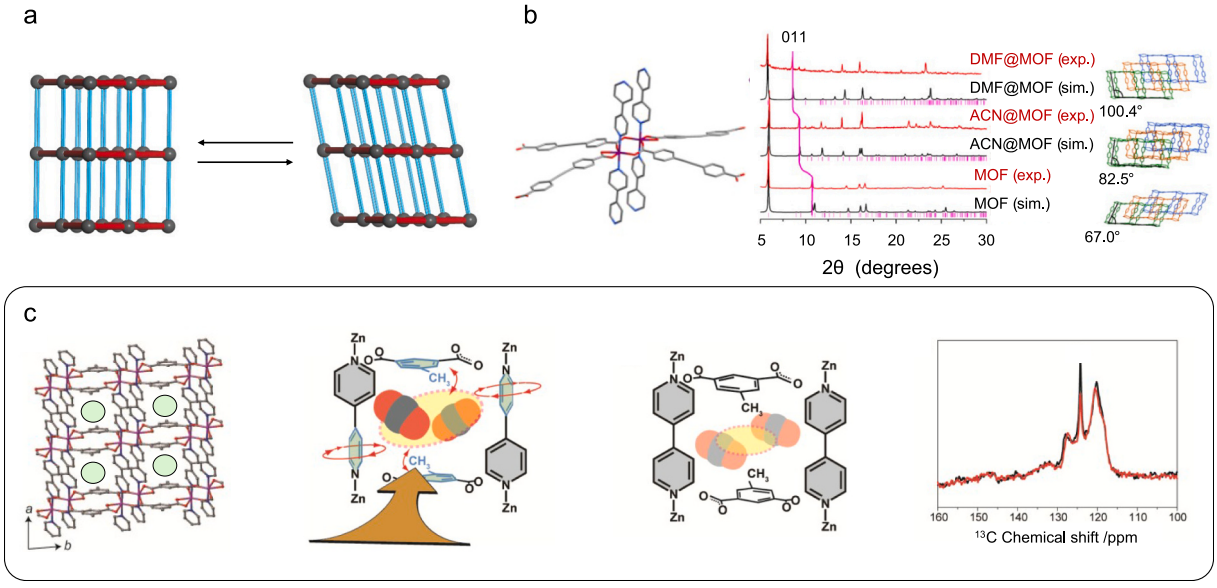


Fig. 10. a) Schematic representation of pillar tilting in double-pillared frameworks. b) *Left*, asymmetric unit of the double-pillared MOF described by Chen et Al. and its PXRD (*middle)* and frameworks (*right*), highlighting the "pendulum effect" triggered by the inclusion of different guests. Reprinted with permission from [231]. c) *Left to right,* structure of CID-Me highlighting the empty pores as green circles, CO_2 adsorption through the rotational rotors at room temperature, CO_2 storage controlled by steric hindrance of the immobile rotors at 195 K and ^{13}C MAS-NMR of CID-Me⊃0.6CO_2 at 304 K before (black line) and after (red line). Reproduced with permission from [230]. (For interpretation of the references to colour in this figure legend, the reader is referred to the web version of this article.)

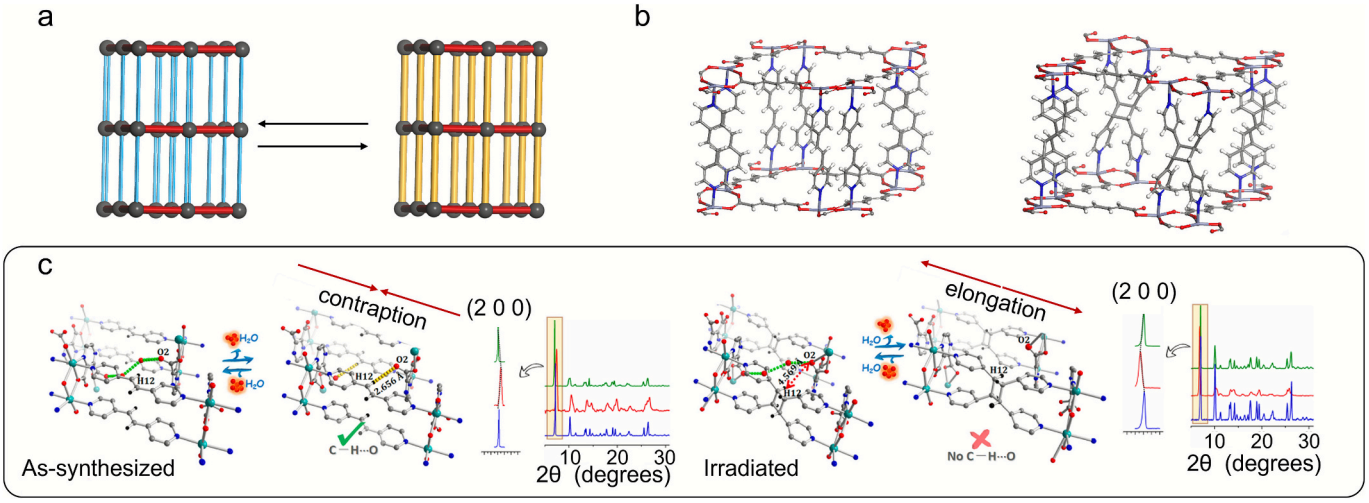


Fig. 11. a) Schematic representation of a generic [2 + 2] cyclization reaction in double-pillared frameworks. b) Structure of the framework of [Zn(1,2-bis(4-pyridyl)ethene)-(muco)] before and after UV irradiation, highlighting the cycloaddition of the pillaring ligand. c) Structure of the as-synthetized and irradiated [[Cd(1,2-bis(4-pyridyl)ethylene)(1,2-bis(4-pyridyl)ethylene)]$_2$·3H$_2$O]$_n$, displaying the presence of noncovalent interactions taking place between guest CO_2 molecules and the framework, or lack thereof, and how these interactions result in a different behavior for the two phases (structural contraption for the as-synthetized and structural elongation for the irradiated sample) clearly visible from the PXRD patterns. Reproduced with permission from [234].

of adjacent BPE ligands undergo a topochemical [2 + 2] cycloaddition reaction (Fig. 11, b). This reaction forms tetrakis(4-pyridyl)cyclobutane within the framework. Crucially, this transformation occurs by a single-crystal-to-single-crystal process, allowing the resulting structures to be analyzed. The structural consequence of this addition is that the newly formed groups diverge from the cyclobutane ring, leading to an increase in the Zn···Zn distance but an overall reduction in the unit-cell volume. [233] Building on this, Hazra and Maji further explored a guest-responsive [2 + 2] cycloaddition in a MOF with a different ligand, [[Cd(1,2-bis(4-pyridyl)ethylene)(1,2-bis(4-pyridyl)ethylene)]$_2$·3H$_2$O]$_n$. This MOF, also undergoes a [2 + 2] cycloaddition reaction upon light irradiation, forming regio cis,trans,trans-tetrakis(4-pyridyl) cyclobutane, similarly proceeding as a single-crystal-to-single-crystal transformation. A key insight from this covalent addition reaction is its profound influence on the MOF guest-responsive structural behavior. In the original MOF, weak C-H···O interactions between the 1,2-bis(4-pyridyl)ethylene pillars and 2,3-pyrazinedicarboxylate (PZDC) layers caused structural contraction upon dehydration. However, after the [2 + 2] cycloaddition, these critical C − H···O interactions are eliminated due to changes in hybridization and oxygen availability of the original ethylenic hydrogens. Consequently, the photomodified framework exhibits structural expansion upon dehydration, a reversal of the behavior seen in the original MOF. This structural change leads to enhanced CO_2 uptake and high selectivity for CO_2 over N_2 and CH_4, significantly lowering the diffusion barrier for adsorbates (Fig. 11, c). [234]

3. Applications of mixed-ligand MOFs: purification, delivery and sensing

As we previously discussed, a MOF might be tailored to host a single specific guest or a class of guests. [232,235] The ability of MOFs to dynamically change their structure is a pivotal feature that allows for a high number of favorable noncovalent interactions to take place between hosts and guests, providing strong anchoring points for volatile or liquid molecules to be trapped inside of the cavities of the MOFs. [236] As a consequence, MOFs can be used to purify and separate gas mixtures without the need of chemical reaction or expensive industrial methods. [112] This behavior, common to many different MOFs, has important practical implications like the avoidance of expensive processes or high energetic expenses. When volatile or liquid guests are trapped into a MOF they can be concentrated inside the channels of the frameworks. This allows for detection (sensing) [237] and study of minority components of complex natural matrices (crystalline sponge method). [238,239] This feature allows molecules to be easily located inside the cavities of a MOF to be structurally characterized. This processes, firstly developed by Fujita *et Al*, permit to use the MOF as crystalline matrices, where, thanks to the formation of supramolecular interaction as hydrogen bonds or π-π stacking interactions, guest molecules can be trapped and crystallographically detailed. This method has allowed the determination of reluctant to crystallize compounds as pharmaceuticals, [240] agrochemical [241] or metal complexes intermediate. [242] Lastly, loading a specific guest into the cavities of a MOF can prove instrumental in using these crystalline compounds as delivery systems for the controlled release of API delivery. [243]

3.1. Separation of chemical mixtures

The separation of chemical mixtures represents a significant industrial challenge, consuming approximately 10–15 % of the earth's energy, largely due to reliance on energy-intensive methods such as distillation. [244] This task becomes particularly arduous when separating gas mixtures comprising molecules with similar physical and chemical properties, often necessitating complex and harsh operating conditions. To overcome this, a novel strategy has emerged, centered on the use of flexible MOFs whose pore structures can be dynamically modified, for instance, by varying pressure conditions, to achieve effective and selective separation. [245,246] While most of the processes nowadays focus on Zeolitic Imidazolate MOF (ZIF) membranes, [247–249] mixed-ligand MOFs are also emerging as an interesting alternative.

In particular, in the critical industrial process of separating acetylene from CO_2 and other light hydrocarbons, zinc-based MOFs offer advanced solutions. **UTSA-300-Zn**, with the chemical formula [Zn(4,4′-dipyridylsulfide)$_2$(SiF$_6$)]$_n$, exhibits pores that facilitate acetylene uptake. Its pore size of 3.5 × 3.9 × 4.1 Å^3 is precisely compatible with acetylene molecules, and it achieves adsorption through a gate-opening effect mediated by linker rotation. [250] Further advancements in zinc-based MOFs for C_2H_2 separation include the series {[Zn$_2$(TPTA)]·2DMA} (**ZJNU-406**), {[Zn$_4$(TPTA)(BDC-F)(OH)$_2$]·0.5DMF·H$_2$O} (**ZJNU-407**), and {[Zn$_4$(TPTA)$_2$(BDC-F)(CH$_3$NH$_3$)$_2$]·5NMF·3EtOH} (**ZJNU-408**) (where TPTA = [1,1′:3′,1″-terphenyl]-4,4′,4″,6′-tetracarboxylate, BDC-F = 2-fluoroterephthalate). These MOFs possess specific adsorption sites

designed to maximize host-guest interactions, such as C-H···O and C-H···F hydrogen bonds between the framework and acetylene, leading to a stronger affinity for acetylene over CO_2 and methane. [251] Similarly, **IITKGP-24** ([Zn_2(1,2-Di(4-pyridyl)ethylene)(1,2,4,5-tetrakis[(4-carboxy)phenoxymethyl]benzene)]$_n$), a chemically robust 3D microporous zinc-MOF (Fig. 12), utilizes its polar pore channels, decorated with alkoxy oxygen atoms, and dynamic functional binding sites to effectively entrap acetylene molecules *via* hydrogen bonding and C-H···π interactions. [252] It exhibits excellent C_2H_2/CO_2 separation selectivity even at ambient conditions (Fig. 12, a, b, c and d) but also of complex quaternary mixtures like $C_2H_2/C_2H_4/C_2H_6/CO_2$ (Fig. 12, e). For C1-C3 alkane separations, the zinc-based MOF [Zn(2,5-bromo1,4-benzenedicarboxylate)$_2$(DABCO)]$_n$, stands out. Despite possessing a rigid topology this MOF demonstrates an intriguing guests-induced self-regulatory strategy. [253] Upon the adsorption of propane molecules, guest molecules sit tightly confined into the pore cavities. This internal adaptation enhances gas diffusion and facilitates the continuous adsorption of subsequent propane molecules without requiring any modification of the MOF structure or the introduction of external species. Although not flexible, for larger hydrocarbons capture, a novel triple catenated Zn-pillared MOF, **PUM210**, has been proposed as a solid-phase microextraction coating. [254] Its channels exhibit a remarkable complementarity in dimensionality between host-pores and guests, enabling smaller molecules like benzene, toluene, ethylbenzene, and xylenes to transit smoothly while effectively blocking larger hydrocarbons. **PUM210** and its fluorinated analogue, **PUM210F**, were also analyzed in their ability to selectively capture CO_2 in a stream of N_2. Both MOFs are built from the rigid dicarboxylate linker NDC, and a pillaring bis-pyridine-bis-amide linker. **PUM210** incorporates N,N′-(1,1′-biphenyl)-4,4′-diylbis-4-pyridinecarboxamide (BPBA), while **PUM210F** its fluorinated analogue, N,N′-(perfluoro-1,1′-biphenyl-4,4′-diyl)-diisonicotinamide (F-BPBA). While both MOFs exhibit permanent porosity and selective adsorption of CO_2, the presence of the perfluorinated biphenyl core in F-BPBA significantly alters the pore environment. Consequently, **PUM210F** shows a marked improvement in CO_2 selectivity over N_2 compared to **PUM210**. The highly electronegative fluorine atoms create a more favorable electrostatic potential within the channels, enhancing the interactions between the framework and the quadrupolar CO_2

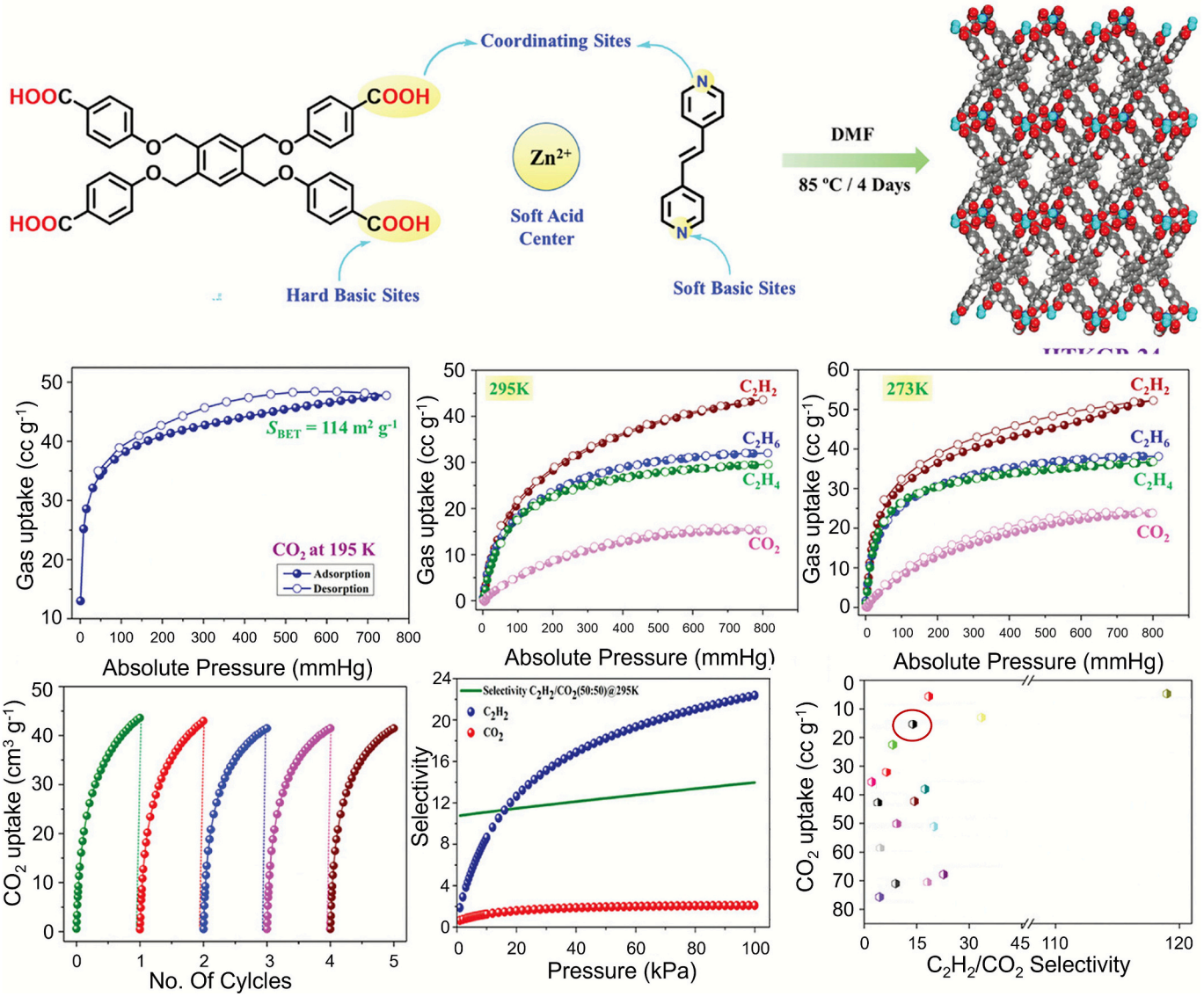


Fig. 12. *Above*, schematic representation of the synthesis of **IITKGP-24**, a mixed-ligand MOF for the separation of mixtures of hydrocarbons. *Below*, a number of experimental analyses routinely used to characterize MOF behavior in mixtures separations. a) CO_2 isotherm at 195 K. b) and c) 295 and 273 K isotherms, respectively, for C_2H_2, C_2H_6, C_2H_4 and CO_2. d) Cyclability of the material. CO_2 adsorption is retained after at least six cycles. e) Selectivity of C_2H_2 over CO_2. f) Schematic selectivity of for a number of different mixtures of different reported MOFs. Reproduced with permission from [252].

molecules. This selective enhancement of host-guest interactions is a successful strategy for tuning gas-sorption properties for applications like flue gas separation. [255]

While the reports of flexible MOFs designed for the separation of chemical mixtures are limited, some important works can be located in literature. One notable example is the flexible-robust zinc-MOF, $[Zn_2(aminotriazole)_2oxalate]_n$ which demonstrates efficient ethylene purification from C_2H_2/C_2H_4 mixtures through a unique guest-dependent stepwise gate-opening mechanism. [256] This material initially presents rigid pores, formed by dimeric [Zn_2 (aminotriazole)$_2$] units in its guest-free phase, which effectively facilitate the adsorption of acetylene molecules at low pressures. Subsequently, a dynamic response, possibly driven by the rotation of oxalate pillars, enables the formation of an intermediate phase that further enhances separation performance across the 298–323 K temperature range. This dual characteristic, combining initial robustness with responsive flexibility, allows for both efficient removal of trace impurities and high gas uptake.

For the challenging separation of C_6 cyclic hydrocarbons, a flexible two-dimensional (2D) layered Zn-MOF, **Zn-BDC** $[Zn(BDC)(H_2O)\cdot DMF]_n$, demonstrates efficient adsorptive separation through a temperature-dependent molecular-sieving mechanism. [257] This MOF, constructed from a $[Zn_2(COO)_4]$ paddlewheel secondary building unit and a 1,4-benzenedicarboxylate (BDC) linker, exhibits fully reversible structural transformations. These transformations occur upon activation, involving the removal of water and DMF molecules, and upon hydrocarbon adsorption, manifesting as guest-induced interlayer expansion. The pore size of the activated **Zn-BDC**, approximately 5.3 Å, is slightly smaller than the kinetic diameters of the targeted C_6 cyclic hydrocarbons (ranging from ~5.85 to 7.4 Å), which effectively triggers and controls the framework expansion. This dynamic, temperature-responsive behavior enables the precise discrimination of individual C_6 cyclic hydrocarbons from binary and ternary mixtures using temperature-programmed protocols, achieving high uptake ratios for C_6H_6/C_6H_{12} and C_6H_{10}/C_6H_{12}. [Zn_2(5,10,15,20-Tetrakis-(4-methoxycarbonylphenyl)porphyri-nato]-PdII)(9,10-Bis(4-pyridyl)-anthracene)]$_n$ ([Zn_2(PdTCPP)(Bpa)]·DMF, **PTA-DMF**) is another excellent example of how the dynamicity of a material can impact its sorption properties. [258] This inherent flexibility, coupled with high adsorption for n-hexane, allows the dynamic framework to self-adapt to the n-hexane molecules, matching their size and/or shape to the pore features of the MOF. A particularly significant finding is that lower temperatures can prompt n-hexane molecules to open the dynamic pores. This leads to an *increase* in both the adsorption rate and efficiency of separation n-hexane as the temperature decreases. Lastly, a tetrahedral **dia** MOF, described by the formula [Zn(4,4′-(4,4,5,5,6,6-hexafluoro-9a,9b-dimethyl-5,6,9a,9b-tetrahydro-4H-indeno[5,4-b:6,7-b']dithiophene-2,8-diyl)dipyridine)(BPDC)·solvents] comprising a diarylethene ligand able to dramatically boost the CO_2 adsorption through photoswitching was recently synthetized. [259] This unit undergoes photo-induced isomerization, involving reversible ring-opening and ring-closing reactions triggered by both UV and visible light. This reversible transformation of the ligand leads to a "local framework movement" within the MOF, the key to its CO_2 capture and release capabilities. [Zn(L)(BPDC)·solvents] photochromic properties enabled significant CO_2 adsorption, reaching a record desorption capacity of 75 % under static irradiation and 76 % under dynamic irradiation, which is attributed to this light-induced local framework flexibility.

3.2. Sensing of hazardous chemicals

In mixed-ligand MOFs, the interactions established between the trapped guest molecules and the material channels may affect the energy transfer processes involving the different linkers and responsible of the MOF luminescence [260]. When a molecule enters the MOF porous structure, it can bind to specific sites *via* hydrogen bonding, π–π interactions, electrostatic forces, or coordination to metal centers. [111] These interactions often induce measurable changes in the MOF physical properties, such as fluorescence, electrical conductivity, or mass, which can be transduced into a detectable signal. For example, luminescent MOFs (LMOFs) exhibit changes in emission intensity or wavelength upon exposure to toxic gases like NO_2, SO_2, or volatile organic compounds (VOCs), enabling rapid and sensitive detection down to parts-per-billion levels [261,262]. In this process, the linker acts as the excitation energy donor, absorbing light in the ultraviolet region. This absorbed energy is then non-radiatively transferred to the bis-pyridine linkers, which serve as acceptors. As a consequence of this intriguing phenomenon, MOFs have emerged as powerful platforms for the detection of dangerous molecules. An interesting application is the detection of explosive compounds. Three distinct pillared MOFs demonstrate varied strategies for explosive detection. Emge et Al. presented $[Zn_2(4,4'\text{-oxybis(benzoate)})_2(4,4'\text{-bipyridine})]_n$. [263] It selectively quenches fluorescence for aromatic nitro-containing compounds like 2,4-dinitrotoluene (DNT) but shows a negligible quenching effect (<1 %) for the aliphatic nitro-containing high explosive 2,3-dimethyl-2,3-dinitrobutane (DMNB). This unique selectivity allows to differentiate between these distinct types of explosives (Fig. 13, b). In contrast, Lan et Al. introduced $[Zn_2(1,4\text{-benzenedicarboxylate})_2(1,2\text{-bipyridylethene})]_n$, [264] which exhibits fluorescence quenching for rapid and reversible detection of both DNT and DMNB. This framework achieved an unprecedented high sensitivity, with approximately 85 % fluorescence quenching for DNT and 84 % for DMNB within ten seconds of exposure. Finally, Kitagawa et Al. utilized $[Zn_2(1,4\text{-benzenedicarboxylate})_2(\text{dipyridyl naphthalenediimide})]_n$ to distinguish small structural differences in aromatic compounds, including potential explosives. [265] This entangled porous framework exhibits a "turn-on" multicolour luminescence where the emission colour is dependent on the chemical substituent of the aromatic guest. This arises from an enhanced dipyridyl naphthalenediimide-aromatic guest interaction, like exciplex fluorescence or phosphorescence, triggered by an induced-fit structural transformation of the framework (Fig. 13, a). The cooperative structural transition also results in a nonlinear sensor response, offering high sensitivity even at low vapor pressures. A different approach is given by Kitagawa et Al. in which, $[Zn_2(1,4\text{-benzenedicarboxylate})_2(\text{triethylenediamine})]_n$ is loaded with a fluorescent reporter molecule, distyrylbenzene. The MOF can then selectively adsorb other gases, such as CO_2, additionally modifying its structure through a "breathing" mechanism. The adsorption of CO_2 induces a further host structural transformation, causing the shrunk rhombic structure to expand back to its original square form. This expansion is directly coupled with the conformational planarization of the distyrylbenzene reporter molecule, resulting in a visible change in its solid-state fluorescence at a specific threshold pressure. [266]

Generally, MOFs also excel in environmental sensing, where they can detect pollutants in air and water with high selectivity and sensitivity [267,268]. Their porous nature allows for preconcentration of analytes, enhancing detection limits and enabling the identification of trace contaminants. In aqueous systems, various MOFs, including mixed ligand Zn-MOFs, have been used to sense anions like phosphate and nitrate, as well as organic toxins such as pesticides and antibiotics. [262] Their ability to function in diverse media makes them adaptable to various sensing platforms, including wearable devices, field-deployable sensors, and integrated lab-on-a-chip systems [267]. Zinc-based MOFs in particular were studied specifically for sensing a range of inorganic ions. Between them, we cite Fe^{2+}, Fe^{3+}, Cd^{2+} Al^{3+}, Cr^{3+}, In^{3+}, Zr^{4+}, CrO_4^{2-}, CrO_7^{2-} and MnO_4^-. [169,269–278] One of the most intriguing applications of this method is the use of scintillating MOFs for radioactive gas detection. In recent years a transformative approach using photoluminescent MOFs was introduced. [279] Zinc-based MOFs were put to the revealing their capacity to concentrate [280] and effectively detect a wide range of radioactive gases, even comprising tritiated dihydrogen, one of the most difficult isotopes to identify due to its low energy emissions [281]. In some cases, flexibility plays a crucial role in

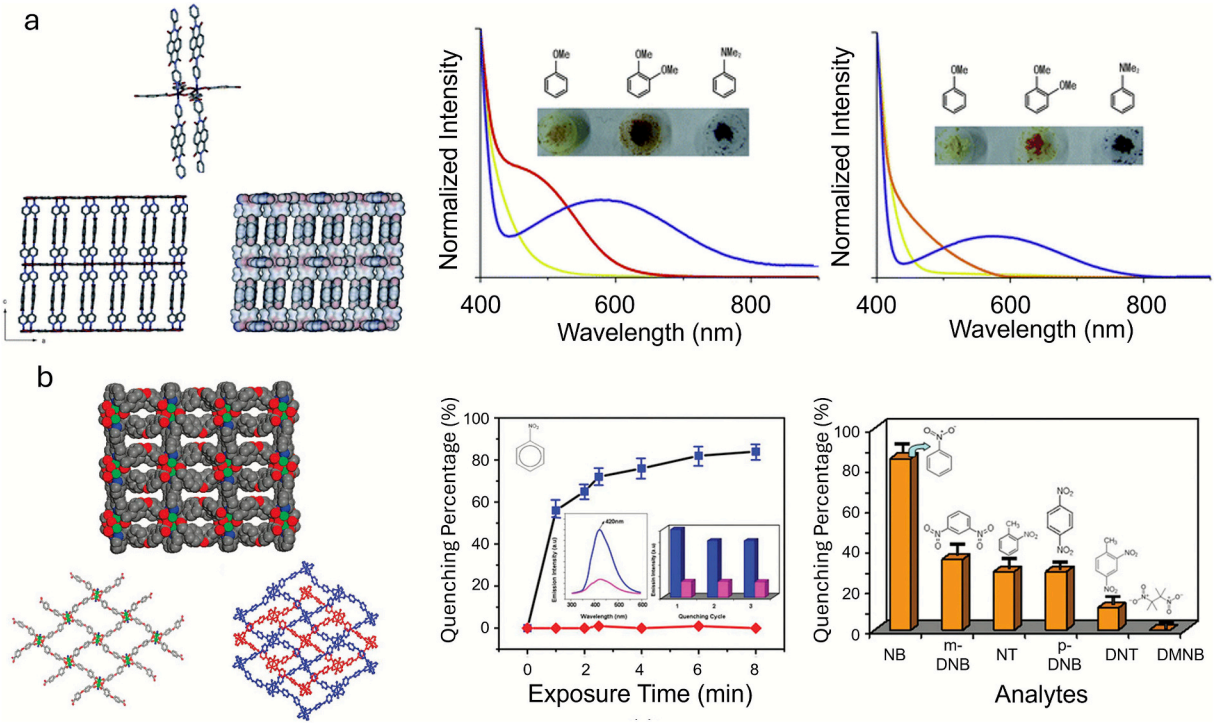


Fig. 13. a) *Left*, crystal structure of {[Zn(thdc)(dpNDI)]·6DMF}$_n$ highlighting the double pillared SBU. *Right*, quenching of {[Zn(thdc)(dpNDI)]·6DMF}$_n$ and [Zn(thdc)(dpNDI)]·10MeOH·2DMF}$_n$ fluorescence from three pollutants. Reproduced with permission from [265]. b) *Left,* Crystal structure [Zn_2(oba)$_2$(bpy)]·DMA. *Center and Right*, luminescence quenching driven by the presence of nitrobenzene (*center*) or other nitro-derivatives (*right*). Reproduced with permission from [263].

encapsulation and sensing. Kamal et Al. report a flexible Zn-MOF that demonstrates a temperature-triggered breathing effect. [282] At a low temperature of 100 K, the MOF exists as a high-symmetry phase, featuring triangular narrow pore channels and a unit cell volume of 1958 Å^3. Upon increasing the temperature to 298 K, the framework undergoes a phase transition to a lower-symmetry form. This transformation involves a significant expansion of the unit cell volume to 7823 Å^3 and a distortion of the channels from triangular narrow pore to rhombic large pore channels. The resulting mesoporous compound is highly efficient for capturing hazardous iodine molecules. The large pore size of low-symmetry phase is significantly greater than the kinetic diameter of iodine (4 Å), which allows numerous iodine molecules to easily pass through these mesoporous channels, thereby enhancing the adsorption capacity.

3.3. API controlled release

Metal-organic frameworks have emerged as highly promising materials for the controlled release of active pharmaceutical ingredients (APIs), offering a sophisticated alternative to conventional drug delivery systems.

The structural versatility of MOFs allows for the encapsulation of a vast range of APIs, additionally tuning the pore channels and materials exterior to accommodate hydrophobic or hydrophilic compounds to improve their bioavailability through solubility, prevention of secondary reaction between the API and the body and passing through biological membranes [283,284]. This adaptability makes them suitable for delivering APIs that are poorly soluble, unstable, or require targeted release. For instance, MOFs can protect sensitive drugs from premature degradation in the gastrointestinal tract or bloodstream, ensuring that the therapeutic agent reaches its intended site of action intact [284,285]. However, their translation into physiological environments necessitates careful evaluation of stability, biocompatibility, and potential toxicity. [286] MOFs must maintain structural integrity under aqueous, saline, and variable pH conditions typical of the human body. Frameworks susceptible to hydrolysis or ligand displacement may release metal ions or degrade prematurely, compromising both efficacy and safety. [287] Biocompatibility is largely influenced by the choice of metal nodes and organic linkers. Zn-MOFs are favored in biomedicine, partly due to the high biocompatibility of zinc, which is considered a safe metal ion for constructing functional MOFs. [288] MOFs with **dia** or **sql** topology are often reported to be water stable [141,193,196] but their trial in biological applications are, to the best of our knowledge, absent from literature, and important works in that regard focus on MOFs that are known to be water unstable (not just pillared and double-pillared MOFs [289], but also IRMOFs [290,291] and ZIFs [292]). Their degradation inside the body, if sufficiently slow, might in fact be regarded as an asset rather than a drawback, allowing the targeted release of the API near the target and subsequent excretion of the MOF component (if nontoxic) without bioaccumulation of the material inside the patient. [293]

Improving the water stability of zinc-based MOFs requires a combination of molecular design, defect control, and protective engineering strategies. At the molecular level, choosing strongly coordinating linkers such as multidentate carboxylates, imidazolates, or triazolates helps reinforce Zn–ligand bonds that otherwise hydrolyze easily. Designing high-connectivity or densely packed topologies further limits water ingress and reduces the likelihood of node dissociation. Introducing hydrophobic substituents, including alkyl, aromatic, or fluorinated groups, can effectively repel moisture and slow hydrolysis. [294]

Capping labile Zn sites with auxiliary ligands or introducing mixed-metal strategies substituting a fraction of Zn with more hydrolytically stable metals like Zr or Co can mitigate water-induced degradation while preserving structure and function. [295]

Defect engineering also plays an essential role. Reducing coordination vacancies and minimizing missing-linker defects through careful control of synthesis conditions, modulators, and activation procedures greatly increase water resistance. [296,297] Finally, incorporating Zn-MOFs into polymer composite matrices can provide physical protection, enhance mechanical stability, and slow water diffusion. [298]

The stability of Zn-MOFs in biological environments is often highly dependent on specific physiological parameters, primarily pH and the presence of anions. A defining characteristic of several common Zn-MOFs is their acid-sensitive nature, which is often exploited for stimuli-responsive drug release within the body. For instance, ZIF-8 exhibits "zero premature release" under neutral physiological conditions (around pH 7.4). However, it readily collapses in the mildly acidic environment (pH 5.4–6.0) characteristic of tumor tissue or endosomes. This degradation is due to the protonation of the 2-methylimidazole linker, which consequently breaks the coordination bonds connecting it to the Zn^{2+} centers. [299,300]

Crucially, studies have shown that Zn-MOFs can possess favorable metabolic pathways. IRMOFs are noted for their water-reactive properties, facilitating their metabolism in the body. For example, PEGylated IRMOF-1 was observed to clear rapidly from mice, with the majority of the material eliminated through the renal route and biliary excretion within approximately one week. This rapid clearance profile suggests promise for their continued development in biomedical applications. [301]

One of the most compelling examples of this approach is given by Yin et Al. In the work, different **IRMOFs** (**IRMOF-1**, **IRMOF-8**, **IRMOF-10**, and **IRMOF-16**) were loaded in oridoin, an antitumoral drug. The drug loading capacity was found to be significantly influenced by the matching of the **IRMOF** pore size to the drug molecule's size. **IRMOF-1**, with its 2.43 nm pore size, demonstrated the highest drug stabilization, showing a drug loading of 57.93 % for oridoin, compared to lower capacities in **IRMOF-8**, **IRMOF-10**, and **IRMOF-16** which have larger pores. Oridoin-loaded **IRMOF-1** exhibited a pH-dependent drug release profile, with 37.86 % release in 10 h at pH 7.4 and a significantly increased release of 66.66 % at pH 5.5. This pH-sensitive release is beneficial for targeting acidic tumor microenvironments. [301]

The same principle can be applied to smart packaging [302,303] and controlled release of APIs for agrochemical applications. [304] In one notable example, thymol, is encapsulated within **Zn-BDC-NH2** and the activity against *E. coli* is evaluated. [305] A second example details the encapsulation of carvacrol using **IRMOF-3**. [306] This loaded MOF is then integrated into sodium alginate films, a natural polysaccharide. Both systems are developed to create bioactive packaging materials with sustained antioxidant and antibacterial activities. It must be noted that most works focus on Zinc Imidazolate or IRMOF frameworks, [307] which are generally considered rigid.

The different applications of the described MOFs are summarized in Table 1, together with their characteristic framework dynamics.

4. A discourse on API delivery from PUM168

To effectively track the details of a guest-exchange process and the subsequent growth of molecular aggregates, MOFs must be carefully designed with specific characteristics. For instance, the pores must be large enough to accommodate multiple guest molecules while being small enough to avoid a chaotic, disordered arrangement. Furthermore, the framework's backbone must be flexible and adaptive, allowing the guests to self-organize within the confined chemical environment. **PUM168**, synthesized from Zn-based paddlewheel SBUs linked by the rigid linear biphenyl 4,4′-dicarboxylate (BPDC) ligand and pillared by the neutral N,N′-(1,1′-biphenyl)-4,4′-diylbis-4-pyridinecarboxamide (BPBA) ligand, fulfills these design criteria (Fig. 14). The BPBA ligand was specifically engineered with two amide moieties that break its rigid sp^2 backbone, imparting the necessary flexibility to the MOF to adapt to the size and shape of its guests. Moreover, amide groups provide good hydrogen bonds anchoring points. The MOF structure is a triple-interpenetrated network of two independent nets, an acentric net (a-

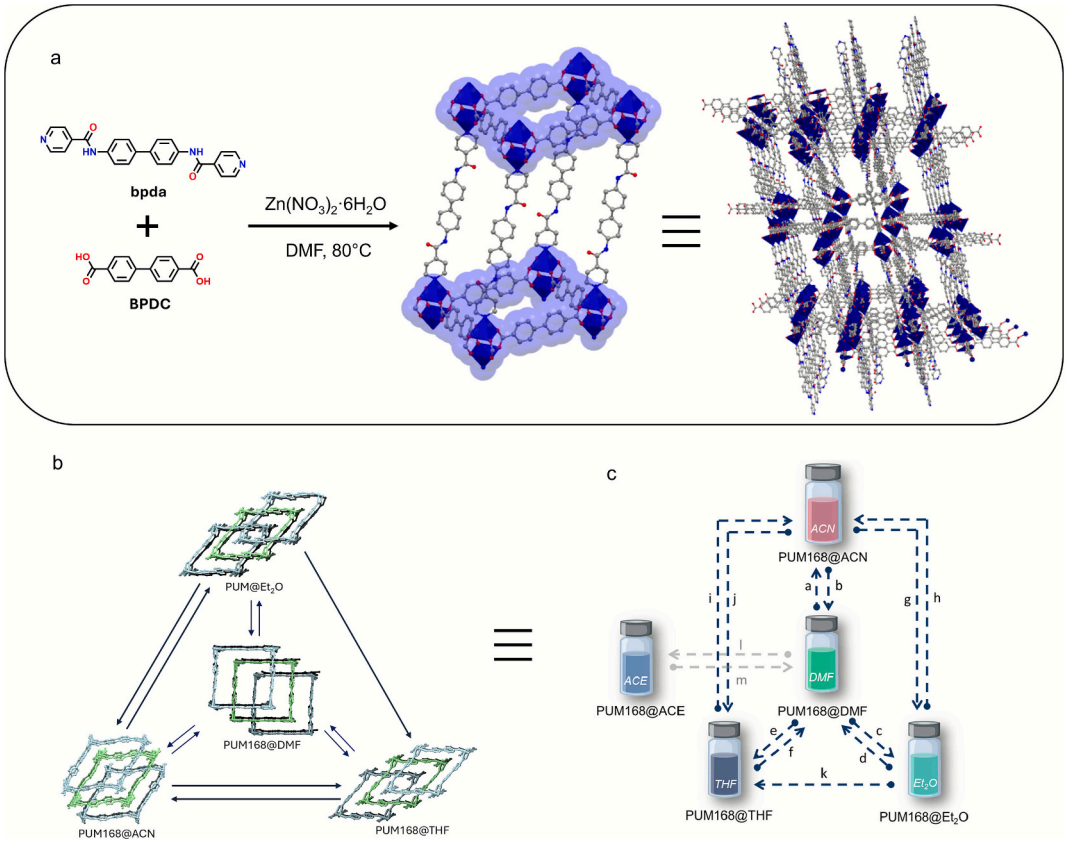


Fig. 14. Schematic representation of **PUM168** synthesis. From *left* to *right*: building block and synthetic conditions; framework of **PUM168** and triply interpenetrated framework of the MOFs. *Below*, Visualization of the flexibility of **PUM168** after soaking in different solvents (DMF; Et_2O; ACN and DMF) and schematic representation of the process. Reproduced with permission from [308].

net) and a centric net (c-net), each formed by a square grid of Zn-BPDC units pillared by BPBA. Despite this interpenetration, the structure contains microporous channels running along the [110] direction. These channels, which correspond up 49.7 % of the total volume, have a pseudo-ellipsoidal shape with a total volume of 2980 $Å^3$ per cavity.

4.1. Solvent induced structural transformation

In **PUM168**, the combination of the coordination geometry achieved by the flexible paddlewheel structure, linked to the presence of ligands that express some degree of flexibility thanks to the presence of the amidic moieties provides several degrees of flexibility to the structures. These capabilities were assessed when the pristine crystals, still containing DMF embedded in the channels, were soaked in acetone, a polar non-protic solvent, maintaining crystallinity and allowing the study of the structure through single crystal X-ray diffraction (SC-XRD). The analysis reveals a pronounced structural transformation. In fact, the crystals underwent a shrinkage of the channels, with a drop in the cell volume from the starting value of 5977 $Å^3$ to 4594 $Å^3$. The major distortion effect was found to be related to the change of the angles between the dicarboxylate in the square dicarboxylate grid ("breathing" phenomenon), while the effect over the bis-amidic bis-pyridinic ligands was much more contained. Other organic solvents like acetonitrile (ACN), tetrahydrofuran (THF), and diethyl ether (Et_2O) were tested in order to establish the effect of substitution with the pristine DMF molecules and for evaluating the tolerance of **PUM168** to these solvents (Fig. 14, bottom). In the cases of acetonitrile, the monitoring of the exchange *via* TGA and ^1H NMR denoted the complete extrusion of DMF, thanks to a good combination of polarity and molecular dimensions. In the case of the less polar solvents THF and Et_2O, the complete extrusion of DMF revealed more difficult and possible only after repeated experiments. The DMF-to-ether exchange provoked a shift of the 2D grids along the a-axis ("breathing") that caused the tilting of the pillar ("pillar tilting") and a decrease of the 2D-grid distance ("plane sliding"). A different situation was found in the ACN-solvated structure. Here, the pillaring ligands twist significantly around their amide groups straightening the framework along the a-axis thus widening the distance between the 2D-grids. Crucially, all these solvent-induced transformations were found to be reversible. The ability of **PUM168** to adapt its microporous framework to different guests without losing crystallinity is a key finding that underscores its potential as a crystalline sponge. [308]

4.2. Guest exchange: DMF to APIs

One of the most illustrative examples of host-induced flexibility in **PUM168** is the exchange of the native solvent DMF with eugenol, a phenolic compound with antibacterial activity. [309] This process is not a simple solvent displacement but a cooperative mechanism involving the MOF scaffold, the departing DMF, and the incoming eugenol. Single-crystal X-ray diffraction studies have shown that the inclusion of eugenol induces significant structural changes in the framework. The interpenetrated networks shift relative to each other, and the pillar ligands undergo conformational adjustments to better accommodate the guest molecules. This reorganization results in a measurable increase in the accessible pore volume, approximately 5 %, demonstrating the breathing capacity of the framework. Importantly, the process is reversible: upon removal of eugenol and reintroduction of DMF, the framework returns to its original configuration. The core of this research was the stepwise investigation of the eugenol loading process. Native **PUM168** crystals were soaked in pure eugenol and the structure was recorded at specific time intervals (1, 4, and 7 days) to track the formation of molecular aggregates (Fig. 15, a,b and c). After one day of soaking, the SC-XRD analysis revealed that eugenol molecules had entered the MOF pores and coexisted with residual DMF (Fig. 15, from a to b and c). The cavities core was occupied by disordered eugenol molecules, which could be deconvoluted into two concomitant and mutually exclusive assemblies. Two disordered eugenol molecules were interacting with the paddlewheel SBU. Other three disordered entities were interacting with the amide groups of the a-net. Here, the native DMF molecules have not been released yet. After 7 days, the structural model showed the progressive displacement of DMF in favor of the gradual organization of eugenol molecules. In this snapshot the eugenol molecules that were disordered acquired defined position, displacing all the molecules of DMF and occupying their spots. The two molecules interacting with the SBU can still be found in the same position. In

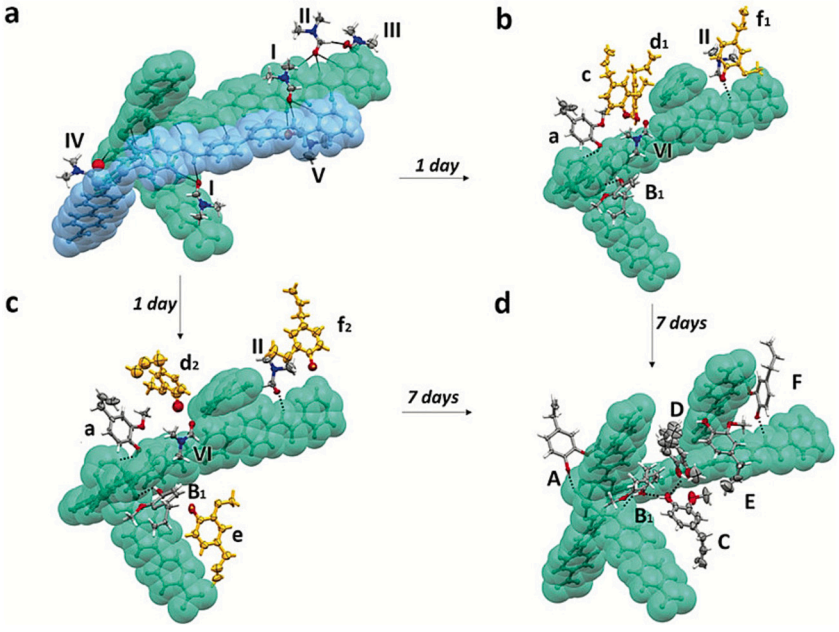


Fig. 15. **S**napshots of the eugenol permeation inside **PUM168**. a) visualization of pristine crystal of **PUM168** with 6 molecules of DMF (I-VI). b) and c) Disposition of eugenol molecules along the frames after 1 day of soaking and d) after 7 days of soaking. Capital letters refers to full occupancy molecules. Reproduced with permission from [309].

conclusion, by the end of the 7-day soaking process, the DMF-to-eugenol exchange was complete (Fig. 15, d). The final SC-XRD model revealed that the eugenol molecules had self-organized into a well-defined trimeric aggregate, demonstrating that **PUM168** actively promotes the self-assembly of guests into an ordered supramolecular structure. The MOF nets rearrange to adapt to the new content, showcasing a tight interplay between the host and the guest.

Beyond eugenol, **PUM168** has been employed to encapsulate other liquid active ingredients, including propofol, carvacrol, and menthone. [310] Each of these guests interacts differently with the framework, leading to distinct structural outcomes. The inclusion of propofol, for instance, is associated with extensive conformational disorder in the amide linker, suggesting a high degree of flexibility in accommodating this molecule. Carvacrol, on the other hand, induces a rearrangement of the BPBA linker, with the torsion angle between amide groups shifting from a cis configuration to approximately 90 degrees. Neither propofol nor carvacrol were able to fully displace the native DMF. In contrast, menthone, which lacks hydroxyl groups and aromaticity, exhibited weak interactions with the framework and a high degree of disorder. This suggests that specific chemical functionalities, such as hydrogen bonding donors or π-systems, are critical for effective guest binding and structural modulation.

4.3. Binary guest mixtures: cooperative and competitive inclusion

The inclusion of binary guest mixtures offers additional insights on the ability of **PUM168** to accommodate multiple guests. Experiments involving mixtures of carvacrol with thymol [311] or eugenol [312] revealed complex cooperative and competitive interactions that influence both the structural response of the framework and the release profiles of the guests. In the eugenol/thymol system, a complementary binding affinity was observed: eugenol preferentially binds to the paddlewheel SBU and forms homodimers, while thymol interacts with the amide groups (Fig. 16, top). This selectivity persists even when thymol is present in excess, indicating a strong preference in binding sites. However, the presence of thymol hinders the complete removal of DMF, suggesting that the simultaneous presence of two guests restricts the mobility of eugenol within the pores. In contrast, the eugenol/carvacrol mixture exhibited more competitive behavior. Carvacrol was found to share binding sites with eugenol and influence the overall stability of the framework (Fig. 16, bottom). These differences in binding behavior translate into distinct controlled release profiles, demonstrating the potential of **PUM168** for designing stimuli-responsive materials with tailored functionalities. Interestingly, the structural response of the framework to binary mixtures was less pronounced than that observed with pure eugenol. In the eugenol/thymol mixture, for example, the overall volume of the framework remained nearly constant, indicating a dampened breathing response. This suggests that the presence of multiple guests can modulate the extent of structural transformation, offering a means to fine-tune the material's behavior.

4.4. Comparison between PUM168 and PUM210, flexibility over rigidity

The comparison between two different frameworks can be considered. **PUM168** and **PUM210** both contain the same bispyridinic ligand BPBA but differ in the carboxylate moiety (**PUM168** contains biphenyl

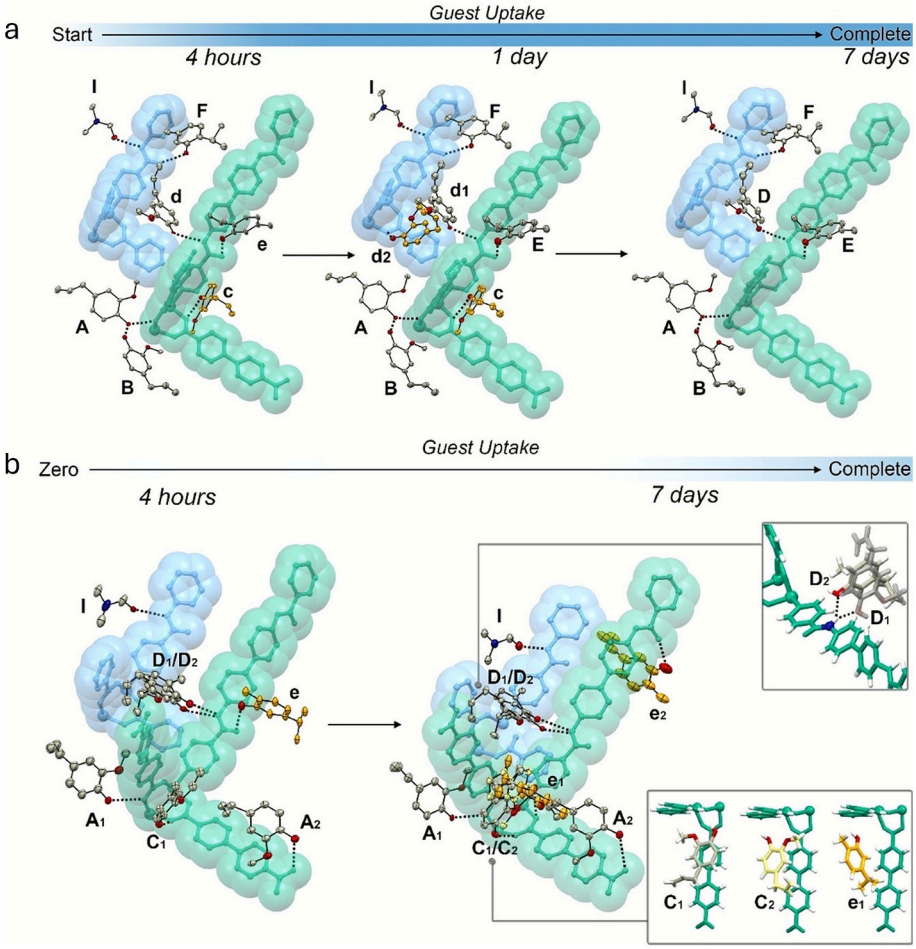


Fig. 16. Crystallographic snapshots of the guest immobilization in the channels of **PUM168** for the mixture of eugenol and thymol (*top*) and eugenol and carvacrol (*bottom*). Molecules of eugenol are dubbed **E**, thymol **T** and carvacrol **C**. Reproduced with permission from [312].

4,4′-dicarboxylic acid, **PUM210** 2,6-naphthalene dicarboxylic acid). [311,313] Albeit possessing a similar network, the final properties differ incredibly, with **PUM210** presenting a much more rigid framework than **PUM168**. Moreover, **PUM210** presents truncated paddlewheel SBUs. Exposing the crystals to an equimolar mixture of thymol and carvacrol, the more flexible framework of **PUM168** allowed a higher uptake, with a preferential inclusion of carvacrol over thymol. Notably, the guest release at room temperature was found to last for 15 days, as determined by GC–MS monitoring. In comparison, the response of the more rigid **PUM210** was found to fade within 24 h, matching the response of the non-encapsulated essential oil mixture (Fig. 17, a). The effect was attributed to the ability of **PUM168** to stepwise adapt its structure to the release of the guest, being able to dynamically anchor guest molecules in various conformations and amounts. Similar conclusions can be drawn when considering the response of the two materials when exposed to N-heterocycle-containing compounds such pyridine and quinoline (Fig. 17, b). In the work, the crystals of the two MOFs were soaked in neat quinoline to determine the positioning of the guests in the cavities. **PUM168** with its flexibility, included in the cavity the molecule of quinoline, while the more rigid **PUM210**, presenting truncated paddlewheel SBU, permitted the coordination-driven capture of the guest. [313] This work nicely demonstrates the important effects that adaptability may impart to the resulting property of a material.

5. Conclusions and future outlook: next-generation of flexible MOFs

Mixed ligand MOFs are extremely tunable materials thanks to the possibility of controlling the coordination geometry of the metal node, the overall framework topology and harnessing the dynamic behavior of flexible ligands. In this review, we have shown how the interplay of these features allows for the *a priori* design and construction of a vast array of different zinc, mixed-ligand based Metal-Organic Frameworks that display a wide range of structural diversity of dynamic modes, generating functional material that can be applied in several different fields of research. These systems, often chemically similar but structurally and topologically diverse, were instrumental in understanding the structure-function relationships of the frameworks, as well as how variation of the synthetic conditions might produce materials with vastly different properties. While often complex and delicate to harness, flexible materials might find applications in many fields, as they provide unique responses to guests. Flexible MOFs, as **PUM168**, are extremely well suited for encapsulation and controlled release of small molecules, finding possible applications like crystalline sponges, in sensing, mixture separations and more. Building on the concepts outlined above, the accumulated understanding of structural dynamics, host-guest interactions, and framework energetics in MOFs provides a strong rationale for viewing flexibility as a now well-established and maturing subfield within MOF science. This foundation not only clarifies the mechanistic origins of phenomena such as gate-opening but enables the deliberate design of next-generation materials in which additional attributes, most notably defects and disorder, can be tuned to yield responsive and adaptive behavior. While traditionally the synthesis of "perfect" MOF crystals was pursued, real crystalline solids inherently possess structural irregularities or defects, defined as local breaks in the regular periodic arrangement of atoms or ions due to missing or dislocated species. Judicious control over these imperfections, known as "defect engineering," provides a powerful strategy beyond mere compositional variation to manipulate MOF structures. Intracrystalline defects, such as missing linker or missing node defects, are specifically targeted for enhancing separation capabilities, contrasting sharply with undesirable intercrystalline defects. [314]

These tailored properties are critical for developing next-generation materials across various domains. In gas separation, defect engineering simultaneously promotes enhanced gas adsorption (increasing the solution coefficient) and accelerated gas transport (increasing the diffusion coefficient), leading to superior performance in MOF-based membranes and Mixed-Matrix Membranes. [245,315] For instance, optimized defect levels can enhance charge separation efficiency, effectively switching on electro or photocatalysis, a functionality typically difficult to achieve in defect-free MOFs. [316] Furthermore, MOF flexibility, defects, and long-range disorder are inherently intertwined. Defects influence mechanical stability, reducing elastic moduli and even introducing anomalous mechanical properties. By exploiting these

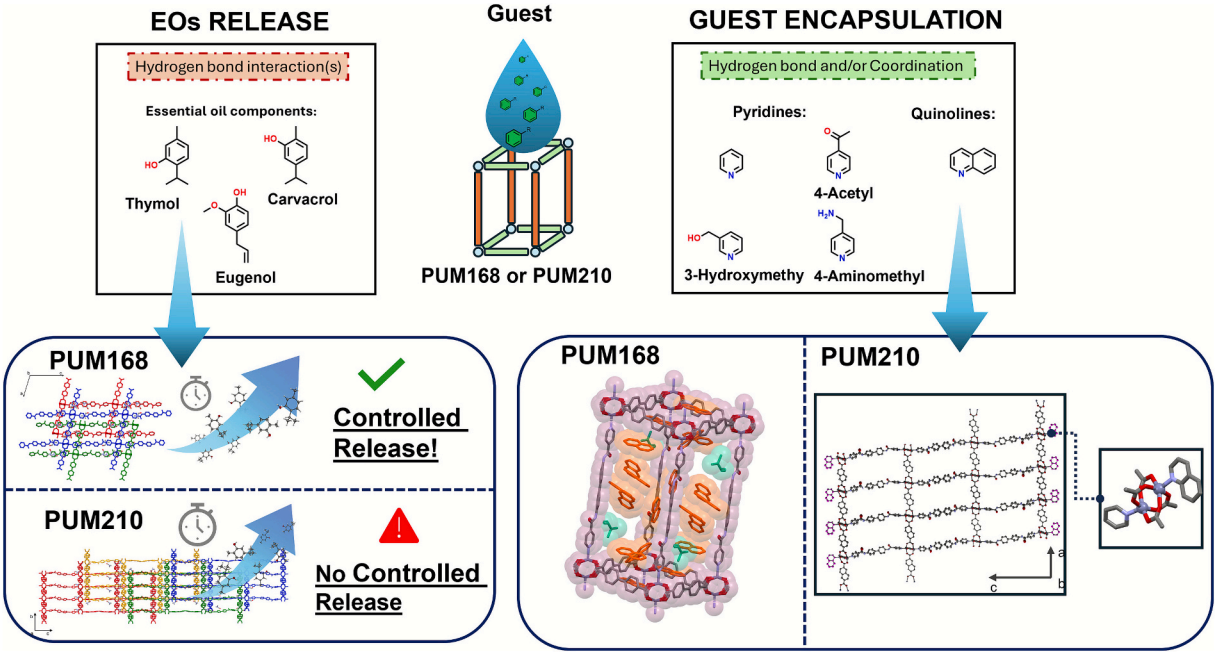


Fig. 17. Representation of the comparative behavior of **PUM168** and **PUM210**, highlighting the effect over inclusion and controlled release of APIs. *Bottom left,* Representation of the different packings of quinoline in **PUM168** and **PUM210**. In the inlets, highlights of the capture of quinoline by weak interactions in **PUM168**, or by coordination in **PUM210**. Reproduced with permission from [311,313].

relationships, defect engineering provides a comprehensive platform for tailoring MOF properties, holding great promise for innovative industrial applications. [317]

The possibility of building next-generation materials with tunable and foreseeable properties based on precise modification to their structure and defects, implies a few challenges that have been tackled in a number of important and seminal works. One of the foremost issues is scalable and reproducible synthesis. Many flexible MOFs require precise conditions to form correctly, and slight variations in temperature, solvent purity, or assembly kinetics can lead to defects or altered flexibility profiles. Economic and environmental factors also play a role. The cost of linkers, solvents, and post-synthetic treatments can be high, and greener, more efficient production routes are needed. Scaling these syntheses from milligram lab batches to kilogram- or ton-scale production without compromising quality remains a major hurdle. Regarding precise syntheses of MOFs, new methodologies are being tested. Mechanochemical synthesis enables rapid, scalable, and solvent-free production of MOFs by grinding metal salts and organic linkers together. It offers excellent reproducibility, reduced waste, and lower energy use. This approach also facilitates difficult reactions, enhances defect control, and supports greener, more cost-effective MOF manufacturing compared to conventional solvothermal methods. [318,319] Flow chemistry enables continuous, controllable MOF synthesis with precise mixing, temperature, and residence-time control. It improves reproducibility, scalability, and crystal uniformity while reducing batch variability. Flow reactors allow rapid optimization, safer operation at high temperatures or pressures, and seamless scale-up through reactor parallelization, supporting industrial-level MOF production. [320,321]

This ties to a second challenge: predictability and control of flexibility. Many flexible MOFs exhibit complex, sometimes abrupt transitions (such as breathing or gate-opening), and accurately modelling and controlling these behaviors outside controlled lab environments is difficult. *In situ* monitoring techniques, such as Raman spectroscopy or X-ray diffraction, provide real-time insight into MOF nucleation and growth, enabling precise control over reaction conditions and early detection of deviations. This improves reproducibility, especially for flexible or defect-sensitive frameworks. Complementing these tools, standardized characterization metrics including surface area, particle size distribution, crystal morphology, and defect concentration create a common basis for comparing results across laboratories. By harmonizing both synthesis monitoring and post-synthesis evaluation, researchers can better understand structure–property relationships, minimize batch variability, and accelerate the transition of MOF materials from exploratory research to reliable, scalable production. [322,323]

Regulatory, safety, and long-term reliability assessments—including toxicity, lifecycle stability, and recyclability—must be addressed before flexible MOFs can be adopted in sectors such as healthcare or environmental remediation. Given the inherent cost of to tackle those challenges, different computational and experimental strategies might guide the development of these materials. First, *in silico* screening of the properties of novel MOFs, including flexibility, have gained attention in recent years to reduce the cost of an experimental screening. [324–327] Comprehensive studies on thermodynamic stability of these materials and property prediction are now possible. Crucially, machine-learning methodologies are being developed recently to speed up the prediction of novel MOFs with tailored properties. [328–331]

Declaration of competing interest

The authors declare that they have no known competing financial interests or personal relationships that could have appeared to influence the work reported in this paper.

Acknowledgements

This work has benefited from the equipment and framework of the COMP-HUB and COMP-R Initiatives, funded by the "Departments of Excellence" program of the Italian Ministry for University and Research (MIUR, 2018–2022 and MUR, 2023–2027). The funding of MIUR within the PRIN2020 project "NICE-Nature Inspired Crystal Engineering" PRIN2020Y2CZJ2 is acknowledged This work also benefitted from the call – Missione 4 "Istruzione e Ricerca" – Componente 2 – Investimento 1.1 "Fondo per il Programma Nazionale di Ricerca e Progetti di Rilevante Interesse Nazionale (PRIN)" with projects "Crystals4Bees" X4BEES PRIN2022-D53D23010140001 and "FLuorInated PePtidEs for Resumption (FLIPPER)" 202224KAX8. P. P. M. also acknowledges the starting grant from the University of Parma 2023-UNPRCLE-0066646.

Data availability

No data was used for the research described in the article.

References

[1] T. Yamada, K. Otsubo, R. Makiura, H. Kitagawa, Designer coordination polymers: dimensional crossover architectures and proton conduction, Chem. Soc. Rev. 42 (2013) 6655, https://doi.org/10.1039/c3cs60028a.
[2] A. Erxleben, Structures and properties of Zn(II) coordination polymers, Coord. Chem. Rev. 246 (2003) 203–228, https://doi.org/10.1016/S0010-8545(03)00117-6.
[3] F. Novio, J. Simmchen, N. Vázquez-Mera, L. Amorín-Ferré, D. Ruiz-Molina, Coordination polymer nanoparticles in medicine, Coord. Chem. Rev. 257 (2013) 2839–2847, https://doi.org/10.1016/j.ccr.2013.04.022.
[4] N. Hosono, A. Terashima, S. Kusaka, R. Matsuda, S. Kitagawa, Highly responsive nature of porous coordination polymer surfaces imaged by in situ atomic force microscopy, Nat. Chem. 11 (2019) 109–116, https://doi.org/10.1038/s41557-018-0170-0.
[5] S.R. Batten, N.R. Champness, X.-M. Chen, J. Garcia-Martinez, S. Kitagawa, L. Öhrström, M. O'Keeffe, M. Paik Suh, J. Reedijk, Terminology of metal–organic frameworks and coordination polymers (IUPAC Recommendations 2013), Pure Appl. Chem. 85 (2013) 1715–1724, https://doi.org/10.1351/PAC-REC-12-11-20.
[6] K. Biradha, A. Ramanan, J.J. Vittal, Coordination polymers versus metal−organic frameworks, Cryst. Growth Des. 9 (2009) 2969–2970, https://doi.org/10.1021/cg801381p.
[7] T. Vermonden, J. van der Gucht, P. de Waard, A.T.M. Marcelis, N.A.M. Besseling, E.J.R. Sudhölter, G.J. Fleer, M.A. Cohen Stuart, Water-soluble reversible coordination polymers: chains and rings, Macromolecules 36 (2003) 7035–7044, https://doi.org/10.1021/ma030353t.
[8] J. Perego, C.X. Bezuidenhout, S. Bracco, S. Piva, G. Prando, C. Aloisi, P. Carretta, J. Kaleta, T.P. Le, P. Sozzani, A. Daolio, A. Comotti, Benchmark dynamics of dipolar molecular rotors in fluorinated metal-organic frameworks, Angew. Chem. Int. Ed. 62 (2023) e202215893, https://doi.org/10.1002/anie.202215893.
[9] T.M. Reineke, M. Eddaoudi, M. O'Keeffe, O.M. Yaghi, A microporous lanthanide-organic framework, Angew. Chem. Int. Ed. 38 (1999) 2590–2594, https://doi.org/10.1002/(SICI)1521-3773(19990903)38:17<2590::AID-ANIE2590>3.0.CO;2-H.
[10] T.J. Barton, L.M. Bull, W.G. Klemperer, D.A. Loy, B. McEnaney, M. Misono, P. A. Monson, G. Pez, G.W. Scherer, J.C. Vartuli, O.M. Yaghi, Tailored porous materials, Chem. Mater. 11 (1999) 2633–2656, https://doi.org/10.1021/cm9805929.
[11] H. Li, M. Eddaoudi, M. O'Keeffe, O.M. Yaghi, Design and synthesis of an exceptionally stable and highly porous metal-organic framework, Nature 402 (1999) 276–279, https://doi.org/10.1038/46248.
[12] S. Noro, S. Kitagawa, M. Kondo, K. Seki, A. New, Methane adsorbent, porous coordination polymer [{$CuSiF_6$(4,4′-bipyridine)$_2$}n], Angew. Chem. Int. Ed. 39 (2000) 2081–2084, https://doi.org/10.1002/1521-3773(20000616)39:12<2081::AID-ANIE2081>3.0.CO;2-A.
[13] S. Noro, S. Kitagawa, M. Yamashita, T. Wada, New microporous coordination polymer affording guest-coordination sites at channel walls, Chem. Commun. 2 (2002) 222–223, https://doi.org/10.1039/b108695b.
[14] L. Shupletsov, A.C. Schieck, I. Senkovska, V. Bon, S. Kaskel, The use of a dynamic solvent system as a novel approach to sustainable MOF crystallization, Green Chem. 27 (2025) 10218–10233, https://doi.org/10.1039/D5GC01029B.
[15] J. Zhang, G.B. White, M.D. Ryan, A.J. Hunt, M.J. Katz, Dihydrolevoglucosenone (Cyrene) as a green lternative to N,N -Dimethylformamide (DMF) in MOF Synthesis, ACS Sustain. Chem. Eng. 4 (2016) 7186–7192, https://doi.org/10.1021/acssuschemeng.6b02115.
[16] P.A. Julien, C. Mottillo, T. Friščić, Metal–organic frameworks meet scalable and sustainable synthesis, Green Chem. 19 (2017) 2729–2747, https://doi.org/10.1039/C7GC01078H.
[17] S. Kitagawa, R. Kitaura, S. Noro, Functional porous coordination polymers, Angew. Chem. Int. Ed. 43 (2004) 2334–2375, https://doi.org/10.1002/anie.200300610.
[18] S. Kitagawa, K. Uemura, Dynamic porous properties of coordination polymers inspired by hydrogen bonds, Chem. Soc. Rev. 34 (2005) 109, https://doi.org/10.1039/b313997m.

[19] S.-H. Lo, L. Feng, K. Tan, Z. Huang, S. Yuan, K.-Y. Wang, B.-H. Li, W.-L. Liu, G. S. Day, S. Tao, C.-C. Yang, T.-T. Luo, C.-H. Lin, S.-L. Wang, S.J.L. Billinge, K.-L. Lu, Y.J. Chabal, X. Zou, H.-C. Zhou, Rapid desolvation-triggered domino lattice rearrangement in a metal–organic framework, Nat. Chem. 12 (2020) 90–97, https://doi.org/10.1038/s41557-019-0364-0.

[20] O. Erhart, P.A. Georgiev, H. Krautscheid, Desolvation process in the flexible metal–organic framework [cu(me-4py-trz-ia)], adsorption of dihydrogen and related structure responses, CrystEngComm 21 (2019) 6523–6535, https://doi.org/10.1039/C9CE00992B.

[21] S. Kumar, S.K. Mandal, Capturing the structural diversification upon thermal desolvation of a robust metal organic framework via a single-crystal-to-single-crystal transformation, CrystEngComm 17 (2015) 8801–8806, https://doi.org/10.1039/C5CE01116G.

[22] K. Uemura, R. Matsuda, S. Kitagawa, Flexible microporous coordination polymers, J. Solid State Chem. 178 (2005) 2420–2429, https://doi.org/10.1016/j.jssc.2005.05.036.

[23] S. Horike, S. Shimomura, S. Kitagawa, Soft porous crystals, Nat. Chem. 1 (2009) 695–704, https://doi.org/10.1038/nchem.444.

[24] C.J. Kepert, M.J. Rosseinsky, Zeolite-like crystal structure of an empty microporous molecular framework, Chem. Commun. 536 (1999) 375–376, https://doi.org/10.1039/a809746a.

[25] A.P. Ferreira, C. Almeida-Aguiar, S.P.G. Costa, I.C. Neves, Essential oils encapsulated in zeolite structures as delivery systems (EODS): an overview, Molecules 27 (2022) 8525, https://doi.org/10.3390/molecules27238525.

[26] A. Schneemann, V. Bon, I. Schwedler, I. Senkovska, S. Kaskel, R.A. Fischer, Flexible metal–organic frameworks, Chem. Soc. Rev. 43 (2014) 6062–6096, https://doi.org/10.1039/C4CS00101J.

[27] N. Li, J. Pang, F. Lang, X.-H. Bu, Flexible Metal–Organic Frameworks: from local structural design to functional realization, Acc. Chem. Res. 57 (2024) 2279–2292, https://doi.org/10.1021/acs.accounts.4c00253.

[28] E.S. Sanz-Pérez, C.R. Murdock, S.A. Didas, C.W. Jones, Direct capture of CO_2 from ambient air, Chem. Rev. 116 (2016) 11840–11876, https://doi.org/10.1021/acs.chemrev.6b00173.

[29] S. Bureekaew, H. Sato, R. Matsuda, Y. Kubota, R. Hirose, J. Kim, K. Kato, M. Takata, S. Kitagawa, Control of interpenetration for tuning structural flexibility influences sorption properties, Angew, Chemie 122 (2010) 7826–7830, https://doi.org/10.1002/ange.201002259.

[30] H. Furukawa, K.E. Cordova, M. O'Keeffe, O.M. Yaghi, The chemistry and applications of metal-organic frameworks, Science (80-.). 341 (2013) 1–12, https://doi.org/10.1126/science.1230444.

[31] Y. Li, Y. Wang, W. Fan, D. Sun, Flexible metal-organic frameworks for gas storage and separation, Dalton Trans. 51 (2022) 4608–4618, https://doi.org/10.1039/d1dt03842g.

[32] A. Kirchon, L. Feng, H.F. Drake, E.A. Joseph, H.C. Zhou, From fundamentals to applications: a toolbox for robust and multifunctional MOF materials, Chem. Soc. Rev. 47 (2018) 8611–8638, https://doi.org/10.1039/c8cs00688a.

[33] B. Zhang, Y. Zheng, T. Ma, C. Yang, Y. Peng, Z. Zhou, M. Zhou, S. Li, Y. Wang, C. Cheng, Designing MOF nanoarchitectures for electrochemical water splitting, Adv. Mater. 33 (2021), https://doi.org/10.1002/adma.202006042.

[34] Z. Ye, Y. Jiang, L. Li, F. Wu, R. Chen, Rational design of MOF-based materials for next-generation rechargeable batteries, Nano-Micro Lett. 13 (2021) 203, https://doi.org/10.1007/s40820-021-00726-z.

[35] T.-W. Liu, Q. Nguyen, A.B. Dieng, D.A. Gómez-Gualdrón, Diversity-driven, efficient exploration of a MOF design space to optimize MOF properties, Chem. Sci. 15 (2024) 18903–18919, https://doi.org/10.1039/D4SC03609C.

[36] A. Lopatka, Creators of metal–organic frameworks honored with chemistry Nobel, Phys. Today 2025 (2025), https://doi.org/10.1063/pt.jups.hccf.

[37] W. Zhang, O. Kozachuk, R. Medishetty, A. Schneemann, R. Wagner, K. Khaletskaya, K. Epp, R.A. Fischer, Controlled SBU approaches to isoreticular metal-organic framework ruthenium-analogues of HKUST-1, Eur. J. Inorg. Chem. 2015 (2015) 3913–3920, https://doi.org/10.1002/ejic.201500478.

[38] M.J. Kalmutzki, N. Hanikel, O.M. Yaghi, Secondary building units as the turning point in the development of the reticular chemistry of MOFs, Sci. Adv. 4 (2018), https://doi.org/10.1126/sciadv.aat9180.

[39] M. Eddaoudi, D.B. Moler, H. Li, B. Chen, T.M. Reineke, M. O'Keeffe, O.M. Yaghi, Modular chemistry: secondary building units as a sasis for the design of highly porous and robust metal−organic carboxylate frameworks, Acc. Chem. Res. 34 (2001) 319–330, https://doi.org/10.1021/ar000034b.

[40] J. Ha, J.H. Lee, H.R. Moon, Alterations to secondary building units of metal–organic frameworks for the development of new functions, Inorg. Chem. Front. 7 (2020) 12–27, https://doi.org/10.1039/C9QI01119F.

[41] D. Jędrzejowski, M. Pander, W. Nitek, W. Bury, D. Matoga, Turning flexibility into rigidity: stepwise locking of interpenetrating networks in a MOF crystal through click reaction, Chem. Mater. 33 (2021) 7509–7517, https://doi.org/10.1021/acs.chemmater.1c02451.

[42] L. Sarkisov, R.L. Martin, M. Haranczyk, B. Smit, On the flexibility of Metal–Organic Frameworks, J. Am. Chem. Soc. 136 (2014) 2228–2231, https://doi.org/10.1021/ja411673b.

[43] J. Andreo, E. Priola, G. Alberto, P. Benzi, D. Marabello, D.M. Proserpio, C. Lamberti, E. Diana, Autoluminescent Metal–Organic Frameworks (MOFs): self-photoemission of a highly stable thorium MOF, J. Am. Chem. Soc. 140 (2018) 14144–14149, https://doi.org/10.1021/jacs.8b07113.

[44] J. Perego, I. Villa, A. Pedrini, E.C. Padovani, R. Crapanzano, A. Vedda, C. Dujardin, C.X. Bezuidenhout, S. Bracco, P.E. Sozzani, A. Comotti, L. Gironi, M. Beretta, M. Salomoni, N. Kratochwil, S. Gundacker, E. Auffray, F. Meinardi, A. Monguzzi, Composite fast scintillators based on high-Z fluorescent metal–organic framework nanocrystals, Nat. Photonics 15 (2021) 393–400, https://doi.org/10.1038/s41566-021-00769-z.

[45] F.A. Almeida Paz, J. Klinowski, S.M.F. Vilela, J.P.C. Tomé, J.A.S. Cavaleiro, J. Rocha, Ligand design for functional metal–organic frameworks, Chem. Soc. Rev. 41 (2012) 1088–1110, https://doi.org/10.1039/C1CS15055C.

[46] D. Zhao, D.J. Timmons, D. Yuan, H.-C. Zhou, Tuning the topology and functionality of metal−organic frameworks by ligand design, Acc. Chem. Res. 44 (2011) 123–133, https://doi.org/10.1021/ar100112y.

[47] M. Eddaoudi, J. Kim, N. Rosi, D. Vodak, J. Wachter, M. O'Keeffe, O.M. Yaghi, Systematic design of pore size and functionality in isoreticular MOFs and their application in methane storage, Science 80 (2002) 469–472, https://doi.org/10.1126/science.1067208.

[48] W. Morris, R.E. Taylor, C. Dybowski, O.M. Yaghi, M.A. Garcia-Garibay, Framework mobility in the metal–organic framework crystal IRMOF-3: evidence for aromatic ring and amine rotation, J. Mol. Struct. 1004 (2011) 94–101, https://doi.org/10.1016/j.molstruc.2011.07.037.

[49] H. Ju, S. Kim, J.H. Jung, S.S. Lee, A series of entangled MOFs constructed from flexible dipyridyl piperazine and rigid dicarboxylate: interpenetration, self-penetration, and polycatenation, CrystEngComm 24 (2022) 7906–7914, https://doi.org/10.1039/D2CE00745B.

[50] S.B. Choi, H. Furukawa, H.J. Nam, D. Jung, Y.H. Jhon, A. Walton, D. Book, M. O'Keeffe, O.M. Yaghi, J. Kim, Reversible interpenetration in a Metal–Organic Framework triggered by ligand removal and addition, Angew. Chem. 124 (2012) 8921–8925, https://doi.org/10.1002/ange.201202925.

[51] M. Singh, S. Neogi, Largely entangled diamondoid framework with high-density urea and divergent metal nodes for selective scavenging of CO_2 and molecular dimension-mediated size-exclusive H-bond donor catalysis, Inorg. Chem. 62 (2023) 871–884, https://doi.org/10.1021/acs.inorgchem.2c03684.

[52] H.-L. Jiang, T.A. Makal, H.-C. Zhou, Interpenetration control in metal–organic frameworks for functional applications, Coord. Chem. Rev. 257 (2013) 2232–2249, https://doi.org/10.1016/j.ccr.2013.03.017.

[53] Y. Fan, H. Li, Z. Ji, J. Liu, M. Wu, Syntheses, structures and photoluminescence of three Zn(II) coordination polymers based on N-containing heterocyclic ligand and varied auxiliary ligands, Inorg. Chem. Commun. 102 (2019) 229–232, https://doi.org/10.1016/j.inoche.2019.02.037.

[54] H. Ju, Y. Habata, S.S. Lee, Temperature-dependent supramolecular isomeric Zn (II)-metal–organic frameworks and their guest exchange, Cryst. Growth Des. 20 (2020) 4640–4648, https://doi.org/10.1021/acs.cgd.0c00443.

[55] Z. Shi, Z. Pan, H. Jia, S. Chen, L. Qin, H. Zheng, Zn(II)/cd(II) terephthalate coordination polymers incorporating bi-, tri-, and tetratopic phenylamine derivatives: crystal structures and photoluminescent properties, Cryst. Growth Des. 16 (2016) 2747–2755, https://doi.org/10.1021/acs.cgd.6b00056.

[56] Y.-F. Hsu, C.-H. Lin, J.-D. Chen, J.-C. Wang, A novel interpenetrating diamondoid network from self-assembly of N,N′ -Di(4-pyridyl)adipoamide and copper sulfate: an unusual 12-fold, [6+6] Mode, Cryst. Growth Des. 8 (2008) 1094–1096, https://doi.org/10.1021/cg701209k.

[57] H. Wu, J. Yang, Z.-M. Su, S.R. Batten, J.-F. Ma, An exceptional 54-fold interpenetrated coordination polymer with 10 3 -srs network topology, J. Am. Chem. Soc. 133 (2011) 11406–11409, https://doi.org/10.1021/ja202303b.

[58] Y. Sakata, S. Furukawa, M. Kondo, K. Hirai, N. Horike, Y. Takashima, H. Uehara, N. Louvain, M. Meilikhov, T. Tsuruoka, S. Isoda, W. Kosaka, O. Sakata, S. Kitagawa, Shape-memory nanopores induced in coordination frameworks by crystal downsizing, Science (80-.). 339 (2013) 193–196, https://doi.org/10.1126/science.1231451.

[59] R. Kitaura, K. Fujimoto, S. Noro, M. Kondo, S. Kitagawa, A pillared-layer coordination polymer network displaying hysteretic sorption: $[Cu_2(pzdc)_2(dpyg)]_n$ (pzdc=pyrazine-2,3-dicarboxylate; dpyg=1,2-di(4-pyridyl) glycol), Angew. Chem. Int. Ed. 41 (2002) 133–135, https://doi.org/10.1002/1521-3773(20020104)41:1<133::AID-ANIE133>3.0.CO;2-R.

[60] J. Hafizovic, M. Bjørgen, U. Olsbye, P.D.C. Dietzel, S. Bordiga, C. Prestipino, C. Lamberti, K.P. Lillerud, The inconsistency in adsorption properties and powder XRD data of MOF-5 is rationalized by framework interpenetration and the presence of organic and inorganic species in the nanocavities, J. Am. Chem. Soc. 129 (2007) 3612–3620, https://doi.org/10.1021/ja0675447.

[61] H. Kim, S. Das, M.G. Kim, D.N. Dybtsev, Y. Kim, K. Kim, Synthesis of phase-pure interpenetrated MOF-5 and its gas sorption properties, Inorg. Chem. 50 (2011) 3691–3696, https://doi.org/10.1021/ic200054b.

[62] D.T. McGrath, V.A. Downing, M.J. Katz, Investigating the crystal engineering of the pillared paddlewheel metal–organic framework Zn_2 (NH_2 BDC)$_2$ DABCO, CrystEngComm 20 (2018) 6082–6087, https://doi.org/10.1039/C8CE00848E.

[63] T.K. Prasad, M.P. Suh, Control of interpenetration and gas-sorption properties of Metal–Organic Frameworks by a simple change in ligand design, Chem. – A Eur. J. 18 (2012) 8673–8680, https://doi.org/10.1002/chem.201200456.

[64] D. Bara, C. Wilson, M. Mörtel, M.M. Khusniyarov, S. Ling, B. Slater, S. Sproules, R. S. Forgan, Kinetic control of interpenetration in Fe–biphenyl-4,4′-dicarboxylate Metal–Organic Frameworks by coordination and oxidation modulation, J. Am. Chem. Soc. 141 (2019) 8346–8357, https://doi.org/10.1021/jacs.9b03269.

[65] D.N. Jordan, P.G. Straßburg, D. Woschko, L.M. Carrella, L.P. Cuignet, K. Eickmeier, R. Dronskowski, Y. Garcia, E. Rentschler, C. Janiak, Interpenetration phenomena via anion template effects in Fe(II) and co(II) coordination networks with a bis-(1,2,4-triazole) ligand, Polymers (Basel). 15 (2023) 3286, https://doi.org/10.3390/polym15153286.

[66] X.-S. Wang, S. Ma, D. Sun, S. Parkin, H.-C. Zhou, A mesoporous metal−organic framework with permanent porosity, J. Am. Chem. Soc. 128 (2006) 16474–16475, https://doi.org/10.1021/ja066616r.

[67] Y.-Q. Zhang, L. Liu, W.-Z. Li, B.-H. Wu, C.-N. Li, J.-Q. Chu, Z.-B. Han, Solvent-induced in(III)-MOFs with controllable interpenetration degree performing high-efficiency separation of CO_2/N_2 and CO_2 /CH_4, Inorg. Chem. 63 (2024) 7705–7713, https://doi.org/10.1021/acs.inorgchem.3c04602.

[68] S. Bureekaew, H. Sato, R. Matsuda, Y. Kubota, R. Hirose, J. Kim, K. Kato, M. Takata, S. Kitagawa, Control of interpenetration for tuning structural flexibility influences sorption properties, Angew. Chem. Int. Ed. 49 (2010) 7660–7664, https://doi.org/10.1002/anie.201002259.

[69] J. Zhang, L. Wojtas, R.W. Larsen, M. Eddaoudi, M.J. Zaworotko, Temperature and concentration control over interpenetration in a metal−organic material, J. Am. Chem. Soc. 131 (2009) 17040–17041, https://doi.org/10.1021/ja906911q.

[70] Y. Qi, H. Xu, X. Li, B. Tu, Q. Pang, X. Lin, E. Ning, Q. Li, Structure transformation of a luminescent pillared-layer Metal–Organic Framework caused by point defects accumulation, Chem. Mater. 30 (2018) 5478–5484, https://doi.org/10.1021/acs.chemmater.8b02511.

[71] R.K. Deshpande, J.L. Minnaar, S.G. Telfer, Thermolabile groups in Metal–Organic Frameworks: suppression of network interpenetration, post-synthetic cavity expansion, and protection of reactive functional groups, Angew. Chem. Int. Ed. 49 (2010) 4598–4602, https://doi.org/10.1002/anie.200905960.

[72] G.J. Halder, S.M. Neville, C.J. Kepert, A highly distorted (10,3)-a coordination framework constructed from alternating T-shaped and trigonal nodes, CrystEngComm 7 (2005) 266, https://doi.org/10.1039/b503352g.

[73] M.A. Withersby, A.J. Blake, N.R. Champness, P.A. Cooke, P. Hubberstey, M. Schröder, Assembly of a three-dimensional polyknotted coordination polymer, J. Am. Chem. Soc. 122 (2000) 4044–4046, https://doi.org/10.1021/ja991698n.

[74] C.-Y. Su, A.M. Goforth, M.D. Smith, H.-C. Zur Loye, Assembly of large simple 1D and rare polycatenated 3D molecular ladders from T-shaped building blocks containing a new, long N,N′-bidentate ligand, Chem. Commun. (2004) 2158–2159, https://doi.org/10.1039/B406126H.

[75] Y.-B. Dong, R.C. Layland, N.G. Pschirer, M.D. Smith, U.H.F. Bunz, H.-C. Zur Loye, New crystalline frameworks formed from 1,2-bis(4-pyridyl)ethyne and $co(NO_3)_2$: interpenetrating molecular ladders and an unexpected molecular parquet pattern from T-shaped building blocks, Chem. Mater. 11 (1999) 1413–1415, https://doi.org/10.1021/cm990082u.

[76] J.-Q. Liu, Y.-Y. Wang, P. Liu, Z. Dong, Q.-Z. Shi, S.R. Batten, Two coordination polymers displaying unusual threefold 1D→1D and threefold 2D→3D interpenetration topologies, CrystEngComm 11 (2009) 1207, https://doi.org/10.1039/b905427h.

[77] Y.-P. Li, J.-H. Zhang, X.-X. Zhang, S.-J. Liu, 2D → 3D polycatenated Zn(II) metal–organic framework with good chemical stability as a fluorescent sensor toward salicylaldehyde, acetylacetone and H2 PO4−, CrystEngComm 25 (2023) 6424–6433, https://doi.org/10.1039/D3CE00961K.

[78] M. Yang, F. Jiang, Q. Chen, Y. Zhou, R. Feng, K. Xiong, M. Hong, Solvent and temperature influence structural variation from nonporous 2D → 3D parallel polycatenation to 3D microporous metal–organic framework, CrystEngComm 13 (2011) 3971, https://doi.org/10.1039/c1ce05263b.

[79] R. Rajak, M. Saraf, A. Mohammad, S.M. Mobin, Design and construction of a ferrocene based inclined polycatenated co-MOF for supercapacitor and dye adsorption applications, J. Mater. Chem. A 5 (2017) 17998–18011, https://doi.org/10.1039/C7TA03773B.

[80] F.-J. Liu, D. Sun, H.-J. Hao, R.-B. Huang, L.-S. Zheng, 3D → 3D interpenetrated and 2D → 3D polycatenated ag(I) networks constructed from 1,4-bis(2-methylimidazol-1-ylmethyl)benzene and dicarboxylates, CrystEngComm 14 (2012) 379–382, https://doi.org/10.1039/C1CE06356A.

[81] L. Carlucci, G. Ciani, D.M. Proserpio, Polycatenation, polythreading and polyknotting in coordination network chemistry, Coord. Chem. Rev. 246 (2003) 247–289, https://doi.org/10.1016/S0010-8545(03)00126-7.

[82] X. Kuang, X. Wu, R. Yu, J.P. Donahue, J. Huang, C.-Z. Lu, Assembly of a metal–organic framework by sextuple intercatenation of discrete adamantane-like cages, Nat. Chem. 2 (2010) 461–465, https://doi.org/10.1038/nchem.618.

[83] N. Faaizatunnisa, R. Ediati, E.N.M. Yusof, A. Fadlan, K. Karelius, U. Kulsum, M. N. Ariesta, The mixed-ligand strategy for structural modification of MOF materials to enhance the photocatalytic degradation and adsorption of organic pollutants: a review, Nano-Struct. ano-Objects 40 (2024) 101366, https://doi.org/10.1016/j.nanoso.2024.101366.

[84] H. Dong, S. Liu, Q. Liu, Y. Li, Z. Xu, Y. Li, Q. Wei, Mixed-ligand-regulated self-enhanced luminous Eu-MOF as an ECL signal probe for an oriented antibody-decorated biosensing platform, Anal. Chem. 94 (2022) 12852–12859, https://doi.org/10.1021/acs.analchem.2c02852.

[85] Y. Bae, K.L. Mulfort, H. Frost, P. Ryan, S. Punnathanam, L.J. Broadbelt, J.T. Hupp, R.Q. Snurr, Separation of CO_2 from CH_4 using mixed-ligand metal−organic frameworks, Langmuir 24 (2008) 8592–8598, https://doi.org/10.1021/la800555x.

[86] X.-B. Yin, Y.-Q. Sun, H. Yu, Y. Cheng, C. Wen, Design and multiple applications of mixed-ligand Metal–Organic Frameworks with dual emission, Anal. Chem. 94 (2022) 4938–4947, https://doi.org/10.1021/acs.analchem.1c02949.

[87] S. Mahajan, M. Lahtinen, 3D zinc–organic frameworks based on mixed thiophene dicarboxylate and 4-amino-3,5-bis(4-pyridyl)-1,2,4-triazole linkers: syntheses, structural diversity, and single-crystal-to-single-crystal transformations, Cryst. Growth Des. 24 (2024) 747–762, https://doi.org/10.1021/acs.cgd.3c01172.

[88] P. Kanoo, T.K. Maji, Construction of a 2D rectangular grid and 3D diamondoid interpenetrated frameworks and their functionalities by changing the second spacers, Eur. J. Inorg. Chem. 2010 (2010) 3762–3769, https://doi.org/10.1002/ejic.201000362.

[89] A. Halder, A. Maiti, S. Dinda, B. Bhattacharya, D. Ghoshal, Unraveling the role of structural dynamism in metal organic frameworks (MOF) for excited-state intramolecular proton transfer (ESIPT) driven water sensing, Cryst. Growth Des. 21 (2021) 6110–6118, https://doi.org/10.1021/acs.cgd.1c00446.

[90] O. Saengsawang, V. Vchirawongkwin, T. Remsungnen, M. Wiebcke, S. Fritzsche, S. Hannongbua, Rotational flexibility of bridging ligands in paddle–wheel layer–pillar metal–organic frameworks studied by quantum calculations, Comput, Theor. Chem. 1001 (2012) 33–38, https://doi.org/10.1016/j.comptc.2012.10.006.

[91] M.R. Ryzhikov, S.G. Kozlova, Understanding structural flexibility of the paddle-wheel Zn-SBU motif in MOFs: influence of pillar ligands, Phys. Chem. Chem. Phys. 21 (2019) 11977–11982, https://doi.org/10.1039/C9CP02483B.

[92] S. Ghosh, G. Pahari, A. Maiti, S. Dinda, D. Ghoshal, Designing of three mixed ligand MOFs in searching of length induced flexibility in ligand for the creation of interpenetration, Polyhedron 218 (2022) 115763, https://doi.org/10.1016/j.poly.2022.115763.

[93] Z. Lin, J. Lu, Z. Lin, J. Lu, Metal–organic frameworks based on flexible ligands (FL-MOFs): structures and applications, Chem. Soc. Rev. 43 (2014) 5867–5895, https://doi.org/10.1039/C3CS60483G.

[94] X. Liu, C. Lu, Structural design and applications of pillar-layered MOFs, Chem. Commun. 61 (2025) 17735–17750, https://doi.org/10.1039/d5cc03773e.

[95] Y. Li, Z. Mo, X. Zhang, K. Zheng, D. Zhou, J. Zhang, A metal−ligand layer compatible with various types of pillars for new porous coordination polymers, Cryst. Growth Des. 20 (2020) 7021–7026, https://doi.org/10.1021/acs.cgd.0c01078.

[96] Y. Lin, Y. Zhang, J. Zhang, X. Chen, Pillaring Zn-triazolate layers with flexible aliphatic dicarboxylates into three-dimensional metal−organic frameworks, Cryst. Growth Des. 8 (2008) 3673–3679, https://doi.org/10.1021/cg800289c.

[97] S. Meng, M. Xu, H. Guan, C. Chen, P. Cai, B. Dong, W. Tan, Y. Gu, W. Tang, L. Xie, Anisotropic flexibility and rigidification in a TPE-based Zr-MOFs with scu topology, Nat. Commun. 14 (2023) 5347, https://doi.org/10.1038/s41467-023-41055-6.

[98] Shing Bo Peh, Avishek Karmakar, Dan Zhao, Multiscale design of flexible Metal–Organic Frameworks, Trends Chem. 2 (2020) 199–213, https://doi.org/10.1016/j.trechm.2019.10.007.

[99] Y.J. Colón, S. Furukawa, Understanding the role of linker flexibility in soft porous coordination polymers, Mol. Syst. Des. Eng 5 (2020) 284–293, https://doi.org/10.1039/c9me00117d.

[100] J. Sun, Y. Zhou, Q. Fang, Z. Chen, L. Weng, G. Zhu, Construction of 3D layer-pillared homoligand coordination polymers from a 2D layered precursor, Inorg. Chem. 45 (2006) 8677–8684, https://doi.org/10.1021/ic0612303.

[101] M.O.F. Crystallization, E. Stavitski, M. Goesten, J. Juan-alcaçiz, A. Martinez-joaristi, P. Serra, A.V. Petukhov, J. Gascon, F. Kapteijn, Kinetic control of metal – organic framework crystallization investigated by time-resolved in situ X-ray scattering, Angew. Chemie 50 (2011) 9624–9628, https://doi.org/10.1002/anie.201101757.

[102] O.M. Linder-patton, W.M. Bloch, C.J. Coghlan, K. Sumida, Particle size effects in the kinetic trapping of a structurally-locked form of a flexible MOF, CrystEngComm 18 (2016) 4172–4179, https://doi.org/10.1039/c6ce00082g.

[103] M.C. Wasson, J. Lyu, T. Islamoglu, O.K. Farha, Linker competition within a metal−organic framework for topological insights, Inorg. Chem. 58 (2019) 1513–1517, https://doi.org/10.1021/acs.inorgchem.8b03025.

[104] P. Smart, G.M. Espallargas, L. Brammer, Competition between coordination network and halogen bond network formation: towards halogen-bond functionalised network materials using copper-iodobenzoate units, CrystEngComm 10 (2008) 1335–1344, https://doi.org/10.1039/b806765a.

[105] M. Kim, J.S. Oh, B.H. Kim, A.Y. Kim, K.C. Park, J. Mun, G. Gupta, C.Y. Lee, Enhanced photocatalytic performance of nanosized mixed-ligand metal−organic frameworks through sequential energy and electron transfer process, Inorg. Chem. 59 (2020) 12947–12953, https://doi.org/10.1021/acs.inorgchem.0c02079.

[106] Z. Han, Y. Yang, J. Rushlow, R. Liang, H. Zhou, Sequential linker installation in metal−organic frameworks, Acc. Chem. Res. 57 (2024) 3217–3226, https://doi.org/10.1021/acs.accounts.4c00564.

[107] S. Yuan, W. Lu, Y. Chen, Q. Zhang, T. Liu, D. Feng, X. Wang, Sequential linker installation: precise placement of functional groups in multivariate metal−organic frameworks, J. Am. Chem. Soc. 137 (2015) 3177–3180, https://doi.org/10.1021/ja512762r.

[108] S.K.A. Schneemann, V. Bon, I. Schwedler, I. Senkovska, R.A. Fischer, Flexible metal–organic frameworks, Chem. Soc. Rev. 43 (2014) 6062–6096, https://doi.org/10.1039/c4cs00101j.

[109] G. Kumari, N.R. Patil, S. Bhadram, R. Haldar, Understanding guest and pressure-induced porosity through structural transition in flexible interpenetrated MOF by Raman spectroscopy, J. Raman Spectrosc. 47 (2016) 149–155, https://doi.org/10.1002/jrs.4766.

[110] J. Perego, S. Bracco, M. Negroni, C.X. Bezuidenhout, G. Prando, P. Carretta, A. Comotti, P. Sozzani, Fast motion of molecular rotors in metal–organic framework struts at very low temperatures, Nat. Chem. 12 (2020) 845–851, https://doi.org/10.1038/s41557-020-0495-3.

[111] P. Rani, A. Husain, K.K. Bhasin, G. Kumar, Zinc(II)-MOF: a versatile luminescent sensor for selective molecular recognition of flame retardants and antibiotics, Inorg. Chem. 63 (2024) 3486–3498, https://doi.org/10.1021/acs.inorgchem.3c04214.

[112] Z. Chang, D. Yang, J. Xu, T. Hu, X. Bu, Flexible Metal–Organic Frameworks: recent advances and potential applications, Adv. Mater. 27 (2015) 5432–5441, https://doi.org/10.1002/adma.201501523.

[113] M. Trueman, R.J.S. Pooley, A.R.B.J. Lutton-gething, A. Hasija, G.F.S. Whitehead, S.J.O. Shea, M.W. Anderson, M.P. Attfield, Nanoscale flexing mechanism of a

metal−organic framework determined by etomic force microscopy, J. Am. Chem. Soc. 147 (2025) 17201–17208, https://doi.org/10.1021/jacs.5c02868.
[114] M. Gelpi, J. García-ben, S. Rodríguez-hermida, J. López-beceiro, R. Artiaga, Á. Baaliña, M. Romero-gómez, J. Romero-gómez, S. Zaragoza, J. Salgado-beceiro, J. Walker, C.J. Mcmonagle, S. Castro-garcía, M. Sánchez-andújar, M.A. Señarís-rodríguez, J.M. Bermúdez-garcía, Empowering CO2 eco-refrigeration with colossal breathing-caloric-like effects in MOF-508b, Adv. Mater. 36 (2024) 2310499, https://doi.org/10.1002/adma.202310499.
[115] J. Garc, L. Jorge, R. Artiaga, J. Salgado-beceiro, I. Delgado-ferreiro, J. Manuel, Discovery of colossal breathing-caloric effect under low applied pressure in the hybrid organic−inorganic MIL-53 (Al) material, Chem. Mater. 34 (2022) 3323–3332, https://doi.org/10.1021/acs.chemmater.2c00137.
[116] Z. Zhou, X. Xing, C. Tian, W. Wei, D. Li, F. Hu, S. Du, A multifunctional nanocage-based MOF with tri- and tetranuclear zinc cluster secondary building units, Sci. Rep. 8 (2018) 3117, https://doi.org/10.1038/s41598-018-21382-1.
[117] J. Wang, Y. Fan, H. Lee, C. Yi, C. Cheng, X. Zhao, M. Yang, Ultrasmall Metal–Organic Framework Zn-MOF-74 nanodots: size-controlled synthesis and application for highly selective colorimetric sensing of Iron(III) in aqueous solution, ACS Appl. Nano Mater. 1 (2018) 3747–3753, https://doi.org/10.1021/acsanm.8b01083.
[118] L. Chen, J.-W. Ye, H.-P. Wang, M. Pan, S.-Y. Yin, Z.-W. Wei, L.-Y. Zhang, K. Wu, Y.-N. Fan, C.-Y. Su, Ultrafast water sensing and thermal imaging by a metal-organic framework with switchable luminescence, Nat. Commun. 8 (2017) 15985, https://doi.org/10.1038/ncomms15985.
[119] J. Venezuela, M.S. Dargusch, The influence of alloying and fabrication techniques on the mechanical properties, biodegradability and biocompatibility of zinc: a comprehensive review, Acta Biomater. 87 (2019) 1–40, https://doi.org/10.1016/j.actbio.2019.01.035.
[120] D. Zhu, I. Cockerill, Y. Su, Z. Zhang, J. Fu, K.-W. Lee, J. Ma, C. Okpokwasili, L. Tang, Y. Zheng, Y.-X. Qin, Y. Wang, Mechanical strength, biodegradation, and in vitro and in vivo biocompatibility of Zn biomaterials, ACS Appl. Mater. Interfaces 11 (2019) 6809–6819, https://doi.org/10.1021/acsami.8b20634.
[121] S. Rojas, F.J. Carmona, C.R. Maldonado, P. Horcajada, T. Hidalgo, C. Serre, J.A. R. Navarro, E. Barea, Nanoscaled zinc pyrazolate Metal–Organic Frameworks as drug-delivery systems, Inorg. Chem. 55 (2016) 2650–2663, https://doi.org/10.1021/acs.inorgchem.6b00045.
[122] R. Safdar Ali, H. Meng, Z. Li, Zinc-based metal-organic frameworks in drug delivery, cell imaging, and sensing, Molecules 27 (2021) 100, https://doi.org/10.3390/molecules27010100.
[123] I. Cockerill, Y. Su, S. Sinha, Y.-X. Qin, Y. Zheng, M.L. Young, D. Zhu, Porous zinc scaffolds for bone tissue engineering applications: a novel additive manufacturing and casting approach, Mater. Sci. Eng. C 110 (2020) 110738, https://doi.org/10.1016/j.msec.2020.110738.
[124] P. Barak, P.A. Helmke, The Chemistry of Zinc, in: Zinc Soils Plants, Springer Netherlands, Dordrecht, 1993, pp. 1–13, https://doi.org/10.1007/978-94-011-0878-2_1.
[125] N.K. Daud, CO2 adsorption performance of AC and Zn-MOF for the use of carbon capture and sequestration (CCS), Mater. Today Proc. (2023), https://doi.org/10.1016/j.matpr.2023.03.231.
[126] Y. Jin, F. Li, Y. Zheng, W. Zhang, S. Wang, W. Yan, B. Yu, J. Zhang, Post-combustion carbon capture and conversion using advanced materials of Zn-based metal-organic frameworks: a mini review, front, Energy 19 (2025) 300–311, https://doi.org/10.1007/s11708-025-1009-1.
[127] A.D. Burrows, M.F. Mahon, P.R. Raithby, A.J. Warren, S.J. Teat, J.E. Warren, The effect of carboxylate and N,N′-ditopic ligand lengths on the structures of copper and zinc coordination polymers, CrystEngComm 14 (2012) 3658, https://doi.org/10.1039/c2ce06709a.
[128] A.M. Cheplakova, K.A. Kovalenko, D.G. Samsonenko, A.S. Vinogradov, V. M. Karpov, V.E. Platonov, V.P. Fedin, Structural diversity of zinc(II) coordination polymers with octafluorobiphenyl-4,4′-dicarboxylate based on mononuclear, paddle wheel and cuboidal units, CrystEngComm 21 (2019) 2524–2533, https://doi.org/10.1039/C9CE00073A.
[129] K.O. Kongshaug, H. Fjellvåg, Coordination polymers constructed from paddle-wheel building units, J. Solid State Chem. 166 (2002) 213–218, https://doi.org/10.1006/jssc.2002.9584.
[130] T.-Y. Xu, J.-M. Li, Y.-H. Han, A.-R. Wang, K.-H. He, Z.-F. Shi, A new 3D four-fold interpenetrated dia-like luminescent Zn(<scp>ii</scp>)-based metal–organic framework: the sensitive detection of Fe^{3+}, $Cr_2O_7^{2-}$, and CrO_4^{2-} in water, and nitrob, New J. Chem. 44 (2020) 4011–4022, https://doi.org/10.1039/C9NJ06056A.
[131] C.-C. Wang, S.-Y. Ke, C.-W. Cheng, Y.-W. Wang, H.-S. Chiu, Y.-C. Ko, N.-K. Sun, M.-L. Ho, C.-K. Chang, Y.-C. Chuang, G.-H. Lee, Four mixed-ligand Zn(II) three-dimensional metal-organic frameworks: synthesis, structural diversity, and photoluminescent property, Polymers (Basel). 9 (2017) 644, https://doi.org/10.3390/polym9120644.
[132] W.-J. Gu, J.-Z. Gu, M.V. Kirillova, A.M. Kirillov, Zn(II) metal–organic architectures from ether-bridged tetracarboxylate linkers: assembly, structural variety and catalytic features, CrystEngComm 24 (2022) 5297–5306, https://doi.org/10.1039/D2CE00722C.
[133] X.-Y. Tian, H.-L. Zhou, X.-W. Zhang, C. Wang, D.-D. Zhou, X.-M. Chen, J.-P. Zhang, Tuning the packing, interpenetration, and porosity of two-dimensional networks by metal ions and ligand side groups, Inorg. Chem. Front. 7 (2020) 3424–3430, https://doi.org/10.1039/D0QI00642D.
[134] O.R. Evans, R.-G. Xiong, Z. Wang, G.K. Wong, W. Lin, Crystal engineering of acentric diamondoid metal-organic coordination networks, Angew. Chem. Int. Ed. 38 (1999) 536–538, https://doi.org/10.1002/(SICI)1521-3773(19990215)38:4<536::AID-ANIE536>3.0.CO;2-3.
[135] D.-C. Hou, G.-Y. Jiang, F. Wang, Polycatenated bilayer structure containing honeycomb-like 63 layers, J. Inorg. Organomet. Polym. Mater. 23 (2013) 766–770, https://doi.org/10.1007/s10904-012-9815-4.
[136] W. Jiang, J. Yang, G. Yan, S. Zhou, B. Liu, Y. Qiao, T. Zhou, J. Wang, G. Che, A novel 3-fold interpenetrated dia metal-organic framework as a heterogeneous catalyst for CO_2 cycloaddition, Inorg. Chem. Commun. 113 (2020) 107770, https://doi.org/10.1016/j.inoche.2020.107770.
[137] X.-Y. Li, C.-X. Han, K.-F. Yue, Y.-L. Liu, C.-S. Zhou, Y.-F. Hou, T. He, N. Yan, Syntheses, structures and properties of three 4-fold interpenetration coordination polymers based on two different dia interpenetrating modes, Polyhedron 87 (2015) 156–162, https://doi.org/10.1016/j.poly.2014.11.019.
[138] L. Wen, L. Zhou, B. Zhang, X. Meng, H. Qu, D. Li, Multifunctional amino-decorated metal–organic frameworks: nonlinear-optic, ferroelectric, fluorescence sensing and photocatalytic properties, J. Mater. Chem. 22 (2012) 22603, https://doi.org/10.1039/c2jm34349e.
[139] X.-M. Lian, W. Zhao, X.-L. Zhao, Topological evolution and photoluminescent properties of a series of divalent zinc-based metal–organic frameworks tuned via ancillary ligating spacers, J. Solid State Chem. 200 (2013) 265–270, https://doi.org/10.1016/j.jssc.2013.01.004.
[140] S. Parshamoni, S. Konar, Selective CO2 adsorption in four zinc(II)-based metal organic frameworks constructed using a rigid N,N′-donor linker and various dicarboxylate ligands, CrystEngComm 18 (2016) 4395–4404, https://doi.org/10.1039/c5ce02542g.
[141] X. Gao, X. Wang, M. Feng, M. Yang, Q. Zhang, An excellent water-stable 3D Zn-MOF with 8-fold interpenetrated diamondoid topology showing "turn-on/turn-off" luminescent detection of Al 3+ and SNT in aqueous media, RSC Adv. 11 (2021) 32622–32629, https://doi.org/10.1039/D1RA06590D.
[142] L. Dang, J. Li, S. Liu, M. Luo, F. Luo, A new acylamide MOF showing uncommon ten-fold interpenetration, Inorg. Chem. Commun. 45 (2014) 30–32, https://doi.org/10.1016/j.inoche.2014.03.030.
[143] K. Tomar, R. Rajak, S. Sanda, S. Konar, Synthesis and characterization of polyhedral-based Metal–Organic Frameworks using a flexible bipyrazole ligand: topological analysis and sorption property studies, Cryst. Growth Des. 15 (2015) 2732–2741, https://doi.org/10.1021/acs.cgd.5b00056.
[144] N. Gcwensa, N. Chatterjee, C.L. Oliver, Interchanged hysteresis for carbon dioxide and water vapor sorption in a pair of water-stable, breathing, isoreticular, 2-periodic, Zn(II)-based mixed-ligand Metal–Organic Frameworks, Inorg. Chem. 58 (2019) 2080–2088, https://doi.org/10.1021/acs.inorgchem.8b03148.
[145] B.-Q. Ma, K.L. Mulfort, J.T. Hupp, Microporous pillared paddle-wheel frameworks based on mixed-ligand coordination of zinc ions, Inorg. Chem. 44 (2005) 4912–4914, https://doi.org/10.1021/ic050452i.
[146] W. Wang, Y. Wen, J. Su, H. Ma, H.Y. Wang, M. Kurmoo, J.L. Zuo, Carbon dioxide (CO_2) fixation: linearly bridged Zn_2 paddlewheel nodes by CO_2 in a metal-organic framework, Inorg. Chem. 58 (2019) 16040–16046, https://doi.org/10.1021/acs.inorgchem.9b02548.
[147] P. Smart, C.A. Mason, J.R. Loader, A.J.H.M. Meijer, A.J. Florence, K. Shankland, A.J. Fletcher, S.P. Thompson, M. Brunelli, A.H. Hill, L. Brammer, Zipping and unzipping of a paddlewheel Metal–Organic Framework to enable two-step synthetic and structural transformation, Chem. – A Eur. J. 19 (2013) 3552–3557, https://doi.org/10.1002/chem.201204492.
[148] H. Chun, H. Jung, J. Seo, Isoreticular metal-organic polyhedral networks based on 5-connecting paddlewheel motifs, Inorg. Chem. 48 (2009) 2043–2047, https://doi.org/10.1021/ic801784j.
[149] T.K. Pal, S. Neogi, P.K. Bharadwaj, Versatile tailoring of paddle-wheel ZnII metal-organic frameworks through single-crystal-to-single-crystal transformations, Chem. - A Eur. J. 21 (2015) 16083–16090, https://doi.org/10.1002/chem.201502648.
[150] X. Yang, Y. Zhang, F. Li, T. Guo, Y. Wu, F. Jin, M. Fang, Y. Lan, Y. Li, Y. Zhou, Z. Zou, Theoretical and experimental studies on three water-stable, isostructural, paddlewheel based semiconducting metal–organic frameworks, Dalton Trans. 46 (2017) 8204–8218, https://doi.org/10.1039/C7DT01560G.
[151] A.-Y. Wang, J. Wang, S. Aghabeygi, J.-G. Wang, H.-P. Xiao, A. Mosali, Zinc(II) Metal–Organic Framework with nano-sized channels based on paddle-wheel units, J. Inorg. Organomet. Polym. Mater. 21 (2011) 730–733, https://doi.org/10.1007/s10904-011-9546-y.
[152] S. Bureekaew, S. Amirjalayer, R. Schmid, Orbital directing effects in copper and zinc based paddle-wheel metal organic frameworks: the origin of flexibility, J. Mater. Chem. 22 (2012) 10249, https://doi.org/10.1039/c2jm15778k.
[153] M.R. Ryzhikov, S.G. Kozlova, Understanding structural flexibility of the paddle-wheel Zn-SBU motif in MOFs: influence of pillar ligands, Phys. Chem. Chem. Phys. 21 (2019) 11977–11982, https://doi.org/10.1039/c9cp02483b.
[154] P.V. Dau, S.M. Cohen, The influence of nitro groups on the topology and gas sorption property of extended Zn(II)-paddlewheel MOFs, CrystEngComm 15 (2013) 9304, https://doi.org/10.1039/c3ce41124a.
[155] J. Yang, X. Wang, F. Dai, L. Zhang, R. Wang, D. Sun, Improving the porosity and catalytic capacity of a zinc paddlewheel metal-organic framework (MOF) through metal-ion metathesis in a single-crystal-to-single-crystal fashion, Inorg. Chem. 53 (2014) 10649–10653, https://doi.org/10.1021/ic5017092.
[156] T. Chatterjee, B. Dutta, S. Khan, S. Islam, A.M. Alanazi, S.M. Wabaidur, S. M. Alam, M.H. Mir, Exploitation of a Zn(II) paddle wheel metal-organic framework as effective sorbent for the quantitative estimation of cationic and anionic dyes, Inorg. Chim. Acta 528 (2021) 120595, https://doi.org/10.1016/j.ica.2021.120595.

[157] Y. Li, J. Li, D. Zhu, J. Wang, G. Shu, J. Li, S. Zhang, X. Zhang, S. Cosnier, H. Zeng, D. Shan, 2D Zn-porphyrin-based co(II)-MOF with 2-methylimidazole sitting axially on the paddle–wheel units: an efficient electrochemiluminescence bioassay for SARS-CoV-2, Adv. Funct. Mater. 32 (2022) 1–9, https://doi.org/10.1002/adfm.202209743.
[158] L. Pan, D.H. Olson, L.R. Ciemnolonski, R. Heddy, J. Li, Separation of hydrocarbons with a microporous Metal–Organic Framework, Angew. Chem. Int. Ed. 45 (2006) 616–619, https://doi.org/10.1002/anie.200503503.
[159] D.A. Gomez, A.F. Combariza, G. Sastre, Confinement effects in the hydrogen adsorption on paddle wheel containing metal-organic frameworks, Phys. Chem. Chem. Phys. 14 (2012) 2508–2517, https://doi.org/10.1039/c2cp23146h.
[160] W. Wang, Y. Wen, J. Su, H. Ma, H.-Y. Wang, M. Kurmoo, J.-L. Zuo, Carbon Dioxide (CO_2) fixation: linearly bridged Zn_2 paddlewheel nodes by CO_2 in a Metal–Organic Framework, Inorg. Chem. 58 (2019) 16040–16046, https://doi.org/10.1021/acs.inorgchem.9b02548.
[161] D.A. Gomez, A.F. Combariza, G. Sastre, Confinement effects in the hydrogen adsorption on paddle wheel containing metal–organic frameworks, Phys. Chem. Chem. Phys. 14 (2012) 2508, https://doi.org/10.1039/c2cp23146h.
[162] X.-R. Hao, G. Yang, K.-Z. Shao, Z.-M. Su, G. Yuan, X.-L. Wang, Design and construction of porous metal–organic frameworks based on flexible BPH pillars, J. Solid State Chem. 198 (2013) 143–148, https://doi.org/10.1016/j.jssc.2012.09.008.
[163] V. Lozovan, V.C. Kravtsov, Y.M. Chumakov, N.V. Costriucova, N. Siminel, O. Petuhov, T. Vlase, G. Vlase, A. Barba, M.S. Fonari, Zn(II) and Cd(II) Metal–Organic Frameworks with Azine-Functionalized Pores: Crystal Structures, Photoluminescence, Solvent Exchange, and Molecular Simulations of Carbon Dioxide Binding Sites, Cryst. Growth Des. 23 (2023) 3171–3185, https://doi.org/10.1021/acs.cgd.2c01345.
[164] D.H. Lee, J. Oh, J. An, T. Kim, K. Ju, I.-H. Park, Solvent-dependent Zn(II) supramolecular isomers and [2 + 2] photocycloaddition reaction via an SCSC transformation, Cryst. Growth Des. 24 (2024) 6431–6437, https://doi.org/10.1021/acs.cgd.4c00713.
[165] Z. Zhang, J. Zhou, H.X. Sun, M. He, W. Li, L. Du, M. Xie, Q.-H. Zhao, R-substituent-induced structural diversity and single-crystal to single-crystal transformation of coordination polymers: synthesis, luminescence, and magnetic behaviors, Cryst. Growth Des. 21 (2021) 5086–5099, https://doi.org/10.1021/acs.cgd.1c00491.
[166] B. Parmar, P. Patel, R.I. Kureshy, N.H. Khan, E. Suresh, Sustainable heterogeneous catalysts for CO_2 utilization by using dual ligand ZnII/CdII Metal–Organic Frameworks, Chem. – A Eur. J. 24 (2018) 15831–15839, https://doi.org/10.1002/chem.201802387.
[167] P. Patel, B. Parmar, R.I. Kureshy, N. Khan, E. Suresh, Efficient solvent-free carbon dioxide fixation reactions with epoxides under mild conditions by mixed-ligand Zinc(II) Metal–Organic Frameworks, ChemCatChem 10 (2018) 2401–2408, https://doi.org/10.1002/cctc.201800137.
[168] D. Balestri, D. Costa, A. Bacchi, L. Carlucci, P. Pelagatti, Linker dependent dimensionality in Zn(II)-coordination polymers containing a flexible bis-pyridyl-bis-amide ligand, Polyhedron 153 (2018) 278–285, https://doi.org/10.1016/j.poly.2018.07.025.
[169] B. Parmar, Y. Rachuri, K.K. Bisht, E. Suresh, Mixed-ligand LMOF fluorosensors for detection of Cr(VI) oxyanions and Fe^{3+}/Pd^{2+} cations in aqueous media, Inorg. Chem. 56 (2017) 10939–10949, https://doi.org/10.1021/acs.inorgchem.7b01130.
[170] I.-H. Park, H. Ju, K. Kim, S.S. Lee, J.J. Vittal, Isomerism in double-pillared-layer coordination polymers – structures and photoreactivity, IUCrJ 5 (2018) 182–189, https://doi.org/10.1107/S2052252518001379.
[171] D. Chisca, L. Croitor, O. Petuhov, O.V. Kulikova, G.F. Volodina, E.B. Coropceanu, A.E. Masunov, M.S. Fonari, Tuning structures and emissive properties in a series of Zn(II) and cd(II) coordination polymers containing dicarboxylic acids and nicotinamide pillars, CrystEngComm 20 (2018) 432–447, https://doi.org/10.1039/C7CE01988B.
[172] G. Férey, Structural flexibility in crystallized matter: from history to applications, Dalton Trans. 45 (2016) 4073–4089, https://doi.org/10.1039/C5DT03547C.
[173] O.T. Qazvini, V.-J. Scott, L. Bondorf, M. Ducamp, M. Hirscher, F.-X. Coudert, S. G. Telfer, Flexibility of a Metal–Organic Framework enhances gas separation and enables quantum sieving, Chem. Mater. 33 (2021) 8886–8894, https://doi.org/10.1021/acs.chemmater.1c03170.
[174] T.R. Ramadhar, S.-L. Zheng, Y.-S. Chen, J. Clardy, Analysis of rapidly synthesized guest-filled porous complexes with synchrotron radiation: practical guidelines for the crystalline sponge method, Acta Crystallogr. Sect. A Found. Adv. 71 (2015) 46–58, https://doi.org/10.1107/S2053273314019573.
[175] J. Berger, S. Terruzzi, H. Bunzen, F. Ballerini, M. Vandone, M. Marelli, L. Braglia, R.A. Fischer, V. Colombo, G. Kieslich, CO_2 and temperature induced switching of a flexible Metal–Organic Framework with surface-mounted nanoparticles, Small 21 (2025) 1–9, https://doi.org/10.1002/smll.202408137.
[176] R.M. Abdelhameed, E. Alzahrani, A.A. Shaltout, H.E. Emam, Temperature-controlled-release of essential oil via reusable mesoporous composite of microcrystalline cellulose and zeolitic imidazole frameworks, J. Ind. Eng. Chem. 94 (2021) 134–144, https://doi.org/10.1016/j.jiec.2020.10.025.
[177] S. Lee, S. Jeong, J. Seong, J. Lim, A. Sharma, S. Won, D. Moon, S. Bin Baek, M. S. Lah, Solvent-mediated framework flexibility of interdigitated 2D layered metal–organic frameworks, Mater. Chem. Front. 5 (2021) 3621–3627, https://doi.org/10.1039/D1QM00251A.
[178] V.I. Nikolayenko, D.C. Castell, D.P. van Heerden, L.J. Barbour, Guest-induced structural transformations in a porous halogen-bonded framework, Angew. Chem. Int. Ed. 57 (2018) 12086–12091, https://doi.org/10.1002/anie.201806399.
[179] A.J. Graham, D.R. Allan, A. Muszkiewicz, C.A. Morrison, S.A. Moggach, The effect of high pressure on MOF-5: guest-induced modification of pore size and content at high pressure, Angew. Chem. Int. Ed. 50 (2011) 11138–11141, https://doi.org/10.1002/anie.201104285.
[180] A. Knebel, C. Zhou, A. Huang, J. Zhang, L. Kustov, J. Caro, Smart metal-organic frameworks (MOFs): switching gas permeation through MOF membranes by external stimuli, Chem. Eng. Technol. 41 (2018) 224–234, https://doi.org/10.1002/ceat.201700635.
[181] A. Schneemann, V. Bon, I. Schwedler, I. Senkovska, S. Kaskel, R.A. Fischer, Flexible metal-organic frameworks, Chem. Soc. Rev. 43 (2014) 6062–6096, https://doi.org/10.1039/c4cs00101j.
[182] B. Garai, V. Bon, S. Krause, F. Schwotzer, M. Gerlach, I. Senkovska, S. Kaskel, Tunable flexibility and porosity of the Metal–Organic Framework DUT-49 through postsynthetic metal exchange, Chem. Mater. 32 (2020) 889–896, https://doi.org/10.1021/acs.chemmater.9b04769.
[183] Q. Guan, Y. Fang, X. Wu, R. Ou, X. Zhang, H. Xie, M. Tang, G. Zeng, Stimuli responsive metal organic framework materials towards advanced smart application, Mater. Today 64 (2023) 138–164, https://doi.org/10.1016/j.mattod.2023.02.013.
[184] S. Hiraide, Y. Sakanaka, H. Kajiro, S. Kawaguchi, M.T. Miyahara, H. Tanaka, High-throughput gas separation by flexible metal–organic frameworks with fast gating and thermal management capabilities, Nat. Commun. 11 (2020) 3867, https://doi.org/10.1038/s41467-020-17625-3.
[185] G. Lee, D. Choi, M. Oh, Activating the gate-opening of a Metal–Organic Framework and maximizing its adsorption capacity, J. Am. Chem. Soc. 147 (2025) 12811–12820, https://doi.org/10.1021/jacs.5c01399.
[186] J. Ethiraj, F. Bonino, J.G. Vitillo, K.A. Lomachenko, C. Lamberti, H. Reinsch, K. P. Lillerud, S. Bordiga, Solvent-driven gate opening in MOF-76-Ce: effect on CO_2 adsorption, ChemSusChem 9 (2016) 713–719, https://doi.org/10.1002/cssc.201501574.
[187] X. Wang, R. Krishna, L. Li, B. Wang, T. He, Y.-Z. Zhang, J.-R. Li, J. Li, Guest-dependent pressure induced gate-opening effect enables effective separation of propene and propane in a flexible MOF, Chem. Eng. J. 346 (2018) 489–496, https://doi.org/10.1016/j.cej.2018.03.163.
[188] Á. Berenguer-Murcia, J.P. Marco-Lozar, D. Cazorla-Amorós, Hydrogen storage in porous materials: status, milestones, and challenges, Chem. Rec. 18 (2018) 900–912, https://doi.org/10.1002/tcr.201700067.
[189] J.-X. Yang, X. Zhang, Y.-Y. Qin, Y.-G. Yao, N-donor auxiliary ligand influence on the coordination mode variations of V-shaped triazole dicarboxylic acid ligand affording seven new luminescent Zn(II) compounds with variable structural motifs, Cryst. Growth Des. 20 (2020) 6366–6381, https://doi.org/10.1021/acs.cgd.0c00449.
[190] H.-C. Kim, S. Huh, J.Y. Kim, H.R. Moon, D.N. Lee, Y. Kim, Zn-MOFs containing flexible α,ω-alkane (or alkene)-dicarboxylates with 1,2-bis(4-pyridyl)ethylene: comparison with Zn-MOFs containing 1,2-bis(4-pyridyl)ethane ligands, CrystEngComm 19 (2017) 99–109, https://doi.org/10.1039/C6CE02122K.
[191] A. Halder, B. Bhattacharya, F. Haque, D. Ghoshal, Structural diversity in six mixed ligand Zn(II) metal-organic frameworks constructed by rigid and flexible dicarboxylates and different N, N′ donor ligands, Cryst. Growth Des. 17 (2017) 6613–6624, https://doi.org/10.1021/acs.cgd.7b01270.
[192] V. Lozovan, V.C. Kravtsov, Y.M. Chumakov, N.V. Costriucova, N. Siminel, O. Petuhov, T. Vlase, G. Vlase, A. Barba, M.S. Fonari, Zn(II) and cd(II) metal-organic frameworks with azine-functionalized pores: crystal structures, photoluminescence, solvent exchange, and molecular simulations of carbon dioxide binding sites, Cryst. Growth Des. 23 (2023) 3171–3185, https://doi.org/10.1021/acs.cgd.2c01345.
[193] F.-H. Zhao, Y.-S. Li, S.-Q. Li, X.-H. Wu, Y.-C. He, Z.-L. Li, A stable two-fold interpenetrated 3D Zn(ii) MOF for fluorescence sensing of uric acid and tryptophan, CrystEngComm 27 (2025) 2223–2232, https://doi.org/10.1039/D4CE01283F.
[194] H. Ju, I.-H. Park, E. Lee, S. Kim, J.H. Jung, M. Ikeda, Y. Habata, S.S. Lee, Guest-triggered assembly of zinc(II) supramolecular isomers with accompanying dimensional change and reversible single-crystal-to-single-crystal transformation, CrystEngComm 18 (2016) 1600–1608, https://doi.org/10.1039/C5CE02194D.
[195] H. Ju, Y. Habata, S.S. Lee, Temperature-dependent supramolecular isomeric Zn (II)-metal-organic frameworks and their guest exchange, Cryst. Growth Des. 20 (2020) 4640–4648, https://doi.org/10.1021/acs.cgd.0c00443.
[196] K. Roztocki, F. Formalik, A. Krawczuk, I. Senkovska, B. Kuchta, S. Kaskel, D. Matoga, Collective breathing in an eightfold interpenetrated Metal–Organic Framework: from mechanistic understanding towards threshold sensing architectures, Angew. Chem. Int. Ed. 59 (2020) 4491–4497, https://doi.org/10.1002/anie.201914198.
[197] K. Roztocki, F. Formalik, V. Bon, A. Krawczuk, P. Goszczycki, B. Kuchta, S. Kaskel, D. Matoga, Tuning adsorption-induced responsiveness of a flexible Metal–Organic Framework JUK-8 by linker halogenation, Chem. Mater. 34 (2022) 3430–3439, https://doi.org/10.1021/acs.chemmater.2c00249.
[198] J.H. Park, W.R. Lee, Y. Kim, H.J. Lee, D.W. Ryu, W.J. Phang, C.S. Hong, Interpenetration control, aorption behavior, and framework flexibility in Zn(II) Metal–Organic Frameworks, Cryst. Growth Des. 14 (2014) 699–704, https://doi.org/10.1021/cg401583v.
[199] W.-X.Z. Chun-Ting He, Pei-Qin Liao, Dong-Dong Zhou, J.-P.Z. Bao-Ying Wang, X.-M. Chen, Visualizing the distinctly different crystal-to-crystal structural dynamism and sorption behavior of interpenetration-direction isomeric coordination networks, Chem. Sci. 5 (2014) 4755–4762, https://doi.org/10.1039/c4sc01505c.

[200] Z. Chen, G. Gallo, V.A. Sawant, T. Zhang, M. Zhu, L. Liang, A. Chanthapally, G. Bolla, H.S. Quah, X. Liu, K.P. Loh, R.E. Dinnebier, Q. Xu, J.J. Vittal, Giant enhancement of second harmonic generation accompanied by the structural transformation of 7-fold to 8-fold interpenetrated Metal–Organic Frameworks (MOFs), Angew. Chem. Int. Ed. 59 (2020) 833–838, https://doi.org/10.1002/anie.201911632.
[201] J.O. Fossum, Physical phenomena in clays, Phys. A Stat. Mech. Its Appl. 270 (1999) 270–277, https://doi.org/10.1016/S0378-4371(99)00124-7.
[202] X. Li, D. Sensharma, K. Koupepidou, X.-J. Kong, M.J. Zaworotko, The effect of pendent groups upon flexibility in coordination networks with square lattice topology, ACS Mater. Lett. 5 (2023) 2567–2575, https://doi.org/10.1021/acsmaterialslett.3c00565.
[203] N.C. Burtch, K.S. Walton, Modulating adsorption and stability properties in pillared Metal–Organic Frameworks: a model system for understanding ligand effects, Acc. Chem. Res. 48 (2015) 2850–2857, https://doi.org/10.1021/acs.accounts.5b00311.
[204] K. Zhu, V.N. Vukotic, C.A. O'Keefe, R.W. Schurko, S.J. Loeb, Metal–Organic Frameworks with mechanically interlocked pillars: controlling ring dynamics in the solid-state via a reversible phase change, J. Am. Chem. Soc. 136 (2014) 7403–7409, https://doi.org/10.1021/ja502238a.
[205] H. Fang, X.-Y. Liu, H.-J. Ding, M. Mulcair, B. Space, H. Huang, X.-W. Li, S.-M. Zhang, M.-H. Yu, Z. Chang, X.-H. Bu, Stimulus-induced dynamic behavior regulation of flexible crystals through the tuning of module rigidity, J. Am. Chem. Soc. 146 (2024) 14357–14367, https://doi.org/10.1021/jacs.4c04809.
[206] Z. Zhu, Z. Wang, Q.-H. Li, Z. Ma, F. Wang, J. Zhang, Porphyrin metal–organic frameworks with bilayer and pillar-layered frameworks and third-order nonlinear optical properties, Dalton Trans. 52 (2023) 4309–4314, https://doi.org/10.1039/D3DT00440F.
[207] T.K. Pal, S. Neogi, P.K. Bharadwaj, Versatile tailoring of paddle-wheel ZnII Metal–Organic Frameworks through single-crystal-to-single-crystal transformations, Chem. – A Eur. J. 21 (2015) 16083–16090, https://doi.org/10.1002/chem.201502648.
[208] S. Sen, S. Neogi, K. Rissanen, P.K. Bharadwaj, Solvent induced single-crystal to single-crystal structural transformation and concomitant transmetalation in a 3D cationic Zn(II)-framework, Chem. Commun. 51 (2015) 3173–3176, https://doi.org/10.1039/C4CC09955A.
[209] L. Feng, R.D. Astumian, J.F. Stoddart, Controlling dynamics in extended molecular frameworks, Nat. Rev. Chem. 6 (2022) 705–725, https://doi.org/10.1038/s41570-022-00412-7.
[210] J. Perego, A. Daolio, C.X. Bezuidenhout, S. Piva, G. Prando, B. Costarella, P. Carretta, L. Marchiò, D. Kubicki, P. Sozzani, S. Bracco, A. Comotti, Solid State machinery of multiple dynamic elements in a Metal–Organic Framework, Angew. Chem. Int. Ed. 63 (2024) e202317094, https://doi.org/10.1002/anie.202317094.
[211] J. Perego, C.X. Bezuidenhout, S. Bracco, G. Prando, L. Marchiò, M. Negroni, P. Carretta, P. Sozzani, A. Comotti, Cascade dynamics of multiple molecular rotors in a MOF: benchmark mobility at a few kelvins and dynamics control by CO_2, J. Am. Chem. Soc. 143 (2021) 13082–13090, https://doi.org/10.1021/jacs.1c03801.
[212] X. Jiang, H. Duan, S.I. Khan, M.A. Garcia-Garibay, Diffusion-controlled rotation of triptycene in a Metal–Organic Framework (MOF) sheds light on the viscosity of MOF-confined solvent, ACS Cent. Sci. 2 (2016) 608–613, https://doi.org/10.1021/acscentsci.6b00168.
[213] M.J. Jellen, X. Jiang, S. Benders, A. Adams, M.A. Garcia-Garibay, Slip/stick viscosity models of nanoconfined liquids: solvent-dependent rotation in Metal–Organic Frameworks, J. Organomet. Chem. 87 (2022) 1780–1790, https://doi.org/10.1021/acs.joc.1c02218.
[214] W. Danowski, T. van Leeuwen, S. Abdolahzadeh, D. Roke, W.R. Browne, S. J. Wezenberg, B.L. Feringa, Unidirectional rotary motion in a metal–organic framework, Nat. Nanotechnol. 14 (2019) 488–494, https://doi.org/10.1038/s41565-019-0401-6.
[215] W. Danowski, F. Castiglioni, A.S. Sardjan, S. Krause, L. Pfeifer, D. Roke, A. Comotti, W.R. Browne, B.L. Feringa, Visible-light-driven rotation of molecular motors in a dual-function Metal–Organic Framework enabled by energy transfer, J. Am. Chem. Soc. 142 (2020) 9048–9056, https://doi.org/10.1021/jacs.0c03063.
[216] I. Liepuoniute, C.M. Huynh, S. Perez-Estrada, Y. Wang, S. Khan, K.N. Houk, M. A. Garcia-Garibay, Enhanced rotation by ground state destabilization in amphidynamic crystals of a dipolar 2,3-difluorophenylene rotator as established by solid state ^{2}H NMR and dielectric spectroscopy, J. Phys. Chem. C 124 (2020) 15391–15398, https://doi.org/10.1021/acs.jpcc.0c05314.
[217] Y. Gu, J. Zheng, K. Otake, K. Sugimoto, N. Hosono, S. Sakaki, F. Li, S. Kitagawa, Structural-deformation-energy-modulation strategy in a soft porous coordination polymer with an interpenetrated framework, Angew, Chemie 132 (2020) 15647–15651, https://doi.org/10.1002/ange.202003186.
[218] B. Chen, C. Liang, J. Yang, D.S. Contreras, Y.L. Clancy, E.B. Lobkovsky, O. M. Yaghi, S. Dai, A microporous Metal–Organic Framework for gas-chromatographic separation of alkanes, Angew. Chem. Int. Ed. 45 (2006) 1390–1393, https://doi.org/10.1002/anie.200502844.
[219] H.-C. Kim, S. Huh, D.N. Lee, Y. Kim, Selective carbon dioxide sorption by a new breathing three-dimensional Zn-MOF with Lewis basic nitrogen-rich channels, Dalton Trans. 47 (2018) 4820–4826, https://doi.org/10.1039/C7DT04134A.
[220] E.R. Engel, A. Jouaiti, C.X. Bezuidenhout, M.W. Hosseini, L.J. Barbour, Activation-dependent breathing in a flexible Metal–Organic Framework and the effects of repeated sorption/desorption cycling, Angew. Chem. Int. Ed. 56 (2017) 8874–8878, https://doi.org/10.1002/anie.201704044.
[221] M. Shivanna, Q. Yang, A. Bajpai, S. Sen, N. Hosono, S. Kusaka, T. Pham, K. A. Forrest, B. Space, S. Kitagawa, M.J. Zaworotko, Readily accessible shape-memory effect in a porous interpenetrated coordination network, Sci. Adv. 4 (2018) 1–7, https://doi.org/10.1126/sciadv.aaq1636.
[222] A. Zhu, Q. Yang, S. Mukherjee, A. Kumar, C. Deng, A.A. Bezrukov, M. Shivanna, M.J. Zaworotko, Tuning the gate-opening pressure in a switching pcu coordination network, X-pcu-5-Zn, by pillar-ligand substitution, Angew. Chem. Int. Ed. 58 (2019) 18212–18217, https://doi.org/10.1002/anie.201909977.
[223] P. Kanoo, R. Haldar, S.K. Reddy, A. Hazra, S. Bonakala, R. Matsuda, S. Kitagawa, S. Balasubramanian, T.K. Maji, Crystal dynamics in multi-stimuli-responsive entangled Metal–Organic Frameworks, Chem. – A Eur. J. 22 (2016) 15864–15873, https://doi.org/10.1002/chem.201602087.
[224] V. Bon, I. Senkovska, D. Wallacher, D.M. Többens, I. Zizak, R. Feyerherm, U. Mueller, S. Kaskel, In situ observation of gating phenomena in the flexible porous coordination polymer Zn_2(BPnDC)$_2$ (bpy) (SNU-9) in a combined diffraction and gas adsorption experiment, Inorg. Chem. 53 (2014) 1513–1520, https://doi.org/10.1021/ic4024844.
[225] R. Kitaura, K. Seki, G. Akiyama, S. Kitagawa, Porous coordination-polymer crystals with gated channels specific for supercritical gases, Angew. Chem. Int. Ed. 42 (2003) 428–431, https://doi.org/10.1002/anie.200390130.
[226] K.L. Mulfort, O.K. Farha, C.D. Malliakas, M.G. Kanatzidis, J.T. Hupp, An interpenetrated framework material with hysteretic CO_2 uptake, Chem. – A Eur. J. 16 (2010) 276–281, https://doi.org/10.1002/chem.200902104.
[227] K.L. Mulfort, J.T. Hupp, Alkali metal cation effects on hydrogen uptake and binding in metal-organic frameworks, Inorg. Chem. 47 (2008) 7936–7938, https://doi.org/10.1021/ic800700h.
[228] R. Dey, B. Bhattacharya, P. Pachfule, R. Banerjee, D. Ghoshal, Flexible dicarboxylate based pillar-layer metal organic frameworks: differences in structure and porosity by tuning the pyridyl based N,N′ linkers, CrystEngComm 16 (2014) 2305, https://doi.org/10.1039/c3ce42028k.
[229] U. Patel, B. Parmar, P. Patel, A. Dadhania, E. Suresh, The synthesis and characterization of Zn(II)/cd(II) based MOFs by a mixed ligand strategy: a Zn(II) MOF as a dual functional material for reversible dye adsorption and as a heterogeneous catalyst for the Biginelli reaction, Mater. Chem. Front. 5 (2021) 304–314, https://doi.org/10.1039/D0QM00611D.
[230] M. Inukai, M. Tamura, S. Horike, M. Higuchi, S. Kitagawa, K. Nakamura, Storage of CO_2 into porous coordination polymer controlled by molecular rotor dynamics, Angew. Chem. Int. Ed. 57 (2018) 8687–8690, https://doi.org/10.1002/anie.201805111.
[231] H. Zhou, J. Bai, X. Tian, Z. Mo, X. Chen, Dynamic pendulum effect of an exceptionally flexible pillared-layer metal-organic-framework, Chin. J. Chem. 39 (2021) 2718–2724, https://doi.org/10.1002/cjoc.202100263.
[232] Y. Hijikata, S. Horike, M. Sugimoto, H. Sato, R. Matsuda, S. Kitagawa, Relationship between channel and sorption properties in coordination polymers with interdigitated structures, Chem. – A Eur. J. 17 (2011) 5138–5144, https://doi.org/10.1002/chem.201003734.
[233] M.H. Mir, L.L. Koh, G.K. Tan, J.J. Vittal, Single-crystal to single-crystal photochemical structural transformations of interpenetrated 3D coordination polymers by [2+2] cycloaddition reactions, Angew. Chem. Int. Ed. 49 (2010) 390–393, https://doi.org/10.1002/anie.200905898.
[234] A. Hazra, T.K. Maji, Guest-responsive reversal in structural transformation after a [2 + 2] topochemical reaction in a 3D pillared layer MOF: uncovering the role of C–H·O interaction, Inorg. Chem. 59 (2020) 12793–12801, https://doi.org/10.1021/acs.inorgchem.0c01844.
[235] R.-B. Lin, S. Xiang, W. Zhou, B. Chen, Microporous metal-organic framework materials for gas separation, Chem 6 (2020) 337–363, https://doi.org/10.1016/j.chempr.2019.10.012.
[236] F. Xie, H. Wang, J. Li, Flexible Metal–Organic Frameworks for adsorptive separation of liquid hydrocarbons, Acc. Chem. Res. 58 (2025) 2016–2027, https://doi.org/10.1021/acs.accounts.5c00217.
[237] Y. Shen, A. Tissot, C. Serre, Recent progress on MOF-based optical sensors for VOC sensing, Chem. Sci. 13 (2022) 13978–14007, https://doi.org/10.1039/D2SC04314A.
[238] M. Hoshino, A. Khutia, H. Xing, Y. Inokuma, M. Fujita, The crystalline sponge method updated, IUCrJ 3 (2016) 139–151, https://doi.org/10.1107/S2052252515024379.
[239] Q. Du, J. Peng, P. Wu, H. He, Review: metal-organic framework based crystalline sponge method for structure analysis, TrAC, Trends Anal. Chem. 102 (2018) 290–310, https://doi.org/10.1016/j.trac.2018.02.014.
[240] F. Sakurai, A. Khutia, T. Kikuchi, M. Fujita, X-ray structure analysis of N-containing nucleophilic compounds by the crystalline sponge method, Chem. – A Eur. J. 23 (2017) 15035–15040, https://doi.org/10.1002/chem.201704176.
[241] R.D.J. Lunn, D.A. Tocher, P.J. Sidebottom, M.G. Montgomery, A.C. Keates, C. J. Carmalt, Applying the crystalline sponge method to agrochemicals: obtaining X-ray structures of the fungicide metalaxyl-M and herbicide S-metolachlor, Cryst. Growth Des. 21 (2021) 3024–3036, https://doi.org/10.1021/acs.cgd.1c00196.
[242] K. Ikemoto, Y. Inokuma, K. Rissanen, M. Fujita, X-ray snapshot observation of palladium-mediated aromatic bromination in a porous complex, J. Am. Chem. Soc. 136 (2014) 6892–6895, https://doi.org/10.1021/ja502996h.
[243] M.X. Wu, Y.W. Yang, Metal–Organic Framework (MOF)-based drug/cargo delivery and cancer therapy, Adv. Mater. 29 (2017) 1–20, https://doi.org/10.1002/adma.201606134.
[244] D.S. Sholl, R.P. Lively, Seven chemical separations to change the world, Nature 532 (2016) 435–437, https://doi.org/10.1038/532435a.

[245] D.-Y. Kang, J.S. Lee, Challenges in developing MOF-based membranes for gas separation, Langmuir 39 (2023) 2871–2880, https://doi.org/10.1021/acs.langmuir.2c03458.
[246] J. Kaur, G. Kaur, Review on flexible metal-organic frameworks, ChemistrySelect 6 (2021) 8227–8243, https://doi.org/10.1002/slct.202101524.
[247] Z. Lai, Development of ZIF-8 membranes: opportunities and challenges for commercial applications, Curr. Opin. Chem. Eng. 20 (2018) 78–85, https://doi.org/10.1016/j.coche.2018.03.002.
[248] V.M. Aceituno Melgar, J. Kim, M.R. Othman, Zeolitic imidazolate framework membranes for gas separation: a review of synthesis methods and gas separation performance, J. Ind. Eng. Chem. 28 (2015) 1–15, https://doi.org/10.1016/j.jiec.2015.03.006.
[249] A. Imtiaz, M.H.D. Othman, A. Jilani, I.U. Khan, R. Kamaludin, O. Samuel, ZIF-filler incorporated mixed matrix membranes (MMMs) for efficient gas separation: a review, J. Environ. Chem. Eng. 10 (2022) 108541, https://doi.org/10.1016/j.jece.2022.108541.
[250] R.-B. Lin, L. Li, H. Wu, H. Arman, B. Li, R.-G. Lin, W. Zhou, B. Chen, Optimized separation of acetylene from carbon dioxide and ethylene in a microporous material, J. Am. Chem. Soc. 139 (2017) 8022–8028, https://doi.org/10.1021/jacs.7b03850.
[251] Z. Song, K. Zhang, K. Zhao, W. Jiang, R. Krishna, J. Li, D. Wang, Cooperative ligand engineering enabling stepwise optimization of Metal–Organic Frameworks for improved C_2H_2 Separation from CO_2 and CH_4, ACS Appl. Mater. Interfaces 17 (2025) 43245–43254, https://doi.org/10.1021/acsami.5c09790.
[252] B. Pramanik, R. Sahoo, R. Krishna, M.C. Das, A chemically robust microporous Zn-MOF for C_2H_2 separation from CO_2 and industrially relevant four component gas mixtures, Small 21 (2025) 1–8, https://doi.org/10.1002/smll.202411456.
[253] P. Hu, J. Hu, L. Li, G. Shi, M. Jiang, Y. Chen, L. Jin, C. Xiong, H. Ji, Self-adjusted MOF pore environment through realigning adsorption orientation of guests for boosting separation of gaseous C1-C3 alkanes, Sep. Purif. Technol. 370 (2025) 133289, https://doi.org/10.1016/j.seppur.2025.133289.
[254] F. Bianchi, A. Pankajakshan, F. Fornari, S. Mandal, P. Pelagatti, A. Bacchi, P. P. Mazzeo, M. Careri, A zinc mixed-ligand microporous metal-organic framework as solid-phase microextraction coating for priority polycyclic aromatic hydrocarbons from water samples, Microchem. J. 154 (2020) 104646, https://doi.org/10.1016/j.microc.2020.104646.
[255] D. Balestri, I. Bassanetti, S. Canossa, C. Gazzurelli, A. Bacchi, S. Bracco, A. Comotti, P. Pelagatti, Changing the dress to a MOF through fluorination and transmetalation. Structural and gas-forption effects, Cryst. Growth Des. 18 (2018) 6824–6832, https://doi.org/10.1021/acs.cgd.8b01062.
[256] P.-D. Zhang, X.-Q. Wu, T. He, L.-H. Xie, Q. Chen, J.-R. Li, Selective adsorption and separation of C 2 hydrocarbons in a “flexible-robust” metal–organic framework based on a guest-dependent gate-opening effect, Chem. Commun. 56 (2020) 5520–5523, https://doi.org/10.1039/D0CC01315C.
[257] F. Xie, L. Yu, T. Jenkins, T. Thonhauser, H. Wang, J. Li, Flexible Layered Metal–Organic Framework for Temperature-Dependent Discrimination of Cyclic Hydrocarbons, ACS Mater. Lett. 7 (2025) 780–786, https://doi.org/10.1021/acsmaterialslett.4c02402.
[258] Q. Chen, S. Xian, X. Dong, Y. Liu, H. Wang, D.H. Olson, L.J. Williams, Y. Han, X. Bu, J. Li, High-efficiency separation of n-hexane by a dynamic metal-organic framework with reduced energy consumption, Angew. Chem. Int. Ed. 60 (2021) 10593–10597, https://doi.org/10.1002/anie.202100707.
[259] F. Luo, C. Bin Fan, M.B. Luo, X.L. Wu, Y. Zhu, S.Z. Pu, W. Xu, G. Guo, Photoswitching CO_2 capture and release in a photochromic diarylethene Metal–Organic Framework, Angew. Chem. 126 (2014) 9452–9455, https://doi.org/10.1002/ange.201311124.
[260] A. Delledonne, M. Orlandini, F. Terenziani, P.P. Mazzeo, A. Bacchi, L. Carlucci, A. Comotti, J. Perego, P. Pelagatti, Luminescence properties of mixed-ligand MOFs containing fluorene scaffolds functionalized with isonicotinoyl arms, CrystEngComm 25 (2023) 2085–2095, https://doi.org/10.1039/D3CE00087G.
[261] X. Wang, G. Clavier, Y. Zhang, K. Batra, N. Xiao, G. Maurin, B. Ding, A. Tissot, C. Serre, A MOF/DNA luminescent sensing platform for detection of potential COVID-19 biomarkers and drugs, Chem. Sci. 14 (2023) 5386–5395, https://doi.org/10.1039/D3SC00106G.
[262] G. Yang, X. Jiang, H. Xu, B. Zhao, Applications of MOFs as luminescent sensors for environmental pollutants, Small 17 (2021) 1–19, https://doi.org/10.1002/smll.202005327.
[263] S. Pramanik, C. Zheng, X. Zhang, T.J. Emge, J. Li, New microporous metal−organic framework demonstrating unique selectivity for detection of high explosives and aromatic compounds, J. Am. Chem. Soc. 133 (2011) 4153–4155, https://doi.org/10.1021/ja106851d.
[264] A. Lan, K. Li, H. Wu, D.H. Olson, T.J. Emge, W. Ki, M. Hong, J. Li, A luminescent microporous Metal–Organic Framework for the fast and reversible detection of high explosives, Angew. Chem. Int. Ed. 48 (2009) 2334–2338, https://doi.org/10.1002/anie.200804853.
[265] Y. Takashima, S. Furukawa, S. Kitagawa, Control of the charge-transfer interaction between a flexible porous coordination host and aromatic guests by framework isomerism, CrystEngComm 13 (2011) 3360, https://doi.org/10.1039/c1ce05201b.
[266] N. Yanai, K. Kitayama, Y. Hijikata, H. Sato, R. Matsuda, Y. Kubota, M. Takata, M. Mizuno, T. Uemura, S. Kitagawa, Gas detection by structural variations of fluorescent guest molecules in a flexible porous coordination polymer, Nat. Mater. 10 (2011) 787–793, https://doi.org/10.1038/nmat3104.
[267] X. Ma, Y. Chai, P. Li, B. Wang, Metal–Organic Framework films and their potential applications in environmental pollution control, Acc. Chem. Res. 52 (2019) 1461–1470, https://doi.org/10.1021/acs.accounts.9b00113.
[268] X. Fang, B. Zong, S. Mao, Metal–Organic Framework-based sensors for environmental contaminant sensing, Nano-Micro Lett. 10 (2018) 64, https://doi.org/10.1007/s40820-018-0218-0.
[269] X. Zhang, J. Hu, B. Wang, Z. Li, S. Xu, Y. Chen, X. Ma, A chiral zinc(II) metal-organic framework as high selective luminescent sensor for detecting trace nitro explosives picric acid and Fe3+ ion, J. Solid State Chem. 269 (2019) 459–464, https://doi.org/10.1016/j.jssc.2018.10.021.
[270] A. Mandal, A. Adhikary, A. Sarkar, D. Das, Naked eye Cd^{2+} ion detection and reversible iodine uptake by a three-dimensional pillared-layered Zn-MOF, Inorg. Chem. 59 (2020) 17758–17765, https://doi.org/10.1021/acs.inorgchem.0c02985.
[271] Z. Xiao, Y. Sun, Y. Bao, Y. Sun, R. Zhou, L. Wang, Two new inorganic–organic hybrid zinc phosphate frameworks and their application in fluorescence sensor and photocatalytic hydrogen evolution, J. Solid State Chem. 269 (2019) 575–579, https://doi.org/10.1016/j.jssc.2018.10.038.
[272] J. Wang, D. Yan, W. Huang, A fluorescence zinc metal-organic framework for the effective detection of Fe^{3+} and Fe^{2+} in water, Inorg. Chem. Commun. 138 (2022) 109282, https://doi.org/10.1016/j.inoche.2022.109282.
[273] J. Cheng, T. Hu, W. Li, Z. Chang, C. Sun, Stable zinc metal-organic framework materials constructed by fluorenone carboxylate ligand: multifunction detection and photocatalysis property, J. Solid State Chem. 282 (2020) 121125, https://doi.org/10.1016/j.jssc.2019.121125.
[274] Q. Hu, J.-L. Liu, Q.-M. Zheng, J.-F. Chang, L.-Z. Wu, M.-D. Zhang, L. Qin, The ligand effect resulted in different fluorescence responses of two similar zinc-based MOFs to high-valence metal ions and amino acids, Microporous Mesoporous Mater. 321 (2021) 111130, https://doi.org/10.1016/j.micromeso.2021.111130.
[275] Y. Cao, Y. Zhang, L. Gu, X. Qin, H.-Y. Li, H.-D. Bian, F.-P. Huang, A $zinc^{2+}$-dpbt framework: luminescence sensing of Cu^{2+}, Ag^{+}, MnO_4^- and Cr(VI) ($Cr_2O_7^{2-}$ and CrO_4^{2-}) ions, New J. Chem. 44 (2020) 10681–10688, https://doi.org/10.1039/D0NJ01535K.
[276] Y. Xie, S. Ning, Y. Zhang, Z. Tang, S. Zhang, R. Tang, A 3D supramolecular network as highly selective and sensitive luminescent sensor for PO_4^{3-} and Cu^{2+} ions in aqueous media, Dyes Pigments 150 (2018) 36–43, https://doi.org/10.1016/j.dyepig.2017.11.008.
[277] H.-R. Fu, X.-X. Wu, L.-F. Ma, F. Wang, J. Zhang, Dual-emission SG7@MOF sensor via SC–SC transformation: enhancing the formation of excimer emission and the range and sensitivity of detection, ACS Appl. Mater. Interfaces 10 (2018) 18012–18020, https://doi.org/10.1021/acsami.8b05614.
[278] L. Shi, N. Li, D. Wang, M. Fan, S. Zhang, Z. Gong, Environmental pollution analysis based on the luminescent metal organic frameworks: a review, TrAC Trends Anal. Chem. 134 (2021) 116131, https://doi.org/10.1016/j.trac.2020.116131.
[279] S.K. Elsaidi, M.H. Mohamed, A.S. Helal, M. Galanek, T. Pham, S. Suepaul, B. Space, D. Hopkinson, P.K. Thallapally, J. Li, Radiation-resistant metal-organic framework enables efficient separation of krypton fission gas from spent nuclear fuel, Nat. Commun. 11 (2020) 3103, https://doi.org/10.1038/s41467-020-16647-1.
[280] M. Orfano, J. Perego, F. Cova, C.X. Bezuidenhout, S. Piva, C. Dujardin, B. Sabot, S. Pierre, P. Mai, C. Daniel, S. Bracco, A. Vedda, A. Comotti, A. Monguzzi, Efficient radioactive gas detection by scintillating porous metal–organic frameworks, Nat. Photonics 17 (2023) 672–678, https://doi.org/10.1038/s41566-023-01211-2.
[281] S. Mauree, V. Villemot, M. Hamel, B. Sabot, S. Pierre, C. Dujardin, F. Belloni, A. Comotti, S. Bracco, J. Perego, G.H.V. Bertrand, Detection of radioactive gas with scintillating MOFs, Adv. Funct. Mater. 33 (2023), https://doi.org/10.1002/adfm.202302877.
[282] S. Kamal, M. Khalid, M.S. Khan, M. Shahid, M. Ahmad, Breathing transition and effective iodine adsorption in a temperature-responsive Zn-based flexible Metal–Organic Framework, Langmuir 41 (2025) 1182–1193, https://doi.org/10.1021/acs.langmuir.4c04860.
[283] S.T. Meek, J.A. Greathouse, M.D. Allendorf, Metal-organic frameworks: a rapidly growing class of versatile nanoporous materials, Adv. Mater. 23 (2011) 249–267, https://doi.org/10.1002/adma.201002854.
[284] S. Mallakpour, E. Nikkhoo, C.M. Hussain, Application of MOF materials as drug delivery systems for cancer therapy and dermal treatment, Coord. Chem. Rev. 451 (2022) 214262, https://doi.org/10.1016/j.ccr.2021.214262.
[285] X. Chen, R. Tong, Z. Shi, B. Yang, H. Liu, S. Ding, X. Wang, Q. Lei, J. Wu, W. Fang, MOF nanoparticles with encapsulated autophagy inhibitor in controlled drug delivery system for antitumor, ACS Appl. Mater. Interfaces 10 (2018) 2328–2337, https://doi.org/10.1021/acsami.7b16522.
[286] M. Ding, X. Cai, Improving MOF stability: approaches and applications, Chem. Sci. 10 (2019) 10209–10230, https://doi.org/10.1039/c9sc03916c.
[287] N.C. Burtch, H. Jasuja, K.S. Walton, Water stability and adsorption in metal – organic frameworks, Chem. Rev. 114 (2014) 10575–10612.
[288] J. Yang, Y. Yang, Metal–Organic frameworks for biomedical applications, 1906846 16, 2020, pp. 1–24, https://doi.org/10.1002/smll.201906846.
[289] B. Dutta, K. Pal, K. Jana, C. Sinha, Fabrication of a Zn(II)-based 2D pillar bilayer metal-organic framework for antimicrobial activity, ChemistrySelect 4 (2019) 9947–9951, https://doi.org/10.1002/slct.201901887.
[290] R.M. Abdelhameed, O.M. Darwesh, J. Rocha, A.M.S. Silva, Biological activity of modified MOFs IRMOF-3 biological activity enhancement by post-synthetic modification, Eur. J. Inorg. Chem. 2019 (2019) 1243–1249, https://doi.org/10.1002/ejic.201801442.
[291] M. Cai, B. Ni, X. Hu, K. Wang, D. Yin, G. Chen, T. Fu, R. Zhu, X. Dong, C. Qu, X. Yin, An investigation of IRMOF-16 as a pH-responsive drug delivery carrier of

curcumin, J. Sci. Adv. Mater. Devices 7 (2022) 100507, https://doi.org/10.1016/j.jsamd.2022.100507.
[292] M. Hoop, C.F. Walde, R. Riccò, F. Mushtaq, A. Terzopoulou, X. Chen, J. Andrew, C.J. Doonan, P. Falcaro, B.J. Nelson, J. Puigmartí-luis, S. Pané, Biocompatibility characteristics of the metal organic framework ZIF-8 for therapeutical applications, Appl. Mater. Today 11 (2018) 13–21, https://doi.org/10.1016/j.apmt.2017.12.014.
[293] M. De Toni, R. Jonchiere, P. Pullumbi, F. Coudert, How can a hydrophobic MOF be water-unstable? Insight into the Hydration Mechanism of IRMOFs, ChemPhysChem 13 (2012) 3497–3503, https://doi.org/10.1002/cphc.201200455.
[294] H. Jasuja, Y. Huang, K.S. Walton, Adjusting the stability of metal−organic frameworks under humid conditions by ligand functionalization, Langmuir 28 (2012) 16874–16880, https://doi.org/10.1021/la304151r.
[295] K. Arya, A. Kumar, S. Mehra, A. Kumar, S. Kumar, R. Kataria, Exploration and removal of multiple metal ions using mixed-linker-architected Zn-MOF in aqueous media, Sep. Purif. Technol. 307 (2023) 122551, https://doi.org/10.1016/j.seppur.2022.122551.
[296] Y. Huang, Y. Jiao, T. Chen, Y. Gong, S. Wang, Y. Liu, D.S. Sholl, K.S. Walton, Tuning the wettability of metal−organic frameworks via defect engineering for efficient oil/water separation, ACS Appl. Mater. Interfaces 12 (2020) 34413–34422, https://doi.org/10.1021/acsami.0c08803.
[297] S. Jamdade, Z. Yu, S.E. Boulfelfel, X. Cai, R. Thyagarajan, H. Fang, D.S. Sholl, Probing structural defects in MOFs using water stability, J. Phys. Chem. C 128 (2024) 3975–3984, https://doi.org/10.1021/acs.jpcc.3c07497.
[298] Y. Zeng, J. Xiao, Y. Cong, J. Liu, Y. He, B.D. Ross, H. Xu, Y. Yin, H. Hong, W. Xu, PEGylated nanoscale metal−organic frameworks for targeted cancer imaging and drug delivery, Bioconjug. Chem. 32 (2021) 2195–2204, https://doi.org/10.1021/acs.bioconjchem.1c00368.
[299] Y. Wang, J. Yan, N. Wen, H. Xiong, S. Cai, Q. He, Y. Hu, D. Peng, Z. Liu, Y. Liu, Metal-organic frameworks for stimuli-responsive drug delivery, Biomaterials 230 (2020) 119619, https://doi.org/10.1016/j.biomaterials.2019.119619.
[300] M.E.A. Safy, M. Amin, R.R. Haikal, B. Elshazly, J. Wang, Y. Wang, C. Wçll, M. H. Alkordi, Probing the water stability limits and degradation pathways of Metal–Organic Frameworks, Chem. - A Eur. J. 26 (2020) 7109–7117, https://doi.org/10.1002/chem.202000207.
[301] M. Cai, W. Liang, K. Wang, D. Yin, T. Fu, R. Zhu, C. Qu, X. Dong, J. Ni, X. Yin, Aperture modulation of isoreticular metal organic frameworks for targeted antitumor drug delivery, ACS Appl. Mater. Interfaces 14 (2022) 36366–36378, https://doi.org/10.1021/acsami.2c07450.
[302] K.L. Yam, P.T. Takhistov, J. Miltz, Intelligent packaging: concepts and applications, J. Food Sci. 70 (2005) R1–R10, https://doi.org/10.1111/j.1365-2621.2005.tb09052.x.
[303] C. Vilela, M. Kurek, Z. Hayouka, B. Röcker, S. Yildirim, M.D.C. Antunes, J. Nilsen-Nygaard, M.K. Pettersen, C.S.R. Freire, A concise guide to active agents for active food packaging, Trends Food Sci. Technol. 80 (2018) 212–222, https://doi.org/10.1016/j.tifs.2018.08.006.
[304] Mc Contreras, P. Salcedo-Abraira, A. Zabala-Lekuona, A. Rodríguez-Diéguez, S. Rojas, Developing a novel agrochemical-based MOF: a multifunctional platform with herbicidal and antibacterial activities, ACS Appl. Mater. Interfaces 17 (2025) 4147–4154, https://doi.org/10.1021/acsami.4c17237.
[305] Y. Wu, Y. Luo, B. Zhou, L. Mei, Q. Wang, B. Zhang, Porous metal-organic framework (MOF) carrier for incorporation of volatile antimicrobial essential oil, Food Control 98 (2019) 174–178, https://doi.org/10.1016/j.foodcont.2018.11.011.
[306] H. Ning, L. Lu, J. Xu, L. Lu, L. Pan, Z. Lin, Development of sodium alginate-based antioxidant and antibacterial bioactive films added with IRMOF-3/carvacrol, Carbohydr. Polym. 292 (2022) 119682, https://doi.org/10.1016/j.carbpol.2022.119682.
[307] G.K. Angeli, M.I. Kotzabasaki, C. Maraveas, Metal organic frameworks for smart storage and delivery of aromatic volatiles and essential oils in agrifood, Appl. Sci. 15 (2025) 5479, https://doi.org/10.3390/app15105479.
[308] D. Giovanardi, P.P. Mazzeo, P. Pelagatti, A. Bacchi, Guest molecules play tug of war in a breathing MOF: the stepwise monitoring of an elastic framework deformation via SC-SC transformations, Cryst. Growth Des. 23 (2023) 8726–8734, https://doi.org/10.1021/acs.cgd.3c00869.
[309] D. Balestri, P.P. Mazzeo, C. Carraro, N. Demitri, P. Pelagatti, A. Bacchi, Stepwise evolution of molecular nanoaggregates inside the pores of a highly flexible Metal–Organic Framework, Angew. Chem. 131 (2019) 17503–17511, https://doi.org/10.1002/ange.201907621.
[310] P.P. Mazzeo, D. Balestri, A. Bacchi, P. Pelagatti, Stabilization of liquid active guests via nanoconfinement into a flexible microporous metal–organic framework, CrystEngComm 23 (2021) 7262–7269, https://doi.org/10.1039/D1CE00899D.
[311] D. Giovanardi, E. Ribezzi, M. Napolitano, M. Orlandini, N. Riboni, P.P. Mazzeo, A. Bacchi, F. Bianchi, M. Careri, P. Pelagatti, Effect of the entanglement of microporous pillared MOFs on the uptake and release profiles of essential oil components, Chem. – A Eur. J. 31 (2025) 1–9, https://doi.org/10.1002/chem.202501167.
[312] D. Balestri, P.P. Mazzeo, R. Perrone, F. Fornari, F. Bianchi, M. Careri, A. Bacchi, P. Pelagatti, Deciphering the supramolecular Organization of Multiple Guests inside a microporous MOF to understand their release profile, Angew, Chemie 133 (2021) 10282–10290, https://doi.org/10.1002/ange.202017105.
[313] D. Giovanardi, G. Cagossi, P.N. Zolotarev, P.P. Mazzeo, A. Bacchi, L. Carlucci, D. M. Proserpio, P. Pelagatti, Collapse or capture? Guest-induced response of two structurally distinct pillared-MOFs upon exposure to pyridines and quinolines, Dalton Trans. 54 (2025) 13540–13548, https://doi.org/10.1039/D5DT01321F.
[314] Z. Fang, B. Bueken, D.E. De Vos, R.A. Fischer, Defect-engineered metal – organic frameworks, Angew. Chem. Int. Ed. 54 (2015) 7234–7254, https://doi.org/10.1002/anie.201411540.
[315] S. Li, W. Han, Q. An, K. Yong, M. Yin, Defect engineering of MOF-based membrane for gas separation, Adv. Drug Deliv. Rev. 2303447 (2023) 1–15, https://doi.org/10.1002/adfm.202303447.
[316] K. Wang, J. Kang, L. Jin, L. Yang, Y. Liu, Y. Li, G. Chen, H. Xu, Defect engineering of MOF toward enhanced electrocatalytic water oxidation, Ionics (Kiel). 29 (2023) 5397–5403, https://doi.org/10.1007/s11581-023-05213-6.
[317] T.D. Bennett, A.K. Cheetham, A.H. Fuchs, F. Coudert, Interplay between defects, disorder and flexibility in metal-organic frameworks, Nat. Publ. Gr. 9 (2017) 11–16, https://doi.org/10.1038/nchem.2691.
[318] G. Sylwia, B. Szcze, Mechanochemistry : toward green synthesis of metal–organic frameworks, Mater. Today 46 (2021) 109–124, https://doi.org/10.1016/j.mattod.2021.01.008.
[319] J. Beamish-cook, K. Shankland, C.A. Murray, P. Vaqueiro, Insights into the mechanochemical synthesis of MOF-74, Cryst. Growth Des. 21 (2021) 3047–3055, https://doi.org/10.1021/acs.cgd.1c00213.
[320] M. Rubio-martinez, C. Avci-camur, D. Maspoch, M.R. Hill, A.W. Thornton, I. Imaz, M. Rubio-martinez, New synthetic routes towards MOF production at scale, Chem. Soc. Rev. 46 (2017) 3453–3480, https://doi.org/10.1039/c7cs00109f.
[321] M.P. Batten, M. Rubio-martinez, T. Hadley, K. Carey, K. Lim, A. Polyzos, M. R. Hill, Continuous flow production of metal-organic frameworks, Curr. Opin. Chem. Eng. 8 (2015) 55–59, https://doi.org/10.1016/j.coche.2015.02.001.
[322] B. He, L.K. Macreadie, J. Gardiner, S.G. Telfer, M.R. Hill, In situ investigation of multicomponent MOF crystallization during rapid continuous flow synthesis, ACS Appl. Mater. Interfaces 13 (2021) 54284–54293, https://doi.org/10.1021/acsami.1c04920.
[323] C. Paula, D. Wisser, M. Rangus, W. Schwieger, M. Hovestadt, M. Kriesten, K. Vanatalu, A. Oss, M. Org, A. Samoson, M. Hartmann, Phase transformations in porous materials studied by in situ solid-state NMR spectroscopy and in situ X-ray diffraction, J. Phys. Chem. C 124 (2020) 19136–19145, https://doi.org/10.1021/acs.jpcc.0c05921.
[324] Z. Zhang, D.S. Valente, Y. Shi, D.K. Limbu, M.R. Momeni, F.A. Shakib, In silico high-throughput design and prediction of structural and electronic properties of low-dimensional metal−organic frameworks, ACS Appl. Mater. Interfaces 15 (2023) 9494–95074, https://doi.org/10.1021/acsami.2c22665.
[325] J.P. Darby, M. Arhangelskis, A.D. Katsenis, J.M. Marrett, T. Fris, A.J. Morris, Ab initio prediction of metal-organic framework structures, Chem. Mater. 32 (2020) 5835–5844, https://doi.org/10.1021/acs.chemmater.0c01737.
[326] D. Nazarian, S. Camp, Y.G. Chung, R.Q. Snurr, D.S. Sholl, Large-scale refinement of metal−organic framework structures using density functional theory, Chem. Mater. 29 (2017) 2521–2528, https://doi.org/10.1021/acs.chemmater.6b04226.
[327] D. Nazarian, P. Ganesh, D.S. Sholl, Benchmarking density functional theory predictions of framework structures and properties in a chemically diverse test set of metal–organic frameworks, J. Ma 3 (2015) 22432–22440, https://doi.org/10.1039/c5ta03864b.
[328] Y. Luo, S. Bag, O. Zaremba, A. Cierpka, J. Andreo, S. Wuttke, P. Friederich, M. Tsotsalas, MOFs and machine learning MOF synthesis prediction enabled by automatic data mining and machine learning, Angew. Chem. Int. Ed. 61 (2022) e202200242, https://doi.org/10.1002/anie.202200242.
[329] R. Batra, C. Chen, T.G. Evans, K.S. Walton, R. Ramprasad, Prediction of water stability of metal–organic frameworks using machine learning, Nat. Mach. Intell. 2 (2020) 704–710, https://doi.org/10.1038/s42256-020-00249-z.
[330] M. Pardakhti, E. Moharreri, D. Wanik, S.L. Suib, R. Srivastava, Machine learning using combined structural and chemical descriptors for prediction of methane adsorption performance of metal organic frameworks (MOFs), ACS Comb. Sci. 19 (2017) 640–645, https://doi.org/10.1021/acscombsci.7b00056.
[331] R. Pétuya, S. Durdy, D. Antypov, M.W. Gaultois, N.G. Berry, G.R. Darling, A. P. Katsoulidis, M.S. Dyer, M.J. Rosseinsky, Machine-learning prediction of metal – organic framework guest accessibility from linker and metal chemistry, Angew. Chem. Int. Ed. 61 (2022) e202114573, https://doi.org/10.1002/anie.202114573.
[332] R. Singh, A. Prasad, B. Kumar, S. Kumari, R.K. Sahu, S.T. Hedau, Potential of dual drug delivery systems: MOF as hybrid nanocarrier for dual drug delivery in cancer treatment, ChemistrySelect 7 (2022), https://doi.org/10.1002/slct.202201288.